ADVANCED SULFUR CONTROL CONCEPTS FOR HOT-GAS DESULFURIZATION TECHNOLOGY

Final Report

April 1994 to October 1998

D.P. Harrison, F.R. Groves, W.-N. Huang, A. Lopez Ortiz, J.D. White, Y. Zeng, S. Zhang

October 1998

DE-AC21-94MC30012 -18

Department of Chemical Engineering
Louisiana State University
Baton Rouge, LA 70803-7303

ACKNOWLEDGMENT

This research was supported by the Federal Energy Technology Center (FETC) of the U.S. Department of Energy under contract DE-AC21-94MC30012. The authors would like to thank Mr. Thomas Dorchak of FETC who served as Contracting Officer's Representative throughout the project. The suggestions, support, and patience provided by Mr. Dorchak are gratefully acknowledged. We also thank Ms. Laura Brandt and Ms. Kelly McDonald, FETC Contracting Specialists, who were extremely helpful to us in meeting the administrative requirements of the contract.

ABSTRACT

This research project examined the feasibility of a second generation high-temperature coal gas desulfurization process in which elemental sulfur is produced directly during the sorbent regeneration phase. Two concepts were evaluated experimentally. In the first, FeS was regenerated in a H_2O-O_2 mixture. Large fractions of the sulfur were liberated in elemental form when the H_2O-O_2 ratio was large. However, the mole percent of elemental sulfur in the product was always quite small (<<1%) and a process based on this concept was judged to be impractical because of the low temperature and high energy requirements associated with condensing the sulfur.

The second concept involved desulfurization using CeO_2 and regeneration of the sulfided sorbent, Ce_2O_2S, using SO_2 to produce elemental sulfur directly. No significant side reactions were observed and the reaction was found to be quite rapid over the temperature range of 500°C to 700°C. Elemental sulfur concentrations (as S_2) as large as 20 mol% were produced.

Limitations associated with the cerium sorbent process are concentrated in the desulfurization phase. High temperature and highly reducing coal gas such as produced in the Shell gasification process are required if high sulfur removal efficiencies are to be achieved. For example, the equilibrium H_2S concentration at 800°C from a Shell gas in contact with CeO_2 is about 300 ppmv, well above the allowable IGCC specification. In this case, a two-stage desulfurization process using CeO_2 for bulk H_2S removal following by a zinc sorbent polishing step would be required.

Under appropriate conditions, however, CeO_2 can be reduced to non-stoichiometric CeO_n ($n<2$) which has significantly greater affinity for H_2S. Pre-breakthrough H_2S concentrations in the range of 1 ppmv to 5 ppmv were measured in sulfidation tests using CeO_n at 700°C in highly reducing gases, as measured by equilibrium O_2 concentration, comparable to the Shell gas.

Good sorbent durability was indicated in a twenty-five-cycle test. The sorbent was exposed for 58 consecutive days to temperatures between 600°C and 800°C and gas atmospheres from highly reducing to highly oxidizing without measurable loss of sulfur capacity or reactivity.

In the process analysis phase of this study, a two-stage desulfurization process using cerium sorbent with SO_2 regeneration followed by zinc sorbent with dilute O_2 regeneration was compared to a single-stage process using zinc sorbent and O_2 regeneration with SO_2 in the regeneration product gas converted to elemental sulfur using the direct sulfur recovery process (DSRP). Material and energy balances were calculated using the process simulation package PRO/II. Major process equipment was sized and a preliminary economic analysis completed. Sorbent replacement rate, which is determined by the multicycle sorbent durability, was found to be the most significant factor in both processes. For large replacement rates corresponding to average sorbent lifetimes of 250 cycles or less, the single-stage zinc sorbent process with DSRP was estimated to be less costly. However, the cost of the two-stage cerium sorbent process was more sensitive to sorbent replacement rate, and, as the required replacement rate decreased, the economics of the two-stage process improved. For small sorbent replacement rates corresponding to average sorbent lifetimes of 1000 cycles or more, the two-stage cerium process

was estimated to be less costly. In the relatively wide middle range of sorbent replacement rates, the relative economics of the two processes depends on other factors such as the unit cost of sorbents, oxygen, nitrogen, and the relative capital costs.

TABLE OF CONTENTS

TABLE OF CONTENTS (Continue)

LIST OF TABLES

LIST OF TABLES (Continued)

LIST OF FIGURES

LIST OF FIGURES (Continued)

LIST OF FIGURES (Continued)

LIST OF FIGURES (Continued)

LIST OF FIGURES (Continued)

EXECUTIVE SUMMARY

Advanced power processes such as the integrated gasification combined cycle (IGCC) have the capability of using the nation's vast coal reserves with increased efficiency and reduced environment impact. Optimal development of the IGCC requires that H_2S formed during gasification be removed at high temperature. High temperature desulfurization processes under current development use zinc-based sorbents which are capable of reducing the H_2S content to 20 ppmv or less. Zinc sorbents must be regenerated using dilute air which produces a product gas containing dilute SO_2. Additional processing is required prevent atmospheric sulfur emissions by converting the SO_2 to elemental sulfur.

The primary purpose of this research project was to identify a second-generation desulfurization sorbent capable of being regenerated with the direct production of elemental sulfur. The research began with a search of the literature to identify concepts having the potential for direct elemental sulfur production. Three concepts based on regeneration with SO_2, partial oxidation, and reaction with steam were identified. The thermodynamics of the reaction of a number of metal oxide sorbents known to have desulfurization capability were then analyzed using each of the candidate sorbents.

The thermodynamic analysis showed that sorbents having the greatest affinity for sulfur removal, including zinc, could not be regenerated to produce elemental sulfur. Sorbents based on cerium and tin were identified as having thermodynamic properties uniquely suited to elemental sulfur production. In addition, the literature suggests that the partial oxidation regeneration of FeS in an oxygen-steam mixture having a large excess of steam could be used to produce elemental sulfur. This reaction is believed to be controlled by kinetics instead of thermodynamics and would, therefore, require careful control of regeneration conditions.

Two systems involving the regeneration of FeS using the partial oxidation concept and the regeneration of cerium sorbent by the reaction of Ce_2O_2S with SO_2 were selected for the experimental phase of the study. The regeneration of FeS was studied using both an electrobalance reactor in which reaction progress was monitored by the change in mass of the reacting solid with time and a fixed-bed reactor where reaction progress was followed by analyzing the composition of the gas product using gas chromatography. The reaction between Ce_2O_2S and SO_2 to form $2CeO_2$ produces no change in solid mass; hence, experimental tests using the cerium sorbent were restricted to the fixed-bed reactor with product gas analysis. In addition, the product of the reaction between CeO_2 and H_2S, Ce_2O_2S, cannot be obtained commercially. Therefore, both the sulfidation and regeneration phases were studied.

In agreement with earlier studies from the literature, we found that large fractions of the sulfur in FeS could be liberated in elemental form under partial oxidation conditions. The steam-to-oxygen ratio of the regeneration feed gas was identified as the most important reaction parameter. Approximately 80% of the initial sulfur were converted directly to elemental sulfur at a steam-to-oxygen molar ratio of 200. However, the product gas contained only small concentrations of elemental sulfur (<1 mol%). The energy required to cool the large flow of

dilute regenerator product gas to condense the elemental sulfur would be prohibitive, and this process concept was judged to be commercially impractical.

In contrast, the thermodynamic of the Ce_2O_2S-SO_2 reaction were extremely favorable. No possible side reactions were identified and large concentrations of elemental sulfur could be produced in the product gas. The limitation on the elemental sulfur concentration was established by condensation to liquid sulfur instead of thermodynamics.

Experimental results were also quite favorable. In early tests, CeO_2 was sulfided to Ce_2O_2S under standard reaction conditions so that the effect of regeneration reaction parameters could be studied. The regeneration reaction was rapid and complete over the temperature range of 500°C to 700°C. 600°C was chosen as the standard regeneration temperature and the effects of the SO_2 content of the feed gas, pressure, and feed gas flow rate were examined. Elemental sulfur concentrations in the regeneration product gas up to 20 mol% were produced. The major experimental problem was found to be preventing elemental sulfur from condensing and plugging reactor product lines. A system in which the sulfur condenser was supplemented by a combination of filters was developed to reduce the condensation and plugging problem to manageable limits.

Apparent H_2S removal during sulfidation was found to be influenced by additional H_2S formed downstream of the sorbent bed by the reaction between elemental sulfur deposited in a previous regeneration test and hydrogen present in the sulfidation feed gas. Alterations in the reactor system to minimize contact with stainless steel and development of a cleaning step in which high temperature air was passed through the reactor until no SO_2 was detected in the product gas were needed to determine the ultimate sulfur removal capability of the cerium sorbent.

A more complete examination of the literature showed that under appropriate conditions CeO_2 could be reduced to non-stoichiometric CeO_n ($n<2$) with the value of n dependent on temperature and the reducing power of the gas. Although reliable thermodynamic data for CeO_n were not available, there was reason to believe that their ability to remove H_2S would be significantly better than CeO_2. Indeed, pre-breakthrough H_2S concentrations of about 1 ppmv were measured using CeO_n in the temperature range of 650°C to 700°C with the pre-breakthrough period lasting until about 30% of the cerium was converted to Ce_2O_2S. Unfortunately, reduction of CeO_2 is possible only in highly reducing gases such as produced in the Shell gasification process. Experimental tests using gas compositions which simulated the reducing power of the Shell gas produced pre-breakthrough H_2S concentrations in the 2 to 5 ppmv range at 700°C. Experimental duplication of the composition of the Shell gas was not practical because of the strong tendency for carbon deposition during feed gas preheat.

Three multicycle tests consisting of from 10 to 25 complete sulfidation-regeneration cycles were carried out to obtain preliminary information on sorbent durability. Results were quite favorable and there were no indications of sorbent deterioration in any of the tests. Results from the 25-cycle test were particularly impressive. This test extended over fifty-eight days, during which the sorbent was continually exposed to a temperature of at least 600°C with the temperature being 800°C for about 90% of that time. The sorbent was alternately exposed to a

H_2/N_2 atmosphere during reduction, $H_2S/H_2/N_2$ during sulfidation, SO_2/N_2 during regeneration, air during reactor cleaning and N_2 purge between each phase.

The majority of the experimental tests used CeO_2 obtained from Rhône Poulenc physically mixed with Al_2O_3 as the sorbent charge. In addition, CeO_2 from five other sources was subjected to limited testing. The alternate materials included lower surface area CeO_2 from Molycorp, $Ce_2(CO_3)_3$ from Molycorp which was calcined to CeO_2 prior to sulfidation, and three sorbents supplied by Gas Desulfurization Corp. in which CeO_2 was deposited on an Al_2O_3 support. These sorbents had been prepared by Engelhard Corp. and were composed of varying proportions of CeO_2 on Al_2O_3, and in one case a mixture of CeO_2 and La_2O_3 on Al_2O_3. Although results of individual tests were highly variable, all alternate sorbents were capable of removing H_2S with high efficiency. Performance differences could be attributed to differences in CeO_2 loading and to structural properties such as surface area.

The process analysis section of the research compared a cerium-sorbent process to a first-generation process using zinc sorbent with the direct sulfur recovery process (DSRP) used to produce elemental sulfur. The cerium process was based on two desulfurization stages with CeO_2 used in the primary reactor for bulk H_2S removal followed by a zinc sorbent polishing step. SO_2 was used to regenerate Ce_2O_2S and produce elemental sulfur directly. ZnS was regenerated using dilute O_2 to produce dilute SO_2 which was recycled to the gasifier where it was reduced to H_2S and ultimately captured as elemental sulfur.

The computer design package PRO/II was used to calculate material and energy balances for both processes based on the assumption that chemical equilibrium was achieved in each of the reactors. Desulfurization and regeneration reactors in both processes were assumed to be fluidized beds. Major process equipment was sized using results from PRO/II and literature guidelines. Capital and operating costs were estimated and converted to annual total levelized cost. The key cost item in both processes was found to be sorbent replacement cost, which depends on sorbent durability and sorbent unit cost. The single-stage process using zinc sorbent was estimated to be more economical when relatively large sorbent replacement rates are required. As the durability of the sorbents increases the costs of both processes decrease, and at some point the two-stage cerium process is less costly. The estimated sorbent durability corresponding to equal cost of the two process occurs at a sorbent replacement rate between 0.1% and 0.4% of the sorbent circulation rate. This relatively broad range is due to the uncertainty in estimated costs of numerous items, including unit sorbent cost. If the durability of the sorbent is such that the sorbent replacement rate is less than 0.1% of the sorbent circulation rate, the two-stage process using cerium sorbent and SO_2 regeneration should be less expensive. In the limit of infinite sorbent life (zero sorbent replacement rate), the two-stage cerium process has the potential for showing a profit through the sale of by-product sulfur and export steam. The profit is estimated to be equivalent to about 1.4 mills/kWh. In contrast, infinite life of the zinc sorbent is estimated to result in an incremental cost of about 3.2 mills/kWh.

CHAPTER 1. INTRODUCTION

1.1 Background

High temperature desulfurization of coal-derived gases is an important component in the optimal development of advanced power processes such as the integrated gasification combined cycle (IGCC). These advanced power processes provide a means of utilizing the nation's vast reserves of coal with increased efficiency and reduced environmental impact. High temperature desulfurization research has been on-going for approximately twenty-five years and has reached the demonstration stage in two clean coal demonstration plants (USDOE 1996a, 1996b).

High temperature desulfurization is based on the noncatalytic gas-solid reaction between H_2S and an appropriate metal oxide sorbent. The reaction can be represented generically by

$$MeO(s) + H_2S(g) \rightarrow MeS(s) + H_2O(g) \quad (1)$$

Process economics requires that the sorbent be regenerable. Most regeneration studies have used oxygen and the generic regeneration reaction is

$$MeS(s) + 1.5\ O_2(g) \rightarrow MeO(s) + SO_2(g) \quad (2)$$

The desirable properties of a sorbent include (1) favorable thermodynamics for both the sulfidation and regeneration reactions, (2) large achievable sulfur capacity, (3) rapid reactivity, (4) stability through a large number of sulfidation-regeneration cycles, (5) for this project ready recovery of elemental sulfur, and (6) low cost and ready availability.

Research in the U.S. has concentrated on zinc-based sorbents primarily because of favorable sulfidation properties. The thermodynamics of the ZnO-H_2S reaction are such that the 20 ppmv H_2S product gas concentration target can be achieved at temperatures of interest (Gangwal et al., 1988). The stoichiometric capacity of pure ZnO, 0.39 g S per g of ZnO, is quite large although the addition of stabilizers such as TiO_2 causes the capacity to be considerably reduced. The sulfidation reaction is rapid and ZnO is relatively plentiful and inexpensive.

The only serious problem associated with ZnO during the sulfidation phase is the tendency for ZnO to be reduced to volatile elemental Zn. This limits the application of ZnO to relatively low temperatures ($\leq$550°) and low reducing power coal gases. The addition of TiO_2 to form the mixed metal oxide, ZnO•xTiO_2, is known to stabilize ZnO against reduction and extend the maximum operating temperature by approximately 50°C (Woods et al., 1990). This is achieved, however, with a loss of sulfur capacity and increased cost of sorbent preparation.

Most of the problems with zinc-based sorbents are associated with the regeneration phase of the cycle. Because of the strong affinity between zinc and sulfur, regeneration can only be accomplished using oxygen. The highly exothermic ZnS-O_2 reaction may create temperature excursions during regeneration which lead to sintering, reduced reactivity, and decreased sorbent lifetime. Diluting the O_2 in the regeneration feed gas, which can be used to moderate the

regenerator temperature excursions, produces a product gas containing dilute SO_2 which complicates the ultimate SO_2 control problem. Finally, at desirable regeneration temperatures the concentrations of O_2 and SO_2 favor the formation of $ZnSO_4$. In addition to limiting the degree of regeneration, sulfate formation is believed to be a major cause of rapid sorbent deterioration. The molar volume of $ZnSO_4$ is two to three times greater than the molar volumes of ZnO and ZnS. The large increase in solid volume is believed responsible for sorbent particle fragmentation.

In spite of the problems, the development of zinc-based high temperature desulfurization sorbents has progressed to the point that demonstration on a commercial scale at the Sierra Pacific Power Company (SPPC) Piñon Pine Station (USDOE, 1996a) and the Tampa Electric (TECO) Polk Power Station (USDOE, 1996b) is scheduled. The SPPC plant is based on a KRW air-blown gasifier with in-bed limestone injection for bulk sulfur removal. Sulfur polishing is accomplished using a zinc-based sorbent in a transport reactor. Ultimate sulfur control in the SPPC plant is accomplished by recycling the regenerator product gas to the gasifier where SO_2 will react with limestone and be sequestered as $CaSO_4$. This creates problems with residual $CaSO_3$ and solid waste disposal. The TECO plant uses a Texaco oxygen-blown gasifier. Traditional low-temperature desulfurization is incorporated, with a 10% slip stream scheduled for high temperature desulfurization using zinc-based sorbent in a moving-bed reactor. The TECO plant produces a regenerator off-gas suitable as feedstock for H_2SO_4 manufacture.

1.2. This Project

The primary purpose of this research project was to examine the feasibility of the direct production of elemental sulfur during the sorbent regeneration step. Elemental sulfur can be separated by condensation and stored and transported with relative ease. Elemental sulfur sales have the potential for off-setting a portion of the desulfurization cost. Most importantly, the direct production of elemental sulfur avoids the solid waste problem associated with limestone capture and eliminates the need for further processing of the regenerator off-gas prior to atmospheric discharge.

The project began with a literature search to identify possible concepts for direct production of elemental sulfur. This was followed by a detailed thermodynamic analysis in which a number of candidate sorbents were evaluated using each of these concepts. Results of this phase of the study were detailed in a topical report (Lopez et al., 1994). A summary of the results is presented in Chapter 2. As a result of this initial work two sorbents and two regeneration concepts were selected for experimental study.

Detailed results of exploratory studies on the regeneration of FeS using the partial oxidation concept and regeneration of Ce_2O_2S with SO_2 were covered in a subsequent topical report (Lopez et al., 1997). The FeS regeneration results are summarized in Chapter 4 of this report, while results of the Ce_2O_2S-SO_2 reaction are presented in Chapter 5. Although the production of elemental sulfur via the partial oxidation of FeS was technically feasible, the large amount of steam required and the resultant low concentration of elemental sulfur in the regeneration product gas were such that the approach was judged to be uneconomic. In contrast, the reaction between Ce_2O_2S and SO_2 preceded rapidly with no side reactions and with the

potential of producing large elemental sulfur concentrations. This system was selected for more detailed experimental investigation. Because the sulfidation product, Ce_2O_2S, is not available commercially, it was necessary to sulfide CeO_2 prior to regeneration. Thus, both the sulfidation and regeneration phases of the cycle were included in the experimental study. Detailed sulfidation results are presented in Chapter 6, and Chapter 7 discusses results of multicycle tests. The majority of the research utilized CeO_2 from Rhône-Poulenc as the starting material. Results of limited tests using other CeO_2 sources are discussed in Chapter 8.

The final phase of the project consisted of process analysis which included material and energy balances for a cerium-based process using the software package PRO/II. A number of case studies were considered and major process equipment was designed. A preliminary economic evaluation was then completed by estimating capital and operating costs. For comparison purposes, similar material and energy balances, equipment design and cost estimation steps were included for a zinc-based sorbent process using the direct sulfur recovery process (DSRP) (Gangwal and Portzer, 1995) for recovery of elemental sulfur from the dilute regeneration product gas. The process and economic analysis results are presented in Chapter 9. Finally, Chapter 10 contains an overall summary of the project along with conclusions and recommendations for additional work.

CHAPTER 2. LITERATURE SEARCH AND THERMODYNAMIC ANALYSIS

A literature search was performed to identify possible concepts for the direct production of elemental sulfur during sorbent regeneration, and to collect relevant thermodynamic, kinetic, and process data. This was followed by thermodynamic analysis, based on free-energy minimization, to evaluate candidate sorbents for possible use with the regeneration concepts. Detailed results from this phase of the study have been presented in a topical report (Lopez et al., 1994). The results are summarized in the following.

2.1. Regeneration Concepts

Three regeneration concepts were identified in the literature search. These are referred to as reaction with SO_2, partial oxidation, and reaction with steam. The latter concept results in the direct formation of H_2S instead of elemental sulfur. However, if H_2S can be produced in sufficiently large concentrations, the well-known Claus process can then be used to produce elemental sulfur.

2.1.1. Reaction With SO_2

The reaction between an appropriate metal sulfide and SO_2 to yield elemental sulfur is well known and can be represented generically as follows

$$2\ MeS(s) + SO_2(g) \rightarrow 2\ MeO(s) + 1.5\ S_2(g) \qquad (3)$$

The problem is to identify metal oxide systems which posses the necessary desulfurization capability, are reactive with SO_2, and are not limited by problems such as sulfate formation and/or the production of volatile metal compounds.

Copeland (1993a, 1993b) reported that SnO_2 is capable of 90 to 99% H_2S removal during the desulfurization phase and that the sulfided product, SnS, will react with SO_2 to produce elemental sulfur. Anderson and Berry (1987) reported similar properties associated with a cobalt titanate sorbent. Several papers on the regeneration of sulfided iron oxide with SO_2 were identified. Schrodt and Best (1978) and Tseng et al. (1981) reported results using a sorbent composed of Fe_2O_3 on SiO_2 (or fly ash) while Patrick et al. (1993) reported the formation of elemental sulfur during regeneration of FeS on Al_2O_3. Questions concerning the rate of the FeS-SO_2 reaction and thermodynamic limits on the maximum partial pressure of S_2(g) in the product were raised. The thermodynamic question is addressed in the following section.

2.1.2. Partial Oxidation

A number of investigators have reported that significant quantities of elemental sulfur are formed when metal sulfide is reacted with oxygen and steam under "O_2-starved" conditions. Although this concept likely involves a number of simultaneous gas-solid and gas phase reactions the overall result may be represented by the stoichiometry

$$MeS(s) + 0.5\ O_2(g) \rightarrow MeO(s) + 0.5\ S_2(g) \quad (4)$$

Since the thermodynamics of the MeS-O_2 reaction favors total oxidation to MeO and SO_2, it will be necessary to operate in an "O_2-starved" atmosphere and at conditions where kinetics instead of thermodynamics controls the product distribution.

Iron appeared to be a prime candidate for this regeneration concept. Joshi et al. (1979) reported that 75% of the sulfur in the regeneration product was in elemental form when FeS on SiO_2 was reacted at 540°C in an atmosphere of 95% H_2O-5% air. Grindley and Steinfeld (1981) reported similar results and also found that increasing the O_2 content resulted in decreased elemental sulfur and increased SO_2. Van der Waal (1987) reported that low temperature, low O_2 concentration, and high space velocity increased the yield of elemental sulfur in his study of FeS regeneration using O_2 and steam.

Kay and Wilson (1989) reported the formation of elemental sulfur when Ce_2O_2S was reacted in 20% O_2-80% N_2 at 900°C. The high regeneration temperature was required to avoid $Ce_2(SO_4)_3$ formation. A follow-up paper (Kay, 1993) mentions that "O_2-starved" conditions promote the formation of elemental sulfur.

2.1.3. Regeneration With H_2O

By reversing the sulfidation reaction, regeneration with the production of H_2S is possible. This concept was considered even though elemental sulfur is not a direct product; conversion of H_2S to elemental sulfur using Claus technology is well developed. Because the regeneration reaction is the reverse of sulfidation, it is obvious that sorbents having the greatest affinity for H_2S, for example ZnO, will be the most difficult to regenerate with steam.

Nielsen et al. (1991) used steam at 500°C to regenerate SnS. 30 moles of steam per mole of sulfur were required. A separation step is required to recover H_2S from excess steam and H_2 by-product before the H_2S is sent to a sulfur recovery unit. Iron and tin have similar affinities for H_2S and studies on the regeneration of iron-based sorbents have been reported by Tamhankar et al. (1985) and Wakker et al. (1993). Tamhankar et al. (1985) found that H_2S, H_2 and Fe_3O_4 were the reaction products when FeS on SiO_2 was regenerated with steam. The reaction rate, however, was slow compared to air oxidation. Wakker et al. (1993) studied the sulfidation of $FeAl_2O_4$ and $MnAl_2O_4$ and commented on the possibility of regeneration with steam to produce a high concentration of H_2S in the product gas.

Sohn and Kim (1987) studied the regeneration of ZnS with steam to produce ZnO and H_2S in an electrobalance reactor over the temperature range 640 to 1200 K. While there was no mention of the steam-to-sulfur ratio required, one would expect the ratio to be large because of the strong affinity of ZnO for H_2S.

2.1.4. Summary

The literature search identified three concepts for the direct production of elemental sulfur during sorbent regeneration. Favorable references to the regeneration of sulfided tin

sorbent with SO_2 and sulfided iron sorbent using each of the three concepts have been published. Other possible sorbents identified were the sulfided versions of zinc, cobalt, manganese, and cerium. While zinc would be a logical sorbent candidate because of its ability to remove H_2S and because of the extensive information base, we felt that regeneration of ZnS to elemental sulfur would not be feasible.

The thermodynamic analysis, which followed, evaluated the metal oxide sorbents identified in the literature search, as well as additional metal oxides, for suitability with each of the regeneration concepts.

2.2. Thermodynamic Analysis

The free-energy minimization program CHEMQ (Kirkpatrick and Pike, 1994) was used to evaluate the sulfidation and regeneration properties of eight metal oxides (see Table 1) as potential sorbents. The reduction-desulfurization analysis was carried out over a temperature range of 600 to 1150 K (327 to 877°C) and pressure range of 1 to 25 atm. Two coal gas compositions representative of products from an O_2-blown Texaco gasifier and air-blown KRW gasifier were used (see Table 2). The H_2S content of each coal gas was arbitrarily set to 1 mol%. The greater reducing power and increased tendency toward carbon deposition associated with the Texaco gas are indicated by the values in the last two rows of Table 2. The reducing power of the gas is important in determining the equilibrium oxidation state of the sorbent, while operating conditions at which carbon deposition is favored should be avoided.

Table 1. Candidate Metal Oxide Sorbents
Considered in the Reduction/Sulfidation Analysis

Metal	Highest Oxidation State
Cerium	CeO_2
Cobalt	Co_3O_4
Copper	CuO
Iron	Fe_2O_3
Maganese	MnO_2
Molybdenum	MoO_3
Tin	SnO_2
Zinc	ZnO

Table 2. Composition of the Texaco Oxygen-Blown And KRW Air-Blown Gasifier Products

	Composition, mol%	
	Texaco	KRW
H_2	31.06	10.0
CO	39.87	15.0
H_2O	16.81	15.0
CO_2	10.62	5.0
H_2S	1.04	1.0
N_2	-----	54.0
NH_3	0.21	-----
CH_4	0.31	-----
$\frac{H_2 + CO}{H_2O + CO_2}$	2.59	1.25
$\frac{C}{O + H}$	0.29	0.22

2.2.1. Reduction-Sulfidation Analysis

The most important question in this phase of the analysis was the equilibrium concentration of H_2S in contact with a given sorbent. Other questions addressed included the oxidation state of excess sorbent in the coal gas, the nature of the sulfided product, and possible formation of molten or volatile species. In most cases, these questions were answered by "contacting" coal gas and sorbent in an initial molar ratio of 10 to 1. This provided a large excess of sorbent over that required for complete removal of H_2S and excess reducing gas to determine the final oxidation state of the sorbent.

Equilibrium fractional removal of H_2S was found to be only weakly dependent on pressure, particularly at temperatures outside the carbon deposition region. Three types of temperature effect were found. With most sorbents the fractional H_2S removal decreased monotonically with increasing temperature, which is characteristic of an exothermic sulfidation reaction. In contrast, fractional H_2S removal using cerium oxide increased with increasing temperature indicating that sulfidation is endothermic. Tin oxide exhibited a maximum in the fractional H_2S removal at an intermediate temperature, indicating a shift of the reaction from endothermic to exothermic.

Decreasing H_2S removal with increasing temperature is illustrated in Table 3 for iron oxide. The thermodynamic limit of carbon deposition is indicated by the horizontal solid line in

Table 3. Reduction/Sulfidation Analysis
of Iron Oxide (Fe_2O_3)

A. Initial Mixture: 1 mol Fe_2O_3 With 10 mols of Texaco Gas

	Fractional Sulfur Removal	
T (K)	P = 1 atm	P = 15 atm
823	0.958	-----
873	0.950	0.926
923	0.941	0.906
973	0.915	0.886
1023	0.881	0.869
1073	0.838	0.831
1123	0.754	0.782
Sulfided Product	FeS	FeS
Excess Fe	FeO	FeO
Volatile Species	None	None

B. Initial Mixture: 1 mol Fe_2O_3 With 10 mols of KRW Gas

	Fractional Sulfur Removal	
T (K)	P = 1 atm	P = 15 atm
623	.988	.982
673	.988	.980
723	.988	.978
773	.981	.976
823	.971	.967
873	.957	.954
923	.938	.936
973	.881	.907
1023	.912	.881
1073	.843	.844
1123	.801	-----
Sulfided Product	FeS	FeS
Excess Fe	Fe_3O_4, $T \leq 723$ K FeO, $T \geq 773$ K	Fe_3O_4, $T \leq 773$ FeO, $T \geq 823$
Volatile Species	None	None

each column. In a Texaco gas at 1 atm carbon deposition is not favored at temperatures equal to or greater than 973K but is favored at 923K or lower. Equilibrium fractional sulfur removal decreases with increasing temperature and is a maximum of 0.988 at 623K and 1 atm in KRW gas. FeS is the sulfided product at all conditions shown while the oxidation state of the excess sorbent is either Fe_3O_4 or FeO, depending on temperature and gas composition. No volatile iron species are favored over the range of conditions shown.

Similar results for cerium oxide are shown in Table 4. No H_2S removal is possible for either gas at lower temperatures. In the KRW gas initial H_2S removal can occur at about 850 K at 1 atm and 950 K at 15 atm. Initial H_2S removal in the Texaco gas may occur at 900 K and 1050 K at 1 and 15 atm, respectively. Above these temperatures, the H_2S removal potential increases and reaches a maximum of 0.878 in the Texaco gas at 1150 K and 1 atm. Cerium oxysulfide, Ce_2O_2S, is the sulfidation product at all conditions shown. No reduction of CeO_2 is predicted and no volatile or molten cerium compounds are favored.

Similarly detailed results for the remaining six candidate sorbents are available in the topical report (Lopez et al., 1994). Iron and cerium results were presented here since these two systems were selected for experimental study. An overall summary of the reduction-desulfurization analysis is presented in Table 5. All potential sorbents except cerium and tin are thermodynamically capable of exceeding 90% H_2S removal at sulfidation conditions where carbon deposition is not favored. The maximum H_2S removals for cerium and tin are both slightly less than 90%. Complete reduction of excess cobalt and copper to the metallic state is favored at all conditions, and, because of this, these systems were not considered in the regeneration analysis. The previously mentioned problem of reduction of ZnO to volatile Zn was identified; this limits the range of operating conditions in which zinc sorbents may be used. The tin system is also limited to certain operating conditions because of the high vapor pressure of SnS and the tendency for excess SnO_2 to be reduced to liquid metallic tin.

2.2.2. Regeneration Analysis

The regeneration properties of the six remaining candidate sorbents were analyzed using the three regeneration concepts. Answers to the following questions were sought. Most importantly, can the sulfided product be regenerated using the concept of interest and, if yes, does the gaseous regeneration product contain substantial quantities of elemental sulfur (or H_2S in the case of steam regeneration)? The concentration of elemental sulfur (or H_2S) in the product gas should be as large as possible. Other questions included the possible formation of metal sulfate, the oxidation state of the regenerated metal oxide, and the possible formation of molten or volatile regeneration products.

2.2.2.1. Reaction with SO_2

This regeneration reaction is represented generically by

$$2\,MeS(s) + SO_2(g) \rightarrow 2\,MeO + 1.5\,S_2(g) \qquad (5)$$

Table 4. Reduction/Sulfidation Analysis
Of Cerium Oxide (CeO_2)

A. Initial Mixture: 1 mol of CeO_2 and 10 mols of Texaco Gas

	Fractional Sulfur Removal		
T(K)	P = 1 atm	P = 5 atm	P = 25 atm
600	0.000	0.000	0.000
650	0.000	0.000	0.000
700	0.000	0.000	0.000
750	0.000	0.000	0.000
800	0.000	0.000	0.000
850	0.000	0.000	0.000
900	0.540	0.000	0.000
950	0.818	0.318	0.000
1000	0.848	0.720	0.000
1050	0.862	0.828	0.500
1100	0.870	0.859	0.760
1150	0.878	0.874	0.825
Sulfided Product	Ce_2O_2S	Ce_2O_2S	Ce_2O_2S
Excess Ce	CeO_2	CeO_2	CeO_2
Volatile Species	None	None	None

B. Initial Mixture: 1 mol of CeO_2 and 10 mols of KRW Gas

	Fractional Sulfur Removal		
T(K)	P = 1 atm	P = 5 atm	P = 25 atm
600	0.000	0.000	0.000
650	0.000	0.000	0.000
700	0.000	0.000	0.000
750	0.000	0.000	0.000
800	0.000	0.000	0.000
850	0.447	0.000	0.000
900	0.590	0.377	0.000
950	0.647	0.579	0.236
1000	0.682	0.664	0.500
1050	0.709	0.705	0.639
1100	0.733	0.732	0.709
1150	0.754	0.754	0.746
Sulfided Product	Ce_2O_2S	Ce_2O_2S	Ce_2O_2S
Excess Ce	CeO_2	CeO_2	CeO_2
Volatile Species	None	None	None

Table 5. Reduction/Sulfidation Analysis Summary

Sorbent System	Highest Oxidation Sate	Sulfided Product	Excess Metal	Volatile Species	90% Desulfurization w/o Carbon Deposition
Cerium	CeO_2	Ce_2O_2S	CeO_2	None	Slightly Below
Cobalt	Co_3O_4	Co_3S_4	Co(s)	None	Yes
Copper	CuO	Cu_2S	Cu(s)	None	Yes
Iron	Fe_2O_3	FeS	FeO, Fe_3O_4	None	Yes
Manganese	MnO_2	MnS	MnO	None	Yes
Molybdenum	MoO_3	MoS_2	MoO_2	None	Yes
Tin	SnO_2	SnS	SnO_2, Sn(P)	SnS(g)	Slightly Below
Zinc	ZnO	ZnS	ZnO, Zn(g)	Zn(g)	Yes

The analysis was carried out by "mixing" one mole of sulfided product with three moles of SO_2 and determining the equilibrium product composition as a function of temperature and pressure. With excess SO_2 complete regeneration is possible and ideal performance would correspond to fractional regeneration of 1.0 with 50% of the sulfur in the gas phase being in elemental form and with an equal quantity of SO_2.

MnS, MoS_2, and ZnS are effectively nonreactive with SO_2 over the temperature and pressure ranges considered (750 to 1200 K and 1 to 25 atm). Moderate reaction with FeS is possible while both SnS and Ce_2O_2S are capable of extensive reaction. Selected results from the Ce_2O_2S-SO_2 and FeS-SO_2 analyses are presented in Table 6.

Complete regeneration of Ce_2O_2S to CeO_2 is possible at all conditions shown except 800K and 5 atm where a small amount of $Ce_2(SO_4)_3$ is favored. The distribution between elemental and oxide sulfur corresponds to the ideal 50-50 split at 750 K and 1 atm and is reasonably near the ideal at all other conditions shown. The reaction between FeS and SO_2 is less favorable as indicated by the fact that substantial quantities of sulfur remain in the solid phase at all conditions shown. $FeSO_4$ formation is favored at 773 K and 25 atm where, under equilibrium conditions, the quantity of sulfur in the solid phase is actually increased. Conversion of FeS to FeS_2 is also favored at the lowest temperature at each pressure. Fe_3O_4 is the regeneration product, but the amount ranges from zero at 773 K and 25 atm to a maximum of 0.18 at 873 K and 1 atm. A relatively small fraction of the gas phase sulfur is in elemental form with the maximum of 0.09 at high temperature and low pressure. While the regeneration of FeS with SO_2 to form elemental sulfur is possible at high temperatures, extremely large quantities of SO_2 will be required to achieve complete conversion to Fe_3O_4 and the elemental sulfur concentration in the regenerator product gas will be quite small. The energy requirements associated with sulfur condensation and SO_2 reheat and recycle will be large.

Regeneration of SnS with SO_2 is qualitatively similar to the Ce_2O_2S results of Table 6. Complete regeneration is possible at conditions above the sulfate decomposition temperature. At these conditions, the fraction of elemental sulfur in the gas phase varies from 0.46 to 0.48,

Table 6. Regeneration of Ce_2O_2S(s) and FeS(s) with SO_2(g)

A. 1 mol Ce_2O_2S plus 3 mol SO_2

Temp., K	750	1100	800	850	1100	900	1100
Press., atm	1	1	5	5	5	25	25
Solid Phase Composition, mol fraction							
CeO_2	1.00	1.00	0.97	1.00	1.00	1.00	1.00
$Ce_2(SO_4)_3$	0.00	0.00	0.03	0.00	0.00	0.00	0.00
Sulfur Distribution (as S), fraction							
Condensed Phase	0.00	0.00	0.05	0.00	0.00	0.00	0.00
Gas Phase	1.00	1.00	0.95	1.00	1.00	1.00	1.00
Sulfur Distribution Within Gas Phase, fraction							
Elemental	0.50	0.48	0.53	0.49	0.47	0.49	0.46
Oxide	0.50	0.52	0.47	0.51	0.53	0.51	0.54

B. 1 mol FeS plus 3 mol SO_2

Temp., K	873	973	1173	773	873	1073	1173
Press., atm	1	1	1	25	25	25	25
Condensed Phase Composition, mol fraction							
FeS	0.00	0.97	0.93	0.00	0.00	0.97	0.96
FeS_2	0.82	0.00	0.00	0.67	0.83	0.00	0.00
Fe_3O_4	0.18	0.03	0.07	0.00	0.17	0.03	0.04
$FeSO_4$	0.00	0.00	0.00	0.33	0.00	0.00	0.00
Sulfur Distribution (as S), fraction							
Condensed Phase	0.30	0.24	0.20	0.42	0.31	0.23	0.22
Gas Phase	0.70	0.76	0.80	0.58	0.69	0.77	0.78
Sulfur Distribution Within Gas Phase, fraction							
Elemental	0.02	0.04	0.09	0.00	0.00	0.04	0.05
Oxidized	0.98	0.96	0.91	1.00	1.00	0.96	0.95

similar to the distribution from the Ce_2O_2S-SO_2 reaction. However, $SnSO_4$ is somewhat more stable than $Ce_2(SO_4)_3$ so that higher decomposition temperatures would be required. Also, gas phase SnS may be formed at high temperatures and low pressures as indicated in Table 5.

2.2.2.2 Partial Oxidation

The desired reaction is represented generically by

$$MeS(s) + 0.5\ O_2(g) \rightarrow MeO(s) + 0.5\ S_2(g) \qquad (6)$$

This reaction, however, is the net result of a number of simultaneous reactions. When O_2 is plentiful, complete oxidation to MeO and SO_2 will occur. Large quantities of excess steam and "O_2-starved" conditions are necessary for the formation of elemental sulfur. The thermodynamic analysis was carried out by "mixing" one mole of sulfided sorbent with one mole of O_2 and one mole of H_2O, and evaluating the equilibrium composition as a function of temperature and pressure. While these conditions do not represent actual regeneration conditions, they provide a valid method to compare the performance of potential sorbents.

All sulfided sorbents should react, at least to some extent, in the O_2-H_2O atmosphere. However, effectively no elemental sulfur can be formed from either MoS_2 or ZnS. A small amount of elemental sulfur can be formed during MnS regeneration, and a somewhat larger amount with FeS. Once again, regeneration of SnS and Ce_2O_2S are favored, and the quantities of elemental sulfur which can be formed are quite significant.

Table 7 summarizes results for the regeneration of Ce_2O_2S and FeS. Complete regeneration of Ce_2O_2S to CeO_2 at temperatures above the sulfate decomposition temperature is favored. Large amounts of elemental sulfur can be formed and care must be taken to avoid elemental sulfur condensation at conditions of low temperature and high pressure. Appreciable quantities of reduced sulfur (H_2S) are formed by the reaction with H_2O. Elemental sulfur formation is favored by low temperature and low pressure (assuming that sulfate formation conditions are avoided), and the proportions of both oxidized (SO_2) and reduced (H_2S) sulfur products increase with increasing temperature and pressure.

Formation of iron sulfate is not favored at any of the conditions shown in Table 7. However, the temperature should be sufficiently high to prevent FeS_2 formation. Fe_3O_4 is the stable oxide product at all conditions shown, but complete regeneration cannot be achieved; between 33% and 48% of the sulfur remains in the solid phase. The vast majority of sulfur in the equilibrium gas is in oxidized form (SO_2) with relatively small proportions of elemental and reduced (H_2S) sulfur. Elemental sulfur formation is the maximum at high temperature and low pressure.

The behavior of SnS is again qualitatively similar to Ce_2O_2S although $SnSO_4$ is somewhat more stable that $Ce_2(SO_4)_3$, and higher regeneration temperatures are required if complete regeneration is to be achieved. In addition, formation of SnS_2 and Sn_2S_3 is favored at certain conditions, and significant quantities of gaseous SnS may be formed at high temperature.

Table 7. Regeneration of Ce_2O_2S(s) and FeS(s) by Partial Oxidation

A. Initial Conditions: 1 mol Ce_2O_2S, 1 mol O_2, and 1 mol H_2O

Temp., K	650	700	1100	750	850	1100
Press., atm	1	1	1	25	25	25
Condensed Phase Composition, mol fraction						
CeO_2(*s*)	0.99	1.00	1.00	0.81	1.00	1.00
$Ce_2(SO_4)_3$(*g*)	0.01	0.00	0.00	0.00	0.00	0.00
S(*l*)	0.00	0.00	0.00	0.19	0.00	0.00
Sulfur Distribution (as S), fraction						
Condensed	0.03	0.00	0.00	0.48	0.00	0.00
Gas	0.97	1.00	1.00	0.52	1.00	1.00
Sulfur Distribution Within Gas Phase, fraction						
Elemental	0.82	0.75	0.63	0.65	0.66	0.49
Oxidized	0.03	0.08	0.14	0.09	0.12	0.19
Reduced	0.15	0.17	0.23	0.26	0.22	0.33

B. Initial Conditions: 1 mol FeS, 1 mol O_2, and 1 mol H_2O

Temp., K	873	973	1173	873	973	1173
Press., atm	1	1	1	25	25	25
Condensed Phase Composition, mol fraction						
FeS	0.00	0.63	0.60	0.00	0.63	0.61
FeS_2	0.48	0.00	0.00	0.49	0.00	0.00
Fe_3O_4	0.52	0.37	0.40	0.51	0.37	0.39
Sulfur Distribution (as S), fraction						
Condensed	---	0.36	0.33	0.48	0.36	0.34
Gas	---	0.64	0.67	0.52	0.64	0.66
Sulfur Distribution Within Gas Phase, fraction						
Elemental	---	0.05	0.10	0.01	0.03	0.06
Oxidized	---	0.92	0.86	0.97	0.93	0.89
Reduced	---	0.03	0.04	0.02	0.05	0.05

2.2.2.3 Reaction With Steam

Since regeneration with steam is the reverse of the sulfidation reaction, it is obvious that sorbents such as ZnO having the greatest affinity for sulfur will be the least amenable to this regeneration concept. For this reason only the SnS and Ce_2O_2S systems were examined. The desired reactions are

$$SnS(s) + 2\,H_2O(g) \rightarrow SnO_2(s) + H_2S(g) + H_2(g) \quad (7)$$

$$Ce_2O_2S(s) + 2\,H_2O(g) \rightarrow 2\,CeO_2(s) + H_2S(g) + H_2(g) \quad (8)$$

The fact that both reactions produce H_2 as well as H_2S would require an additional separation step for H_2 removal.

The thermodynamic analysis showed that these reactions should proceed as written with no appreciable formation of by-products. The key parameter was found to be the steam-to-sorbent ratio. While only two moles of steam per mole of sorbent are required by stoichiometry, thermodynamic limitations require the use of excess steam if regeneration is to be complete. Figure 1 shows the minimum steam-to-sorbent ratio required for complete regeneration of both SnS and Ce_2O_2S as a function of temperature at 15 atm. Both reactions are essentially independent of pressure since there is no change in the number of gas phase moles. The quantity of steam required for SnS regeneration is relatively independent of temperature at a ratio of about 22 to 1. Ce_2O_2S is more amenable to reaction with steam and the minimum steam requirement increases from about 3 moles per mole Ce_2O_2S at 650K to 9 moles per mole Ce_2O_2S at 1100K. At the higher temperatures, trace quantities of SnS(g), SO_2, and elemental sulfur may be formed during SnS regeneration. No by-products are favored during regeneration of Ce_2O_2S except at temperatures above 1050 K where trace quantities of elemental sulfur may be formed. There was no indication of the formation of volatile cerium compounds at even the maximum temperature considered.

2.2.3. Conclusions

Thermodynamic analysis of the three regeneration concepts showed clearly that sorbents having the greatest affinity for H_2S during sulfidation would be the most difficult to regenerate with elemental sulfur as a direct product. For practical purposes, elemental sulfur cannot be produced during the regeneration of ZnS, MnS, and MoS_2. Iron-based sorbents are somewhat less effective for H_2S removal, but are somewhat more amenable to elemental sulfur production. The most promising concept appears to be partial oxidation in which FeS is regenerated in a steam-oxygen atmosphere containing a large H_2O-to-O_2 ratio. Several simultaneous reactions would occur and the formation of significant quantities of elemental sulfur would be governed by kinetics instead of thermodynamics. The feasibility of kinetically controlled partial oxidation regeneration of FeS is supported by literature reports (Joshi et al., 1979; Grindley and Steinfield, 1981) indicating that complete regeneration is possible with as much as 70% of the sulfur liberated in elemental form. Direct regeneration of FeS with SO_2 to produce elemental sulfur or with steam to product H_2S is technically feasible although large quantities of either SO_2 or steam

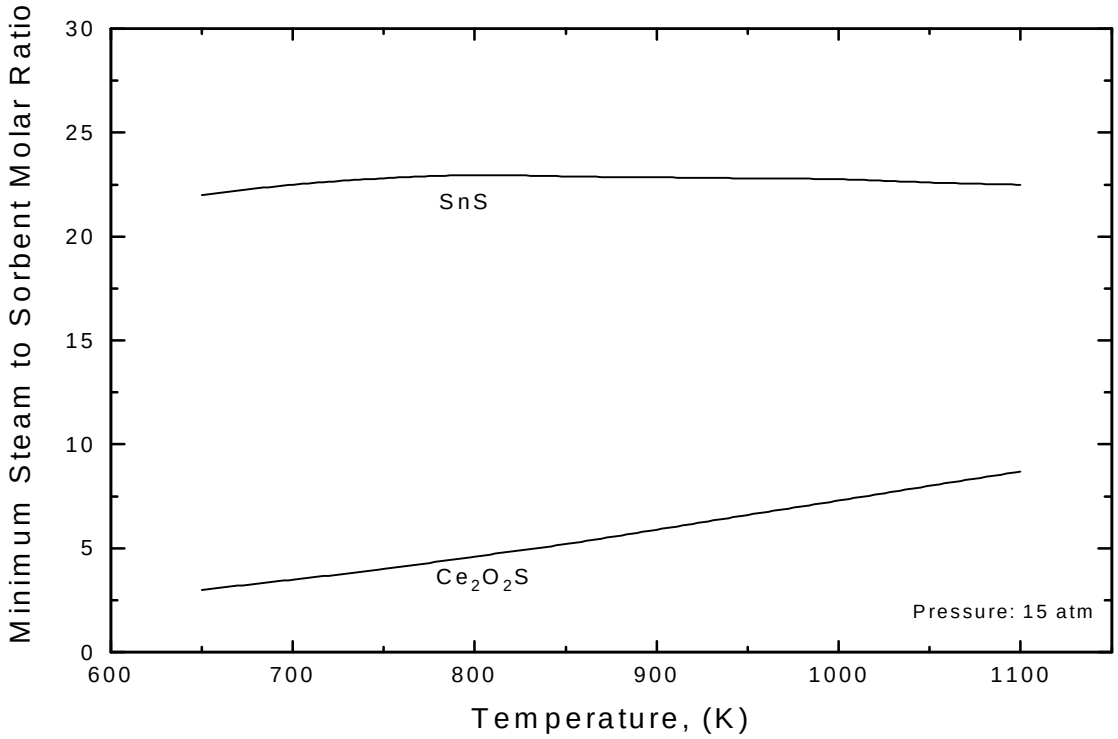

Figure 1. Minimum Ratio of Steam to Sulfided Sorbent Required for Complete Regeneration of SnS and Ce_2O_2S.

would be required. The low concentration of product (either elemental sulfur or H_2S) coupled with energy requirements for condensation and recycle gas reheat are felt to be prohibitive.

The thermodynamic properties of both SnS and Ce_2O_2S make these systems uniquely suited to elemental sulfur production during regeneration. They are, however, not as efficient for H_2S removal. At desulfurization conditions of interest, i.e., outside the carbon deposition region and at temperatures and pressures where formation of volatile or molten metal species is not favored, the H_2S removal capability of both is in the 85% to 90% range. Although the general thermodynamic characteristics of SnS and Ce_2O_2S are similar with respect to elemental sulfur production, there are significant differences in their properties.

The condensed phase products of SnS regeneration are more complex. Either SnS_2 or Sn_2S_3 may be produced from SnS under appropriate conditions. $SnSO_4$ is moderately stable and high temperatures are required to prevent its formation, particularly at high pressure. The reduction of SnO_2 to liquid metallic Sn may occur in coal gas having sufficiently high reducing strength. Finally, the sulfided product, SnS, may volatilize at appropriate conditions, a potential problem in both the sulfidation and regeneration cycles. Avoiding all of the above problems may leave only a small window, or no window at all, at which the tin sorbent can operate.

In contrast, the condensed phase of the cerium system is less complex. Ce_2O_2S is not volatile and there is no danger of reducing CeO_2 to the metal. Indeed, the sulfidation potential of CeO_2 improves with increasing temperature and in more highly reducing coal gas. The

permissible operating window for cerium sulfidation and regeneration is larger than the operating window of the tin system. The drawbacks of cerium are its limited sulfidation capability, relatively low theoretical capacity of 0.093 g S per gram of sorbent, and its availability and cost. However, no other sorbent system approaches cerium in terms of the potential for producing elemental sulfur during regeneration.

A two-stage desulfurization process such as shown in Figure 2 may be required to reduce the H_2S concentration to the sub-20 ppmv IGCC target level. The primary reactor containing CeO_2 would be used for bulk sulfur removal. This would be followed by a polishing reactor containing zinc-based sorbent for final H_2S removal. Regeneration of the sulfided zinc sorbent in the polishing reactor would be accomplished in the traditional manner using dilute O_2, and the product gas containing dilute SO_2 would be recycled to the gasifier. Regeneration of Ce_2O_2S would use one of the previously described concepts, most probably reaction with SO_2. Elemental sulfur would be condensed from the regeneration product and excess SO_2 would be reheated and recycled. The relatively small quantities of SO_2 needed and the large elemental sulfur concentrations in the product gas would reduce the energy demand and make this concept feasible.

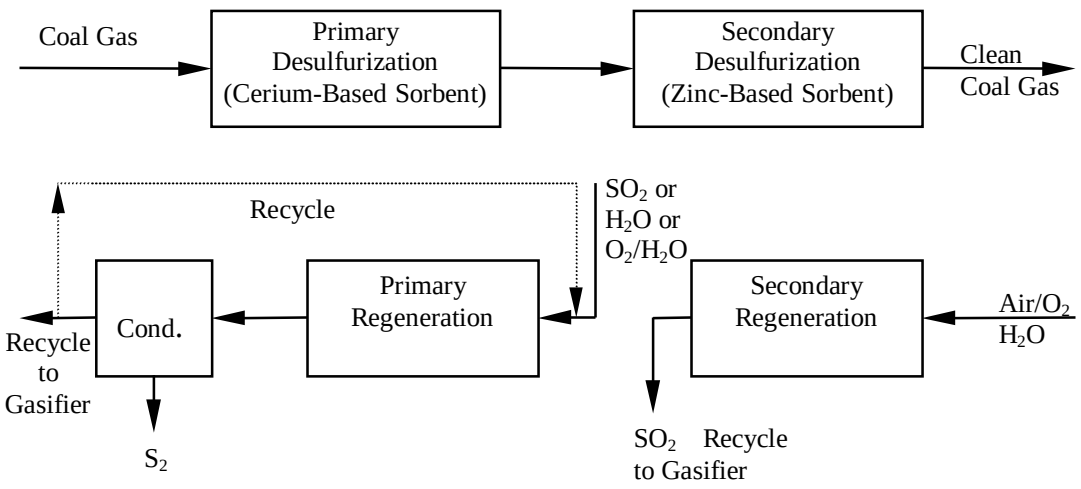

Figure 2. Two-Stage Desulfurization-Regeneration Concept.

As a result of the thermodynamic analysis, two systems were selected for experimental study during the exploratory phase of the research. The regeneration of FeS using the partial oxidation concept was selected based on favorable results in the literature and "feasible" thermodynamics. The regeneration of Ce_2O_2S using the reaction with SO_2 was selected based on the extremely favorable thermodynamics.

Chapter 3 describes the experimental apparatus used during the study while results from the FeS regeneration study are presented in Chapter 4. The FeS results have been described in detail in a previous topical report (Lopez et al., 1997) and only key results are presented in Chapter 4. Detailed results of the cerium studies are presented in Chapters 5 through 9.

CHAPTER 3. EXPERIMENTAL APPARATUS

Many of the experimental tests on the regeneration of FeS and almost all of the tests using cerium sorbent utilized a fixed-bed reactor. The progress of the reaction in these tests was followed by analyzing the composition of the product gas as a function of time. In addition, both atmospheric pressure and high-pressure electrobalance reactors were used to examine the regeneration of FeS and the reduction of CeO_2 to the sub-stoichiometric oxide CeO_n. The progress of the reaction in electrobalance tests was followed by monitoring the weight of the solid as a function of time.

A description of the reactor systems and procedure is presented in this chapter. Presentation and discussion of experimental results begins in Chapter 4. A more detailed description of the apparatus and procedure has been presented in an earlier topical report (Lopez et al., 1997).

3.1. Electrobalance Reactor

A schematic of the high-pressure electrobalance reactor system is shown in Figure 3. The housing and reactor hangdown tube were 316 stainless steel capable of operating at 1500 psi and 600°C. The inner surface of the hangdown tube was alonized to minimize interaction between H_2S and metal. The solid was held in a platinum pan and suspended from the balance mechanism with a nichrome wire.

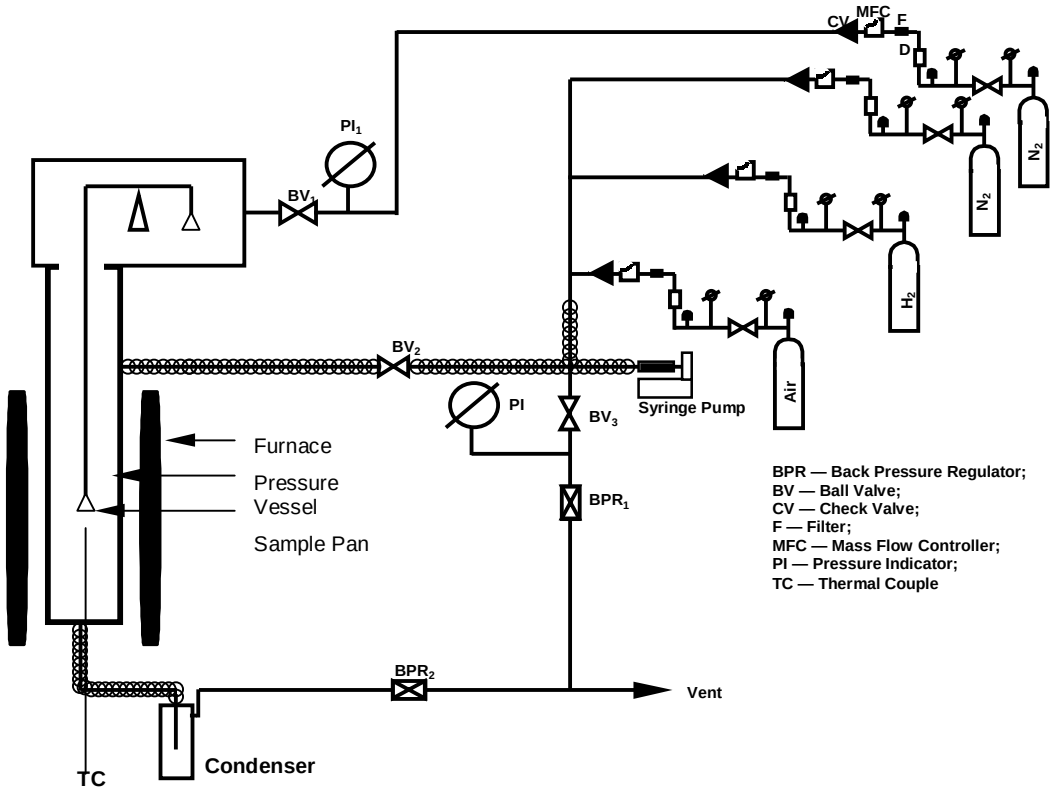

Figure 3. High Pressure Electrobalance Schematic

Ultra high purity (UHP) N_2 was fed through the electrobalance housing to prevent diffusion of reactive gases into the balance mechanism. Additional UHP N_2 and reactive gases were fed through an opening in the side of the hangdown tube. Combined gases flowed downward over the solid reactant. Gas flow rates were controlled using high-pressure mass flow controllers. Steam was generated from water fed from a high-pressure syringe pump; the feed line was heat traced to vaporize the water and preheat the feed gas. Valves in the side-arm permitted flow rates to be established and diverted to vent while desired reaction conditions were established in inert N_2. Reactor product gases passed through a condenser and were vented through a backpressure regulator.

The raw data from the electrobalance are affected by aerodynamic drag and because of a time delay between switching the side-arm valves and reactive gases contacting the sorbent. Delay time corrections based on system volume between the side-arm valve and the sorbent, temperature, pressure, and gas flow rate were calculated on the basis of plug flow and applied to the raw data. Aerodynamic drag corrections as a function of temperature, pressure, and flow rate were experimentally determined and also applied to the raw data.

The atmospheric pressure electrobalance functioned in the same way. The housing and hangdown tube were of glass and quartz, respectively, so that pressure was limited to one atmosphere. Gas flow was controlled using needle valves and calibrated rotameters instead of mass flow controllers.

3.2. Fixed-Bed Reactor (FeS Regeneration)

A diagram of the fixed-bed reactor system used in the FeS regeneration study is shown in Figure 4. The gas flow arrangement was similar to that used in the electrobalance reactor. Air and N_2 were obtained from high-pressure cylinders and flow rates were controlled using high pressure mass flow controllers. Liquid water was fed using a high-pressure syringe pump and feed lines were heat traced to insure vaporization and to preheat the feed gases. N_2, O_2, and steam rates could be established and directed to vent while inert N_2 flowed through the reactor as temperature and pressure were being adjusted. Reactive gases were fed to the reactor by switching valve positions in the feed gas line. The feed gases entered near the top of the reactor and flowed downward through the sorbent bed.

The sorbent was contained in an Alonized stainless steel insert within the pressure vessel. Sorbent was supported by a layer of quartz wool which was placed on top of a porous quartz disc. High temperature o-rings at the top of the insert provided a seal between the insert and pressure vessel and prevented gas bypassing.

Product gas exited from the bottom of the reactor and entered the analytical system shown in Figure 5. Exit lines were maintained at high temperature to prevent elemental sulfur condensation. The product gas was split into two streams, with one portion flowing through a capillary flow restrictor into an oxidation chamber at 1050°C where all sulfur compounds were oxidized to SO_2. Excess H_2O was removed using a membrane dryer and total sulfur concentration was determined using a calibrated UV-Fluorescence detector. Gas flow through the upper leg of the analytical system was determined by the reactor pressure and the resistance

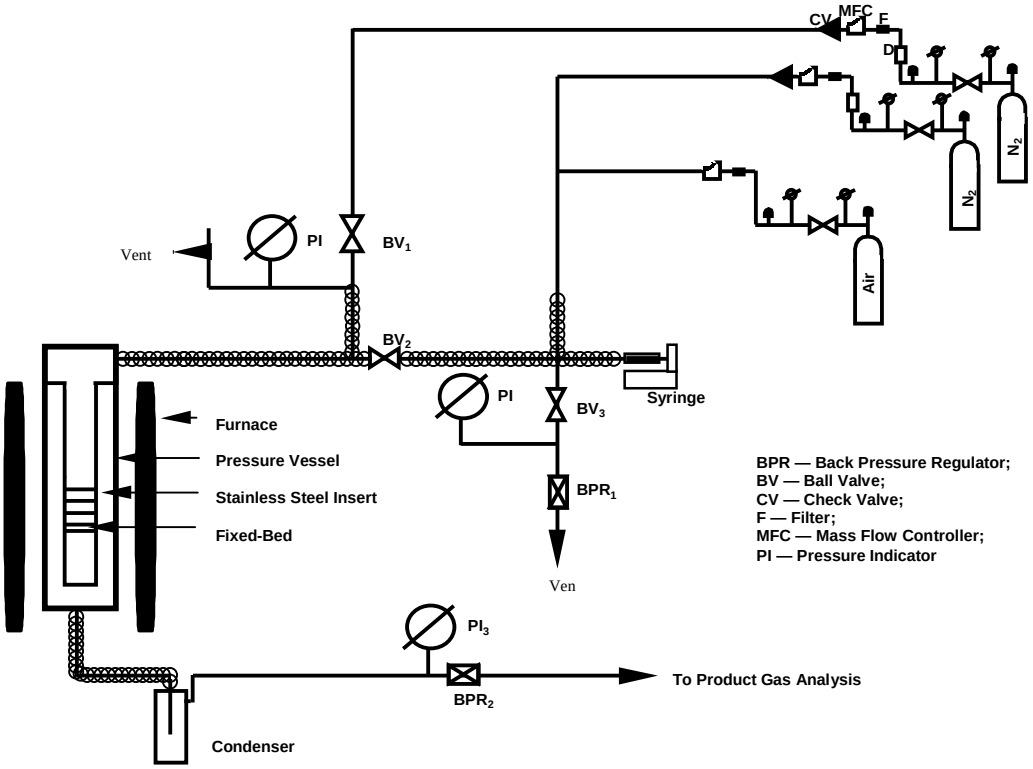

Figure 4. Fixed-Bed Reactor Schematic (FeS Regeneration)

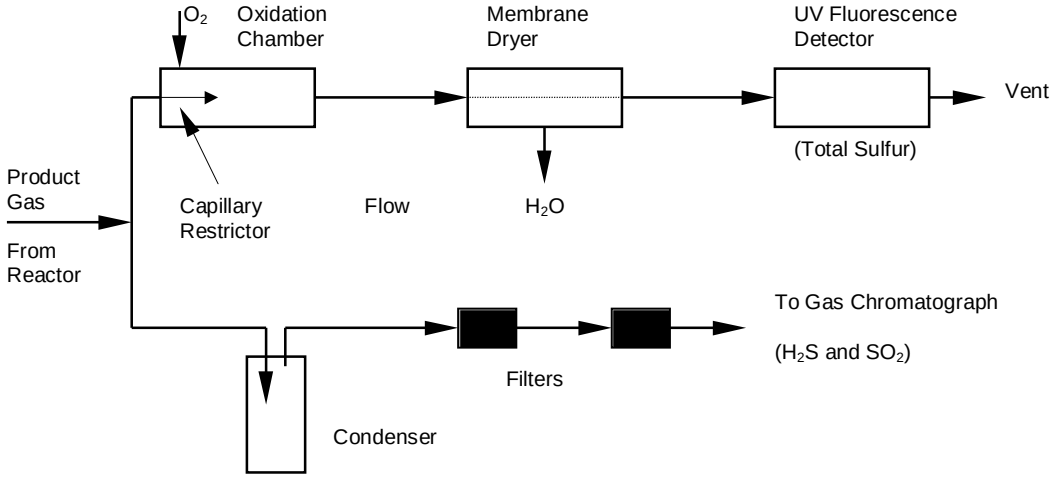

Figure 5. Product Gas Analysis System (FeS Regeneration)

of the capillary restrictor. This portion of the system was troubled by varying capillary resistance due to particulate carryover from the reactor; frequent recalibration was required.

The remainder of the product gas entered the bottom leg of the analytical system and passed through a condenser and series of filters where elemental sulfur was separated from the permanent gases. H_2S and SO_2 concentrations were then determined by gas chromatography using a thermal conductivity detector. Although the technique involved the determination of elemental sulfur by difference (total sulfur - H_2S - SO_2), it provided reasonable accuracy when the concentration of elemental sulfur was sufficiently large.

3.3. Fixed-Bed Reactor (Cerium Sorbent Studies)

The fixed-bed reactor system used in the cerium sorbent studies is shown in Figure 6. The overall system was similar to that used to study FeS regeneration (Figure 4). The gas feed system was modified to handle H_2, H_2S, and SO_2, as well as N_2 and steam. These flow rates were controlled by mass flow controllers. Product gas exited from the bottom of the reactor, and passed through a condenser, a sequence of filters, and a back pressure regulator to the gas chromatograph for analysis. The exit line between the reactor and condenser was heat traced to minimize condensation of elemental sulfur upstream of the condenser.

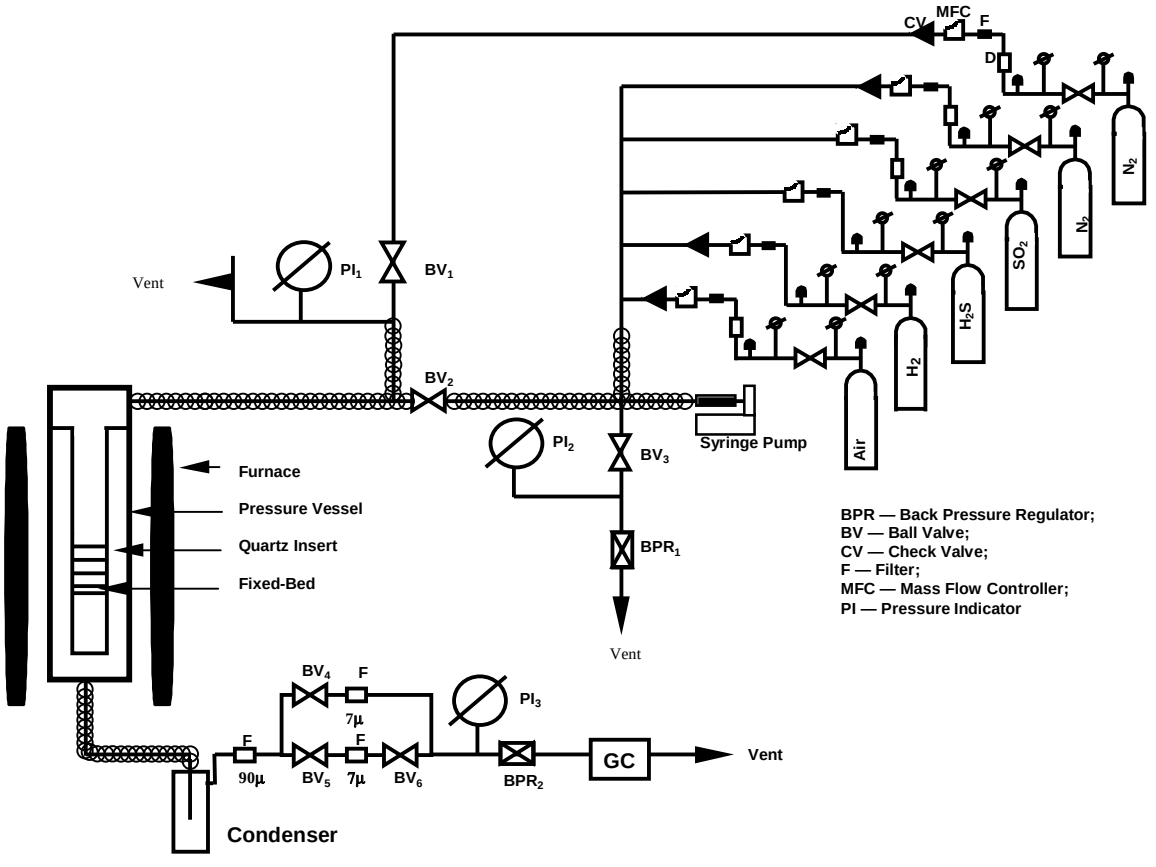

Figure 6. Fixed-Bed Reactor System Used in Cerium Tests

Cerium sorbent was contained within the reactor pressure vessel in a quartz (instead of stainless steel) insert to reduce contact between H_2S and stainless steel during sulfidation tests. In spite of the fact that the stainless steel insert had been Alonized, reaction between the insert walls and H_2S occurred. A quartz liner was also added inside the pressure vessel to further minimize contact between H_2S and high temperature steel surfaces.

The primary operational problem was caused by elemental sulfur condensing and plugging the tubing and filters between the reactor and chromatograph. The condenser was loosely packed with glass wool to improve heat transfer characteristics and provide increased surface area to promote condensation. A complex arrangement of series and parallel filters gradually evolved as successive problem areas were identified and corrected. While sulfur deposition outside the condenser was never eliminated, it was reduced to a manageable level.

Product gas analysis during the early stages of the cerium tests was performed using gas chromatography with a thermal conductivity detector (TCD). The progress of the sulfidation reaction was followed by monitoring the H_2S content of the product gas as a function of time. In a similar fashion, the regeneration reaction was followed by measuring the SO_2 content of the product gas as a function of time. Since both reactions were stoichiometricially "clean," it was not necessary to use the total sulfur analyzer, and the gas analysis was greatly simplified compared to the FeS partial oxidation regeneration tests.

The TCD was adequate for monitoring SO_2 concentrations during regeneration. However, the H_2S detection limit of about 100 ppmv did not provide the sensitivity needed for monitoring H_2S pre-breakthrough concentrations during some of the sulfidation tests. A flame photometric detector (FPD) which provided the capability of detecting H_2S to about 1 ppmv was subsequently installed in the chromatograph. The FPD was installed in parallel with the TCD, and the product gas sample could be directed to either detector using a three-way valve. Thereafter, the TCD was used for regeneration tests and the FPD for most sulfidation tests. However, the maximum H_2S concentration for the FPD was limited to about 100 ppmv so that only pre-breakthrough concentrations could be monitored. In order to follow the H_2S concentration throughout a sulfidation run, it was necessary to switch from the FPD to the TCD during the run. Switching produced a data gap lasting approximately 30 minutes because of the time required for the TCD to equilibrate after being turned on. Consequently, in most tests only one detector was used. The FPD was used when minimum pre-breakthrough concentrations were of primary interest while the TCD was used if establishing the overall breakthrough curve was primary interest.

Further changes in the reactor system and operating procedure were required to reliably measure H_2S concentration at the sub-10 ppmv level. The reactor had to be thoroughly cleaned between regeneration and sulfidation tests. The reaction between H_2 in the sulfidation gas and elemental sulfur deposited downstream of the sorbent bed during the previous regeneration test produced H_2S in sufficient quantity to overwhelm the H_2S emerging from the sorbent bed.

Contact between H_2S and steel surfaces had to be further reduced to obtain reliable measurements of sub-10 ppmv H_2S concentrations. Teflon-lined stainless steel tubing was used from the pressure vessel exit. The condenser and all but one filter were removed from the

product line and all tubing downstream of the backpressure regulator was teflon. In the final system only four stainless steel parts — a nipple at the bottom the pressure vessel, one filter, the backpressure regulator, and the chromatograph automatic sampling valve — contacted the sulfidation product gas. Only the nipple at the bottom the pressure vessel was at high temperature.

CHAPTER 4: FeS PARTIAL OXIDATION REGENERATION STUDIES

We propose that four simultaneous reactions are important in the partial oxidation regeneration of FeS.

$$2\ FeS(s) + 3.5\ O_2(g) \rightarrow Fe_2O_3(s) + 2\ SO_2(g) \quad (9)$$

$$3\ FeS(s) + 4\ H_2O(g) \rightarrow Fe_3O_4(s) + 3H_2S(g) + H_2(g) \quad (10)$$

$$2\ H_2S(g) + SO_2(g) \rightarrow 2\ H_2O(g) + 1.5\ S_2(g) \quad (11)$$

$$2\ Fe_3O_4(s) + 0.5O_2(g) \rightarrow 3\ Fe_2O_3(s) \quad (12)$$

The first reaction represents the traditional regeneration method with fully oxidized Fe_2O_3 and SO_2 as the products. Regeneration with steam liberates H_2S (and H_2) and produces Fe_3O_4. At high temperature in the presence of O_2 the Fe_3O_4 will be quickly oxidized to Fe_2O_3. Formation of elemental sulfur is attributed to the gas phase reaction between SO_2 and H_2S, the Claus reaction. The elemental sulfur product is represented as S_2 for convenience. In reality, varying quantities of gaseous sulfur allotropes S_n with $1 \leq n \leq 8$, may be formed, depending on temperature and pressure. With this four reaction model as background, the objective of the study was to determine reaction conditions most favorable for elemental sulfur formation.

4.1 FeS Properties

FeS from Johnson Mathey Co. was used in the electrobalance tests. The composition and selected properties, as supplied by Johnson Mathey and measured at LSU are presented in the top section of Table 8. The FeS used in the fixed-bed test was from Strem Chemicals; composition and selected properties are found in the bottom section of Table 8. The FeS used in the fixed-bed tests was physically mixed with inert Al_2O_3 to minimize sintering; selected properties of the Al_2O_3 are also found in Table 8.

4.2 Electrobalance Test Results

The electrobalance reactor was used to study the individual reactions of FeS with O_2 and with H_2O over temperature and pressure ranges of 600 to 800°C and 1 to 15 atm, respectively. The feed gas contained from 0.5 to 3.0% O_2 in N_2 or from 10 to 40% H_2O in N_2. A limited number of tests were conducted using O_2-H_2O-N_2 mixtures with the H_2O content fixed at 30% and the O_2 content varied from 0.05 to 0.5%.

Experimental time-fractional conversion results including corrections for delay time and aerodynamic drag are shown in Figure 7 for a series of O_2 regeneration tests at 700°C, 5 atm, and 800 sccm total flow rate. Normalized sorbent mass, M/M_0, where M_0 is the initial mass, is plotted versus time. The horizontal dashed line at $M/M_0 = 0.909$ represents the theoretical value corresponding to the complete regeneration of pure FeS to Fe_2O_3. The experimental final values of M/M_0 in Figure 7 range from 0.900 to 0.902. The fact that final values of M/M_0 were

Table 8. FeS Composition and Properties

Electroblance Tests	
FeS Source	Johnson Matthey
Composition (Mass%)	
Fe	61.78
Al	<0.01
Ca	<0.01
Co	<0.01
Cu	0.02
Mg	<0.01
Mn	<0.01
Ni	<0.01
Particle Size Range	<100 mesh
Specific Surface Area	5.3 m^2/g (Measured by LSU)

Fixed-Bed Tests	
FeS Source	Strem Chemicals
FeS Content	99.2 ± 0.1%
Particle Size Range	60 to 200 mesh
Al_2O_3 Source	Sigma Chemicals
Particle Size Range	800 to 200 mesh

generally less than theoretical is attributed to the sulfur content exceeding the stoichiometric level corresponding to FeS. The Figure 7 results show that the FeS-O_2 reaction is rapid at 700°C and is a strong function of O_2 concentration.

Time-conversion results showing the effects of temperature and pressure are found in Figures 8 and 9, respectively. In all cases, the final normalized masses are slightly below theoretical. The effect of temperature, Figure 8, at 5 atm using 1% O_2 at 800 sccm is relatively small. Between 11 and 12 minutes were required for M/M_0 to reach the theoretical value of 0.909 at 600°C while 7 to 8 minutes were required at 800°C. The effect of pressure, Figure 9, at 700°C, 1% O_2 and 800 sccm was surprising. A relatively small increase in rate was observed from 1 to 5 atm, but the rate at 15 atm was smaller than the 1 atm rate. One would expect the rate to increase with pressure since the O_2 concentration is proportional to pressure. The results shown in Figures 7, 8, and 9 were typical of results at other reaction conditions.

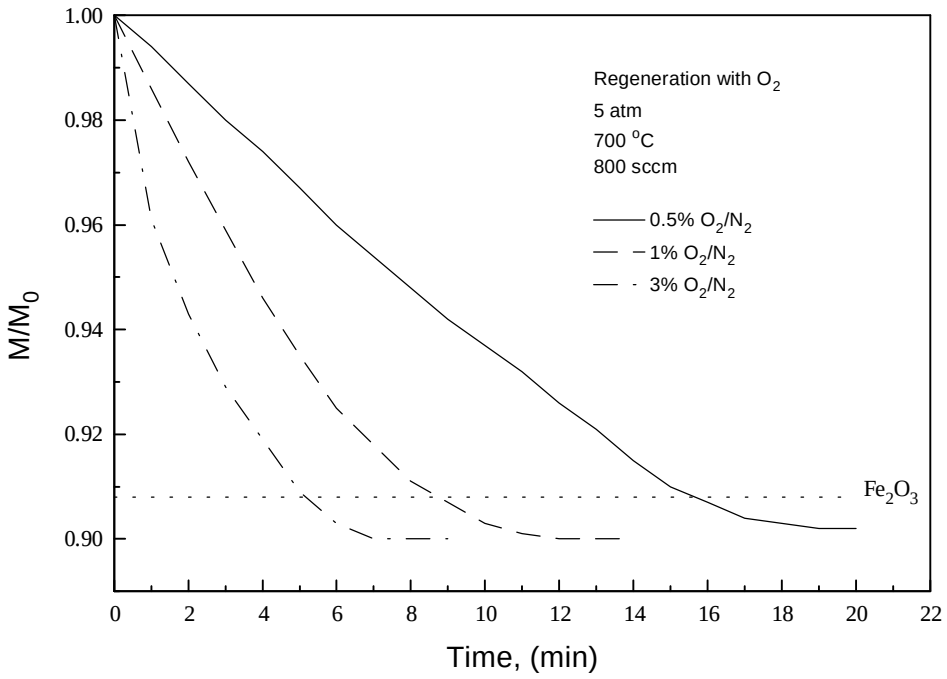

Figure 7. FeS Regeneration with O_2: The Effect of O_2 Concentration

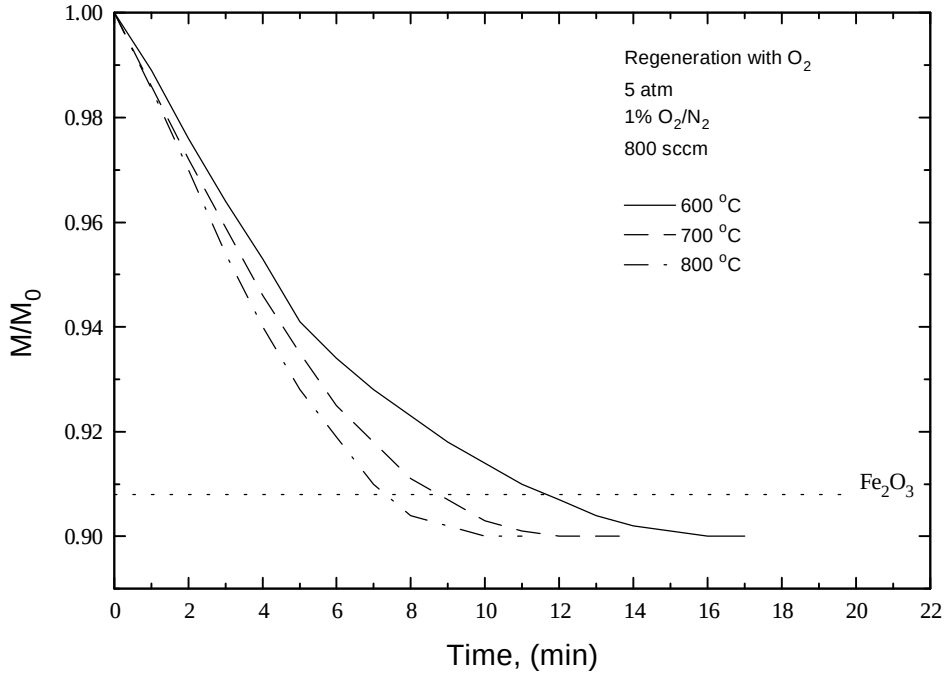

Figure 8. FeS Regeneration with O_2: The Effect of Temperature

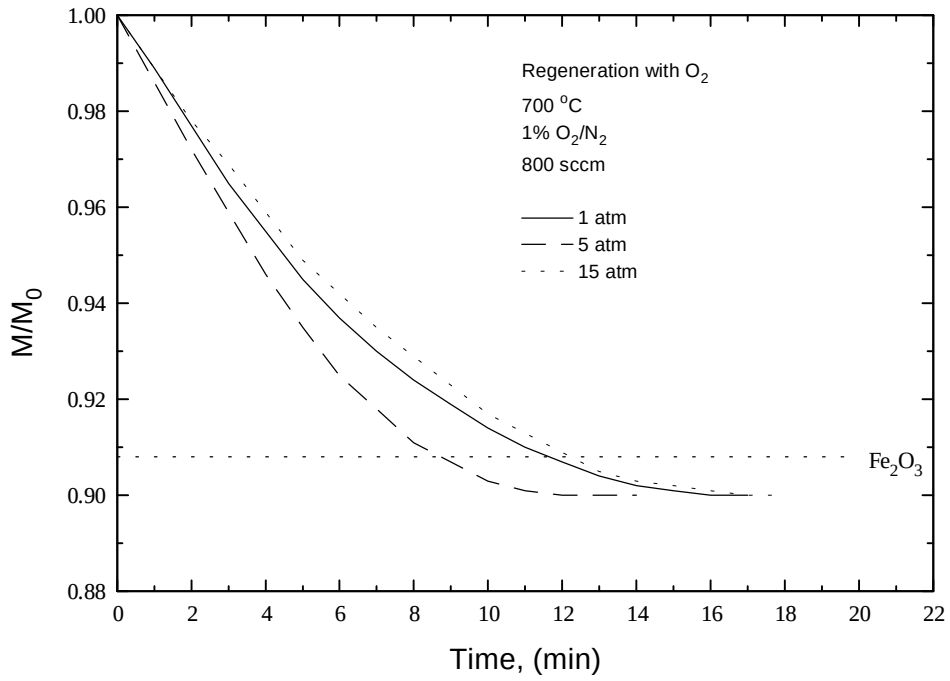

Figure 9. FeS Regeneration with O_2: The Effect of Pressure

Similar results for the FeS-H_2O reaction showing the effects of H_2O concentration, temperature, and pressure are shown in Figures 10, 11, and 12. The horizontal dashed line in these figures at $M/M_0 = 0.878$ corresponds to the stoichiometric value associated with complete conversion of pure FeS to Fe_3O_4. There was greater scatter in the final values of M/M_o with results both above and below the stoichiometric value.

The reaction rate was a strong function of H_2O concentration (Figure 10), a somewhat stronger function of temperature (Figure 11), and exhibited the same unexpected effect of pressure (Figure 12), with all comparisons based on the FeS-O_2 reaction. As expected, the FeS-O_2 reaction was must faster. For example, at 700°C and 5 atm, approximately 18 minutes were required for complete regeneration in 0.5% O_2 while almost 25 minutes were required in 40% H_2O at the same temperature and pressure.

A limited number of electrobalance tests were carried out using both O_2 and H_2O. The H_2O content was held constant at 30% while the O_2 was varied from 0.05 to 0.5% to produce H_2O to O_2 ratios ranging from 60 to 600. Normalized mass-time results as a function of O_2 content are shown in Figure 13. The final value of M/M_0 was slightly less than the stoichiometric value of Fe_2O_3 and was effectively equal to the value obtained in the FeS-O_2 tests, thus showing that any Fe_3O_4 formed by the FeS-H_2O reaction was subsequently oxidized to Fe_2O_3.

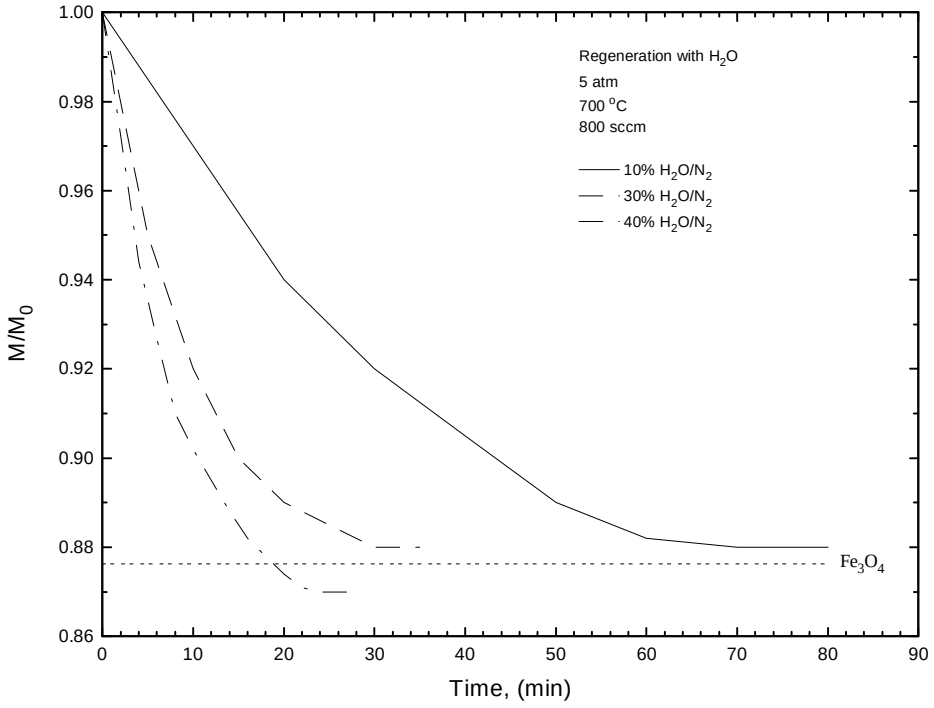

Figure 10. FeS Regeneration with H_2O: The Effect of H_2O Concentration

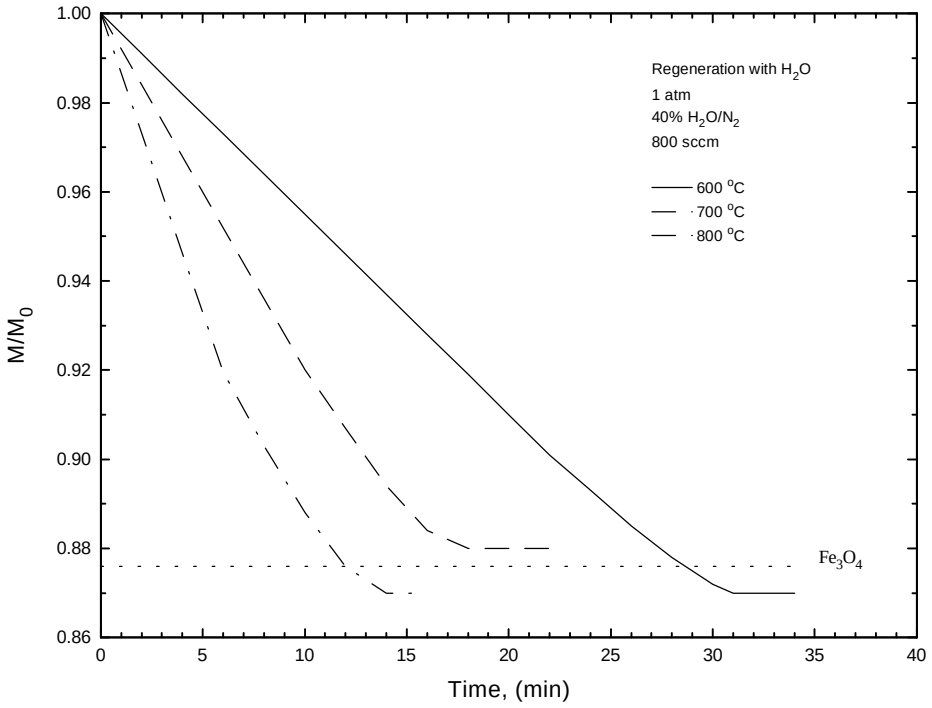

Figure 11. FeS Regeneration with H_2O: The Effect of Temperature

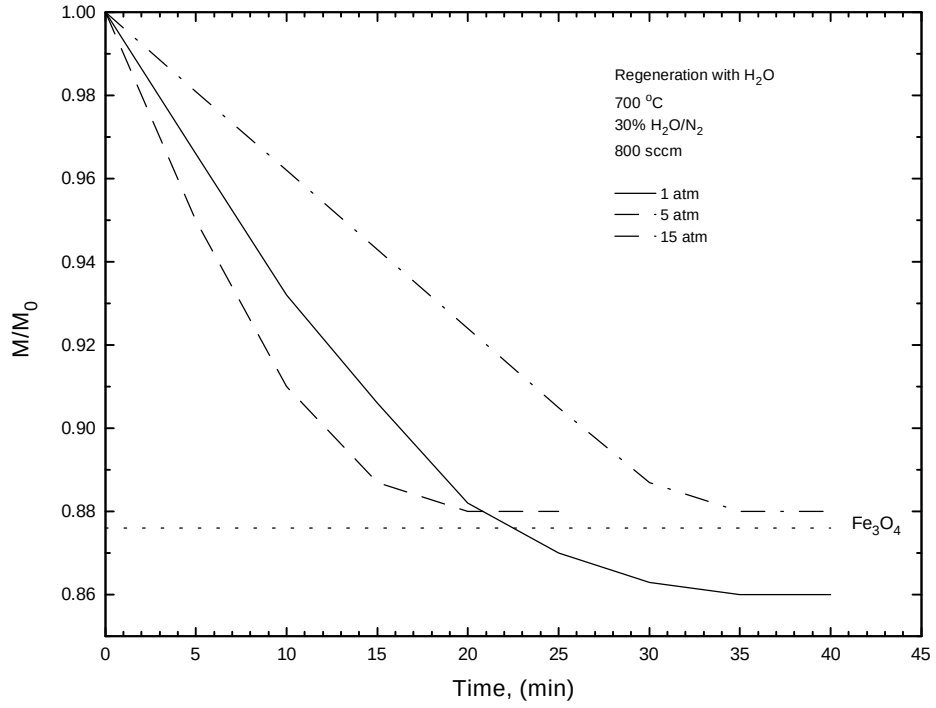

Figure 12. FeS Regeneration with H_2O: The Effect of Pressure

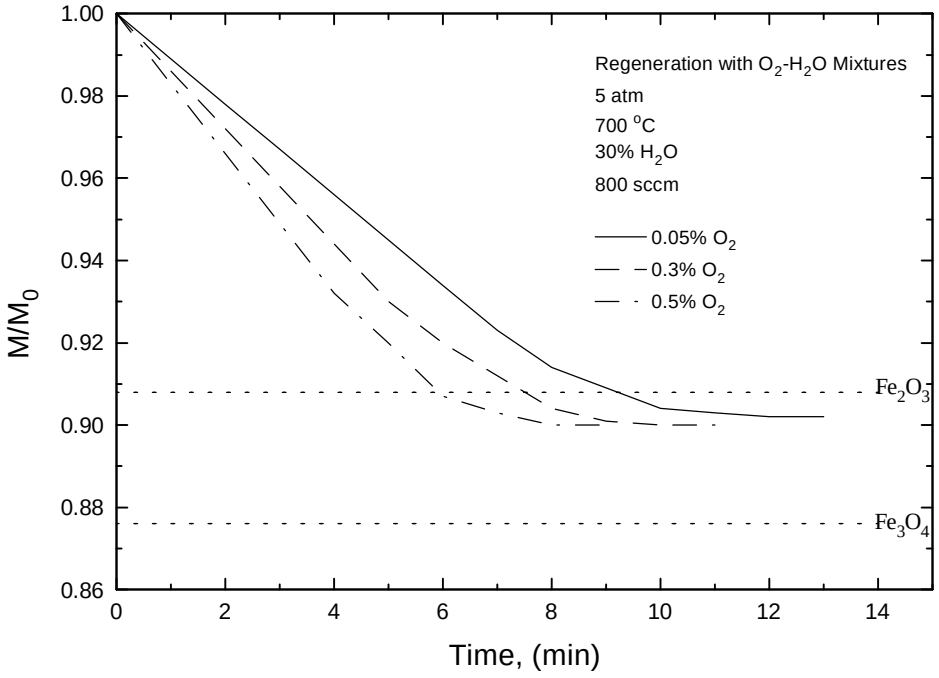

Figure 13. FeS Regeneration with O_2 and H_2O: The Effect of O_2 Concentration

The large H_2O/O_2 ratios were such that both the FeS-O_2 and FeS-H_2O reactions contributed significantly to the total reaction rate. For example, about 30 minutes were required for complete reaction using 30% H_2O and no O_2 (Figure 10), compared to 10 minutes for complete reaction when 0.05% O_2 was added to the same H_2O concentration (Figure 13). Similarly, the 18 minutes required for complete reaction in 0.5% O_2 (Figure 7) were reduced to 8 minutes when 30% H_2O was added (Figure 13). The effects of temperature and pressure for the combined FeS-O_2-H_2O reactions were qualitatively similar to the effects observed with the single reactions.

4.3 Fixed-Bed Reactor Test Results

Pressure was held constant at 4.4 atm in the fixed bed tests while temperature was varied between 550 and 700°C. The feed gas contained from 0 to 1.5% O_2, 0 to 52% H_2O, and balance N_2. When the feed gas contained both H_2O and O_2, the H_2O/O_2 ratio ranged from 6.0 to 200. Volumetric feed rate ranged from 300 to 600 sccm. Reaction conditions, in particular temperature and feed gas composition, were selected on the basis of the electrobalance test results.

With O_2 as the only reactive component in the feed gas, all sulfur should be liberated as SO_2. Figure 14 shows the mole fraction SO_2 in the product gas as a function of dimensionless time, t*. Dimensionless time is defined so that t* = 1 would correspond to complete regeneration of FeS and complete conversion of O_2 if the reaction occurred at an infinitely fast rate. After a brief delay, the SO_2 concentration increased to about 0.0085 mole fraction and was approximately constant until the reaction neared completion. The reaction was quite rapid as indicated by the steepness of the SO_2 concentration decrease near the end of the run and the facts that the "steady-state" SO_2 concentration was near the stoichiometric value corresponding to complete O_2 consumption (indicated by the dashed horizontal line) and that the reaction was almost complete at t* = 1.

With H_2O as the only reactive component in the feed gas, all sulfur was liberated as H_2S. This reaction was quite slow as shown in Figure 15. The steady-state H_2S concentration was only about 1.7% of stoichiometric, even thought the regeneration temperature was 100°C higher. Regeneration was only about 12% complete when the run was terminated after 8 dimensionless time steps.

When the regeneration feed gas contained both O_2 and H_2O, elemental sulfur was formed in the product gas. The amount of elemental sulfur depended on the relative quantities of SO_2 and H_2S, and the position within the sorbent bed where they were formed. The H_2O-to-O_2 ratio was the most important parameter in determining the amount of elemental sulfur with a large ratio resulting in large sulfur production.

Results of a run in which the feed gas contained H_2O and O_2 in a 80-to-1 ratio are shown in Figure 16 as a function of dimensional time. After a brief delay, both the total sulfur and H_2S concentrations increased rapidly with the total sulfur reaching a maximum of 0.0025 mole fraction after 0.9 hours and the H_2S maximum of 0.00065 mole fraction occurring after 1.7 hours. SO_2 concentration was effectively zero during the first hour and then gradually increased

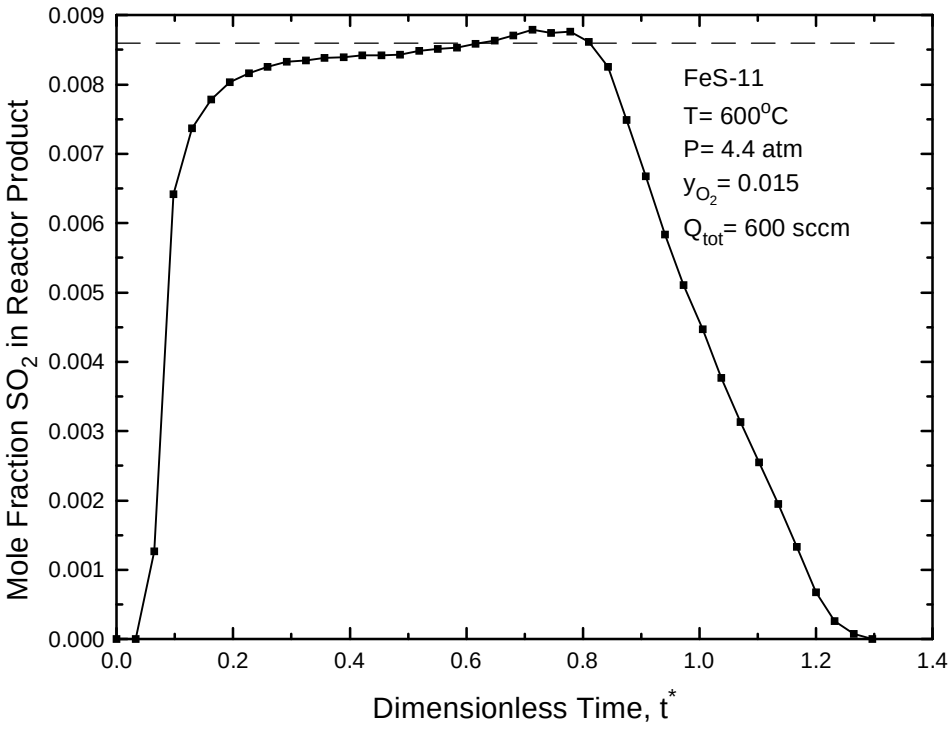

Figure 14. Fixed-Bed Reactor Response: FeS Regeneration with O_2, Run FeS-11

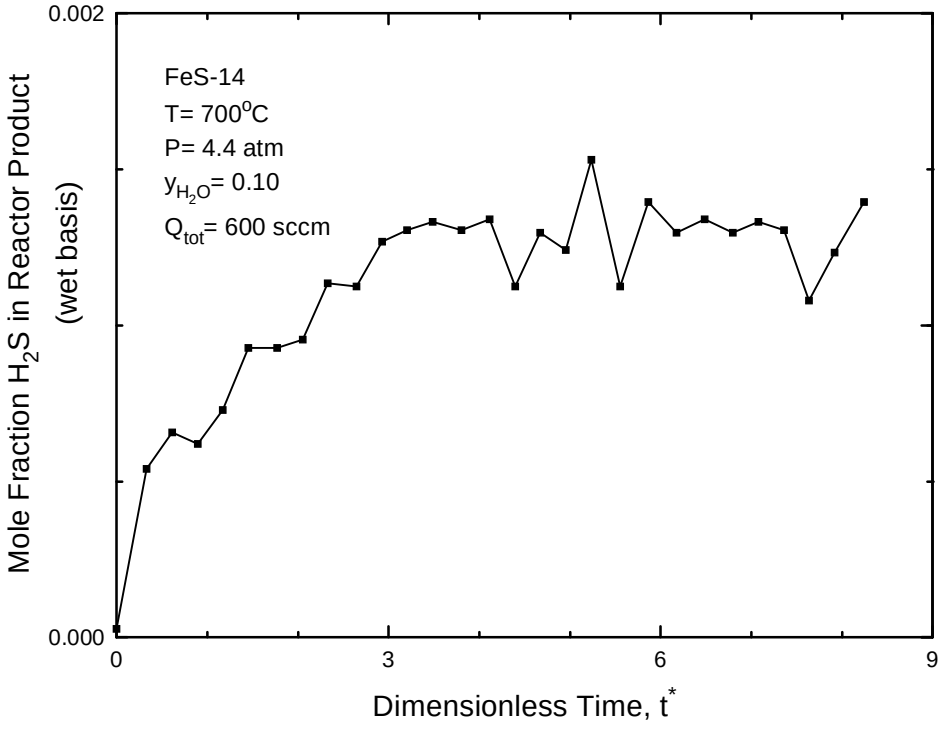

Figure 15. Fixed-Bed Reactor Response: FeS Regeneration with H_2O, Run FeS-14

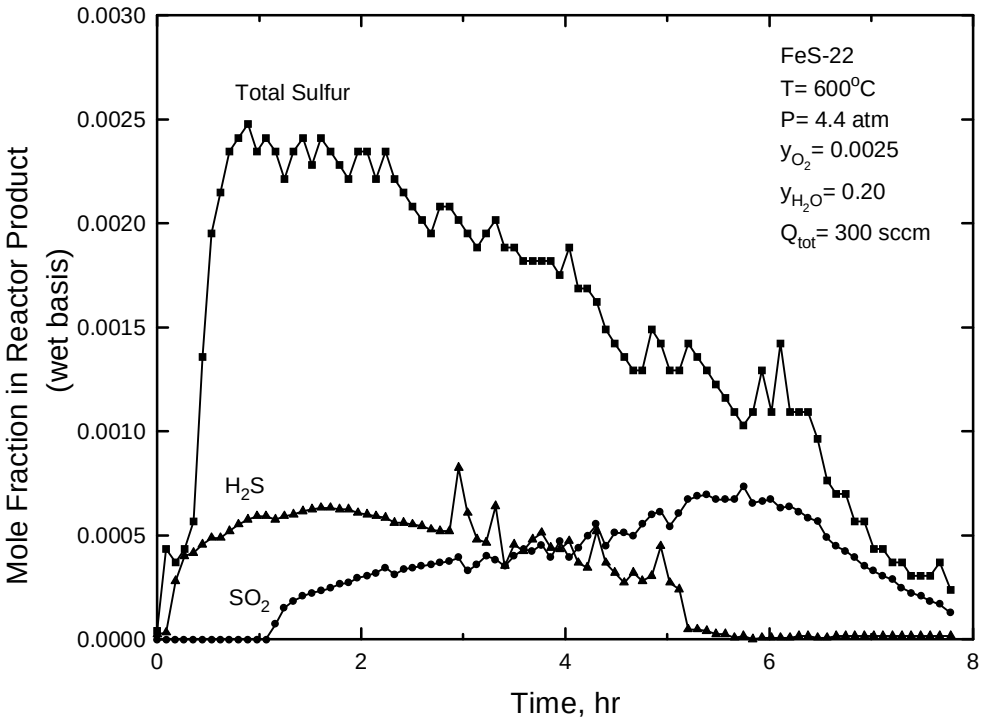

Figure 16. Fixed-Bed Reactor Response: FeS Regeneration with O_2 and H_2O, Run FeS-22

to a maximum of 0.00072 mole fraction after 6 hours. After reaching their maxima, all concentrations decreased gradually with the H_2S concentration approaching zero after 5.1 hours and the total sulfur and SO_2 concentrations simultaneously approaching zero after 8 hours.

The cumulative production of each sulfur species as a function of time was determined by numerical integration of the concentration-time data, with the cumulative amounts produced at the end of the run providing a check on the overall sulfur material balance. Results of the numerical integration of the Figure 16 data are shown in Figure 17. The production of H_2S, H_2S + SO_2, and total sulfur, all expressed as a fraction of the theoretical sulfur associated with the initial FeS charge, are plotted versus reaction time. The amount of H_2S produced increased gradually and accounted for 21% of the theoretical sulfur after 5.1 hours; no additional H_2S was produced after that time. The H_2S and H_2S + SO_2 curves coincided for the first hour when no SO_2 was produced. The curves diverged when SO_2 production began and the cumulative H_2S + SO_2 production was 45% of theoretical by the end of the run; this corresponds to cumulative SO_2 production of 24% of theoretical. The total sulfur material balance for this run was quite good as the cumulative production of total sulfur by the end of the run was 99% of theoretical. Thus, about 55% of the sulfur was liberated in elemental form.

The instantaneous selectivity to elemental sulfur is shown in Figure 18, with selectivity defined by

$$S(t) = \frac{ElementalSulfur}{TotalSulfur} = \frac{TotalSulfur - (SO_2 + H_2S)}{TotalSulfur} \qquad (13)$$

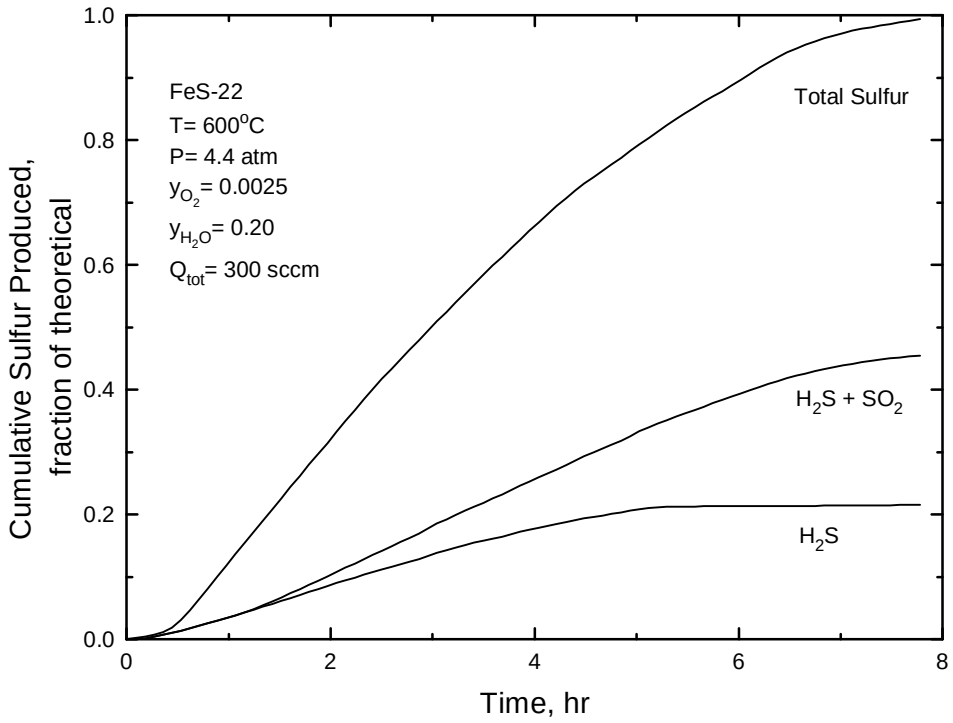

Figure 17. Cumulative Production of H_2S, ($H_2S + SO_2$), and Total Sulfur, Run FeS-22

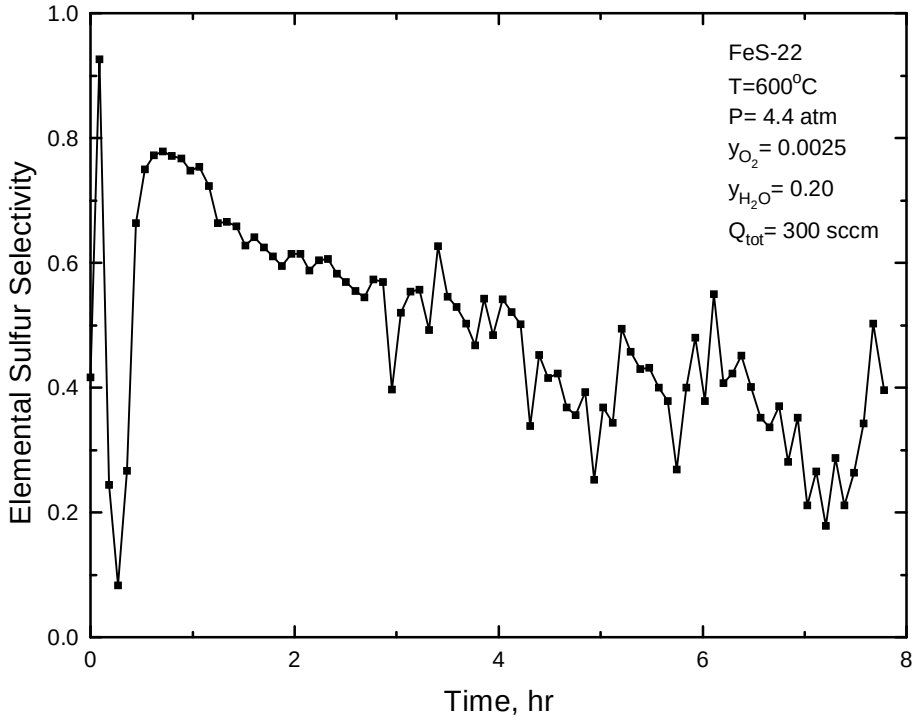

Figure 18. Instantaneous Selectivity to Elemental Sulfur, Run FeS-22

Although there is significant scatter in the data, particularly near the beginning and end of the run when (H_2S + SO_2) concentration was approximately equal to total sulfur concentration, there was a clear trend to the data. Near the beginning of the run about 80% of the sulfur was released in elemental form. This decreased more or less linearly to near 20% at the end of the run. The cumulative, or time average, selectivity was 55% as shown in Figure 18.

Results of a 100°C increase in regeneration temperature, with other regeneration parameters constant, are shown in Figure 19. Some aspects of the concentration-time curves in Figures 16 and 19 are similar. H_2S and total sulfur concentrations increased quickly while the SO_2 concentration remained near zero for the first hour. H_2S concentration approached zero after 5 hours while SO_2 and total sulfur concentrations simultaneously approached zero at the end of the run. However, the maximum SO_2 concentration was about 50% larger and occurred at an earlier time. Similarly the H_2S concentration maximum increased to about two-fold and also occurred at an earlier time. The increased concentrations and extended times meant that larger amounts of SO_2 and H_2S were produced, and, as a consequence, smaller amounts of elemental sulfur. The cumulative production of elemental sulfur obtained by numerically integrating the Figure 19 data was only about 40% of theoretical, compared to 55% of theoretical at 600°C.

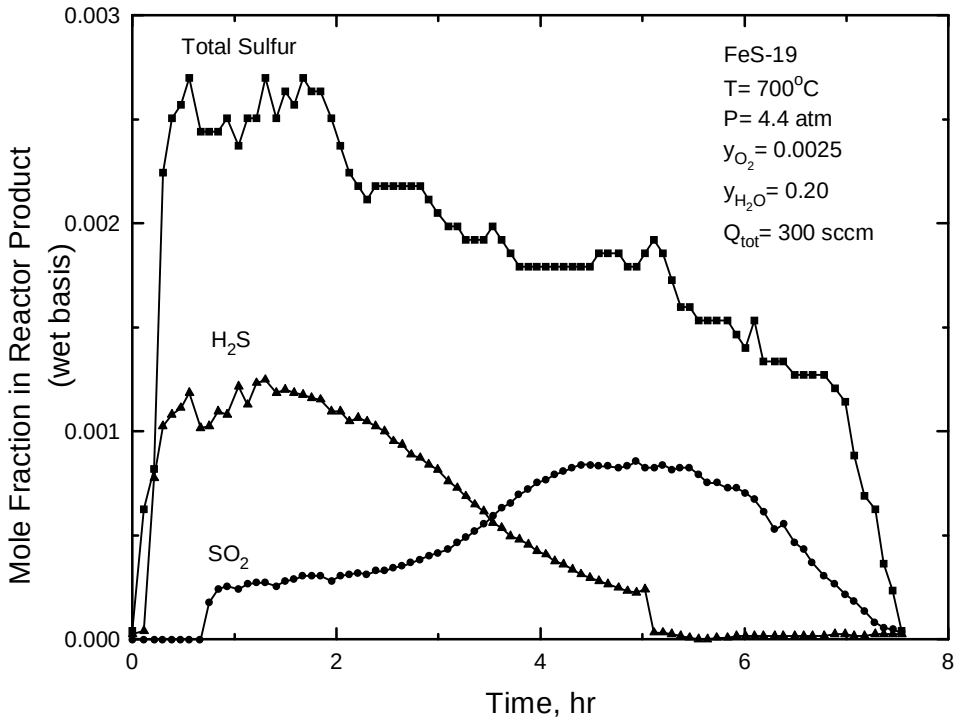

Figure 19. Fixed-Bed Reactor Response: FeS Regeneration With O_2 and H_2O: Run FeS-19

Varying the H_2O-to-O_2 feed ratio produced the largest effect on elemental sulfur production. This is seen from Figure 20 where concentration-time results from a run using a H_2O-O_2 ratio of 200 are presented. The cumulative elemental sulfur produced in this run was 75% of theoretical. When the H_2O to O_2 ratio was decreased to 6.7 (along with an increased temperature), very little elemental sulfur was formed as shown in Figure 21. Here the sum of the

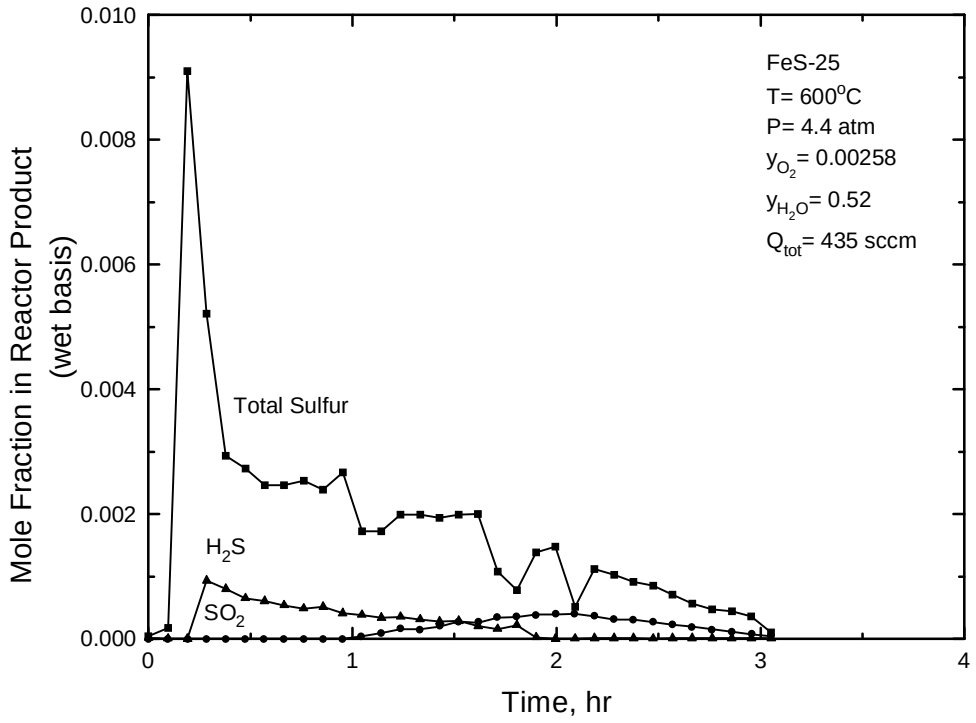

Figure 20. Fixed-Bed Reactor Response: FeS Regeneration with O_2 and H_2O, Run FeS-25

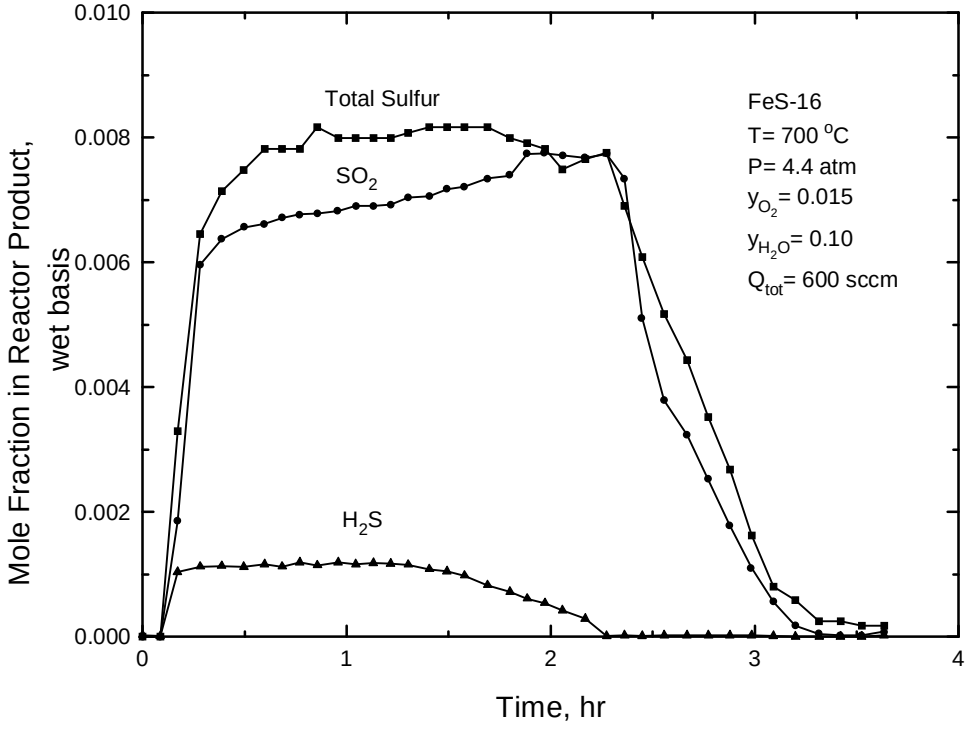

Figure 21. Fixed-Bed Reactor Response: FeS Regeneration with O_2 and H_2O, Run FeS-16

H_2S and SO_2 concentrations was approximately equal to the total sulfur concentration. Increasing the regeneration gas feed rate, which corresponds to decreasing the gas residence time in the sorbent bed, also had a moderately negative effect on elemental sulfur product.

4.4 Interpretation of the Fixed-Bed Results

The results of the fixed-bed FeS regeneration tests may be interpreted on the basis of reactions 9 through 12. Consider Figure 22a which shows proposed solid and gas concentration profiles within the sorbent bed during the early stages of the reaction. These profiles should correspond to a reaction time just less than 1 hour in Figure 16. The interface between solid FeS and Fe_2O_3 is quite steep because of the large rate of the FeS-O_2 reaction. A small amount of Fe_3O_4, represented by the almost horizontal line separating Fe_3O_4 and FeS is formed downstream of the Fe_2O_3-FeS interface as a result of the slow FeS-H_2O reaction. Fe_3O_4 exists only downstream of the FeS-Fe_2O_3 interface since it would be quickly oxidized to Fe_2O_3 whenever O_2 is present in the gas phase.

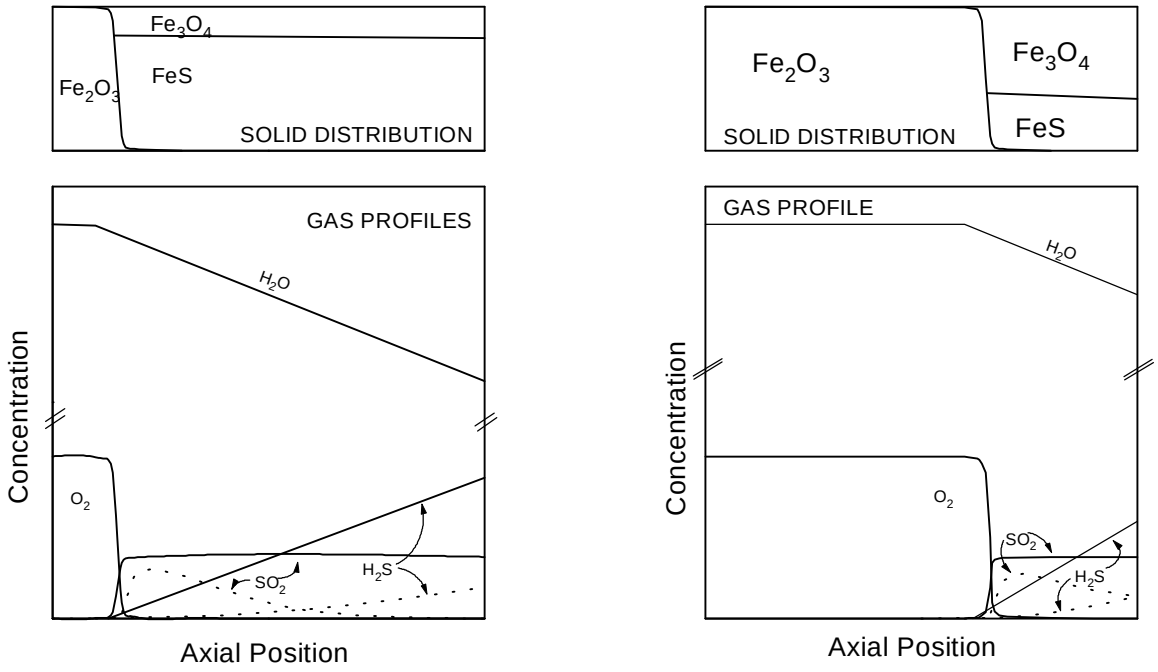

(a) At an Early Stage of the Reaction (b) At an Intermediate Stage of the Reaction

Figure 22. Proposed Solids Distribution and Gas Concentration Profiles within the Sorbent Bed

The shape of the gas phase O_2 concentration profile is approximately equal to the FeS-Fe_2O_3 interface, with only minor distortion due to the additional O_2 consumed in converting Fe_3O_4 to Fe_2O_3. Inlet H_2O concentration is much larger than inlet O_2 concentration (H_2O/O_2 = 80 in Figure 16), and no H_2O reacts upstream of the FeS-Fe_2O_3 interface. Downstream of the interface there is a small, almost linear decrease in H_2O concentration because of the slow FeS-H_2O reaction.

SO_2 and H_2S concentration profiles in the absence of the Claus reaction are shown by the solid lines in Figure 22a. The SO_2 concentration increases rapidly at the position of the FeS-Fe_2O_3 interface to a value of 57% of the inlet O_2 concentration as specified by the stoichiometry of the FeS-O_2 reaction. The SO_2 profile is then horizontal since no additional O_2 is available to react with FeS. The H_2S concentration is zero to the position of the Fe_2O_3-FeS interface and increases almost linearly from there to the bed exit. The final H_2S concentration is equal to 75% of the change in the H_2O concentration according to the stoichiometry of the FeS-H_2O reaction.

At positions within the reactor where SO_2 and H_2S co-exist, they may react by the Claus reaction to form elemental sulfur; the SO_2 and H_2S concentration profiles are modified as shown by the dotted lines in Figure 22a. Since no additional SO_2 may be formed downstream of the FeS-Fe_2O_3 interface because no addition O_2 is available, the SO_2 concentration reaches a maximum at some interior bed position and decreases thereafter. In this case the SO_2 concentration decreases to effectively zero since there is no SO_2 in the product gas. In contrast, H_2S formation begins downstream of the FeS-Fe_2O_3 interface. Most of this H_2S is consumed by reaction with SO_2 to form elemental sulfur. However, additional H_2S formed downstream of the point where the SO_2 concentration is zero appears in the product gas.

The quantity of SO_2 formed within the bed is almost independent of time prior to O_2 breakthrough. The only difference is the axial position within the bed at which the SO_2 is formed. In contrast, the amount of H_2S formed is maximum initially and decreases continuously with time as the FeS-Fe_2O_3 interface progresses through the bed. The maximum H_2S concentration coupled with the maximum H_2S-SO_2 contact time is responsible for the maximum initial elemental sulfur selectivity. The selectivity then decreased as less H_2S is available to react with the fixed amount of SO_2 and contact time decreases.

As the reaction progresses, the FeS-Fe_2O_3 interface moves further into the bed and the concentration profiles are modified as shown in Figure 22b. This corresponds to approximately 4 hours into the run shown in Figure 16. The shape of the FeS-Fe_2O_3 interface is similar to that shown in Figure 22a, but displaced to the right. No Fe_3O_4 exists upstream of the FeS-Fe_2O_3 interface and the FeS-Fe_3O_4 interface is again represented by an almost horizontal line. However, the Fe_3O_4 concentration has increased due to the increased reaction time. The O_2 concentration profile is also similar to the earlier profile, but again displaced to the right. The H_2O profile upstream of the FeS-Fe_2O_3 interface remains flat, and less H_2O reacts downstream because of the reduced contact time. In the absence of the Claus reaction (solid lines) the SO_2 profile is unchanged except for being shifted downstream. Initial H_2S formation is delayed because of the shift in the FeS-Fe_2O_3 interface, and less H_2S is formed because of the reduced reaction time. When elemental sulfur is produced by the Claus reaction (dashed lines), not all SO_2 is consumed because less H_2S is present and the contact time is reduced. Both SO_2 and H_2S are present in the product gas and less elemental sulfur is produced.

At a later stage in the reaction, say about 6 hours into the run shown in Figure 16, O_2 breakthrough has not yet occurred and the amount of SO_2 formed is still constant. Even less H_2S is formed since the FeS-Fe_2O_3 interface is further downstream. Essentially all H_2S is consumed by reacting with SO_2 (zero H_2S concentration in the product gas) but the SO_2 product concentration is even larger than at 4 hours. At still longer times, after initial O_2 breakthrough,

no H_2S can be formed, no elemental sulfur can be produced, and the SO_2 and total sulfur concentrations in the product become equal.

The observed effects of feed gas flow rate, H_2O/O_2 ratio, and temperature are consistent with this interpretation. Increasing the feed gas rate increased the selectivity to SO_2, had little effect on H_2S selectivity, and, as a consequence, decreased the elemental sulfur selectivity. The increased feed rate caused no change in the SO_2 production rate but decreased the H_2S production rate because of the decreased residence time. However, there was less time for the Claus reaction. These effects tended to cancel and produce no change in H_2S production, but an increase in SO_2 and a decrease in elemental sulfur production.

Higher temperature increased the H_2S yield, had little effect on the amount of SO_2 produced, and caused the elemental sulfur selectivity to decrease. This is consistent with electrobalance results, which showed the FeS-H_2O reaction to have greater temperature sensitivity than the FeS-SO_2 reaction. Although more H_2S was formed at the higher temperature, it was formed downstream of the FeS-Fe_2O_3 interface and had less opportunity to react with SO_2 to form elemental sulfur.

The strong effect of H_2O/O_2 ratio on elemental sulfur formation is due to the large difference in the reaction rates of FeS with O_2 and H_2O. Large elemental sulfur selectivity requires that a large fraction of the FeS react with H_2O to liberate H_2S, and, of equal importance, that H_2S and SO_2 be formed at positions within the bed which provide sufficient time for the Claus reaction to occur. H_2S formed near the bed exit is swept out of the reactor within having time to be converted to elemental sulfur.

While reasonably large selectivities to elemental sulfur are possible at large H_2O/O_2 ratios, low temperatures, and low regeneration gas feed rate, the elemental sulfur concentration in the product gas was always quite small. The maximum total sulfur concentration of about 0.009 mole fraction was measured at a H_2O/O_2 ratio of 200. The low temperature required to condense the sulfur would also result in the condensation of large quantities of steam. Thus, the large steam requirements, the large heat duty of the sulfur condenser, and the difficulty in handling the sulfur-water mixture are believed to make the partial-oxidation of FeS an impractical regeneration concept.

CHAPTER 5: CERIUM OXYSULFIDE REGENERATION

The product of the sulfidation of cerium oxide, Ce_2O_2S, is not available commercially and had to be produced before regeneration of Ce_2O_2S with SO_2 could be studied. A set of standard sulfidation parameters was selected in order to produce Ce_2O_2S and the sulfidation phase of all tests described in this chapter was carried out at these conditions. As the study progressed, however, it became apparent that by combining reduction with sulfidation, it would be possible to reduce H_2S concentrations to below the levels associated with the CeO_2-H_2S reaction thermodynamics discussed in Chapter 2. Hence, additional experimental tests were conducted in which the reduction-sulfidation reactions were of primary interest. The commercial application of any high temperature desulfurization process will require that the sorbent maintain its capacity and reactivity through many sulfidation-regeneration cycles. Most tests used CeO_2 from Rhône Poulenc as the starting material, but a limited number of tests used CeO_2 from other sources. Hence, the results of the cerium sorbent studies are presented in four chapters. This chapter presents results from the tests using Rhône Poulenc CeO_2 to investigate the effect of regeneration parameters. Standard sulfidation conditions were used. The next chapter contains the results of the detailed tests to determine the effect of reaction parameters on the reduction-sulfidation phase of the cycle using Rhône Poulenc CeO_2. Regeneration was omitted from this series of tests. Multicycle test results are then presented in Chapter 7. Results from the limited number of tests using other sources of CeO_2 are compared with the Rhône-Poulenc results in Chapter 8.

5.1 Cerium Oxide from Rhône-Poulenc

In preliminary tests using as-received CeO_2, a bed pressure drop of about 3 atm resulted because of the extremely small particle size of the CeO_2. Sintering was also encountered in preliminary tests in which pure CeO_2 was used. At the end of a run the sorbent was removed from the reactor as a lightly bound and highly porous single cylinder. The excessive pressure drop problem was solved by dry-pressing the as-received CeO_2 at 25,000 psi to form tablets which were subsequently crushed and sieved. Particle diameter ranges between 75 and 150 microns and between 150 and 300 microns were then used in the reaction tests. The sintering problem was solved by physically mixing CeO_2 and inert Al_2O_3 having a particle size range from 80 to 200 microns to form the packed bed. Both 1-to-1 and 2-to-1 (by weight) mixtures of CeO_2-to-Al_2O_3 were tested. No significant differences were observed when the two ratios were tested, and the 2-to-1 mixture of CeO_2-to-Al_2O_3 was selected as the standard sorbent charge. The bed pressure drop was reduced to about 5 psi and the CeO_2-Al_2O_3 mixtures emerged from the reactor as free-flowing particles even after multicycle sulfidation-regeneration tests.

Independent electrobalance tests showed that the Rhône Poulenc CeO_2 lost 9% of its original weight when heated to 600°C in an inert atmosphere. Hence, cerium oxide fractional conversion calculations were based on the CeO_2 being 91% pure. On a microscopic scale, mixing CeO_2 with Al_2O_3 did not prevent sintering as shown by the BET surface area results summarized in Table 9. The surface areas of as-received CeO_2 and Al_2O_3 were both approximately 220 m^2/g. The tableting, crushing, and sieving treatment reduced the CeO_2 surface area to 156 m^2/g and the CeO_2-Al_2O_3 mixture charged to the reactor had a surface area of

181 m^2/g. Clear evidence of sintering is shown by the fact that the mixture surface area was reduced to 23 m^2/g after 10 sulfidation-regeneration cycles. However, the sorbent mixture after this multicycle run remained a free-flowing powder, and, as will be shown in the chapter reporting multicycle run results, the reduction in surface area did not cause significant deterioration in the sulfidation-regeneration performance.

Table 9. BET Surface Areas of CeO_2 and Al_2O_3

	Surface Area, m^2/g
Rhone-Poulenc CeO_2	
as-received	220
after tabletting, crushing and sieving	156
Sigma Al_2O_3	
as received	217
Sorbent charge	
$2CeO_2$: $1Al_2O_3$ by mass	181
Sorbent product	
$2CeO_2$: $1Al_2O_3$ by mass, after 10-cycle run	23

5.2 CeO_2 Sulfidation

In those runs where sorbent regeneration was of primary interest, regeneration was proceeded by sulfidation at standard reaction conditions shown in Table 10. Preliminary tests showed that the effect of temperature on the sulfidation reaction was small over the range of 700°C to 850°C. 800°C was chosen to take advantage of the improved sulfidation thermodynamics (see Table 4) at high temperature. Sulfidation pressure was limited to 5 atm to avoid experimental complications when operating near the room temperature vapor pressure of H_2S.

The H_2S content of the feed gas was chosen to be 1% so that complete CeO_2 sulfidation could be achieved in a reasonably short time period using the feed gas rate of 400 sccm. Hydrogen was added as required by the sulfidation reaction and to minimize H_2S decomposition at the high temperature. No H_2O, CO, or CO_2 was added to the feed gas to keep the experimental aspects of the sulfidation phase as simple as possible.

In this highly reducing feed gas the equilibrium H_2S content of the product gas is near the 100 ppmv detection limit of thermal conductivity detector. However, in preliminary tests a pre-breakthrough H_2S plateau of 2000 ppmv or larger H_2S was often measured. This large pre-breakthrough concentration was traced to the reaction of elemental sulfur deposited in the product transfer line during the previous regeneration cycle with H_2 from the sulfidation product gas. Evidence of this contamination is presented in Figure 23. Following a regeneration test, the reactor and downstream tubing were heated to 800°C and 350°C, respectively. 150 sccm of

sulfur-free feed gas containing 10% H_2, balance N_2 was feed to the reactor. Initial H_2S concentrations in excess of 0.4% (> 4000 ppmv) were measured. The H_2S concentration then decreased to about 0.2% and remained constant for approximately 2 hours. At that time the temperature of the transfer line was reduced to 25°C and the gas flow increased to 400 sccm. The H_2S concentration quickly decreased to about 0.01% (–100 ppmv). More extensive efforts to reduce sulfur contamination, including using a teflon-lined transfer tube during sulfidation and a separate transfer line for regeneration were adopted for sulfidation studies following installation of the flame photometric detector. Results of these tests are described in the next chapter.

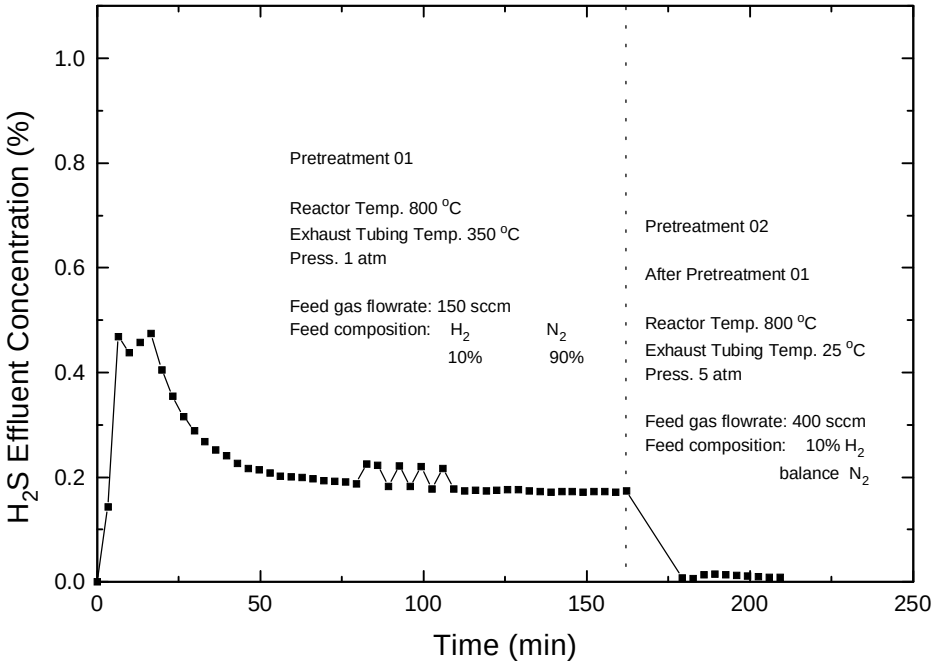

Figure 23. Reactor Cleaning Test: H_2S Formed by the Reaction of H_2 and Elemental Sulfur

The sulfidation breakthrough curve from the first test following adoption of the previously described cleaning procedure is shown in Figure 24. Standard sulfidation conditions shown in Table 10 were used. Results of a non-reacting (cerium-free) tracer test at the same reaction conditions are shown for comparison. The H_2S concentration during the first 20 minutes of about 0.01% corresponds to 99% H_2S removal and is approximately equal to both the detection limit of the TCD and the equilibrium concentration of H_2S in the standard gas composition. The H_2S concentration during the first 80 minutes corresponded to greater than 95% H_2S removal. Active breakthrough began at about 85 minutes and the sulfidation reaction was effectively complete when the test was terminated after 130 minutes. The shaded area between the two curves is proportional to the amount of Ce_2O_2S formed. Numerical integration of this area corresponded to 87% conversion of CeO_2.

Table 10. Standard Sulfidation Conditions Used to Study the Effect of Regeneration Reaction Conditions

Temperature	800°C
Pressure	5 atm
Feed Gas Composition	
H_2S	1 mol %
H_2	10 mol %
N_2	Balance
Feed Gas Rate	400 sccm (SV ≈ 3700 hr^{-1} (STP))
Sorbent Charge	
CeO_2	6.0g
Al_2O_3	3.0g

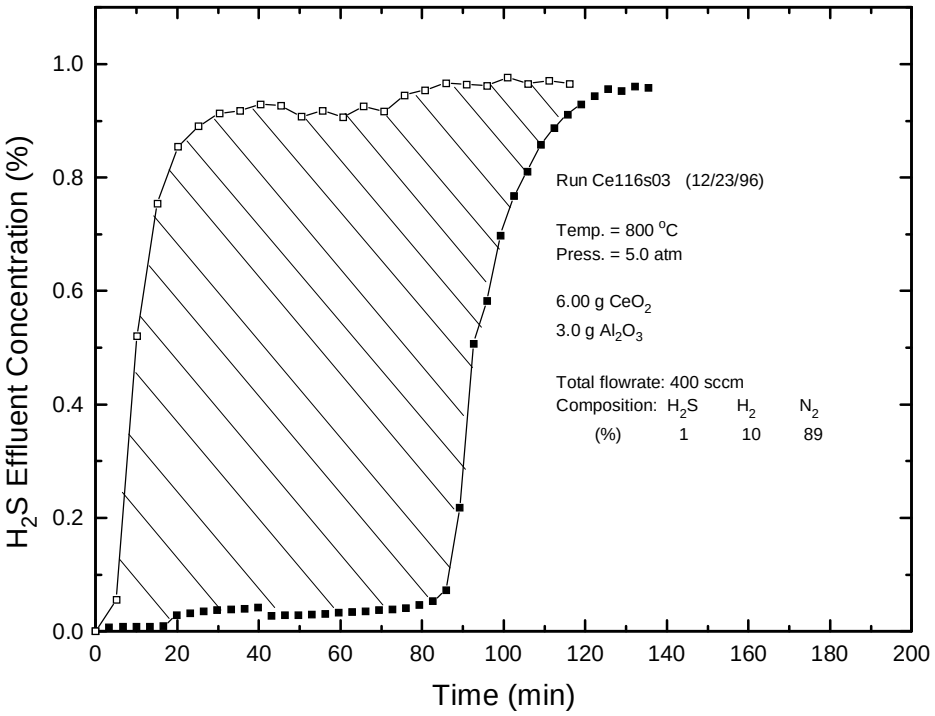

Figure 24. Fixed-Bed Sulfidation Response: H_2S Breakthrough Curve, Run Ce116s03

5.3 Ce_2O_2S Regeneration

All regeneration tests were preceded by sulfidation at the conditions previously described, and the sorbent was almost completely converted to Ce_2O_2S. Regeneration reaction parameters and the range of conditions studied are presented in Table 11. The key parameters were temperature and the SO_2 content of the feed gas. The pressure in most runs was limited to 1 atm because of the low room temperature vapor pressure of SO_2 (–3.4 atm). Higher pressure regeneration tests used premixed cylinders containing 12% SO_2 in N_2. The regeneration gas flow rate was fixed at 200 sccm in most tests so that the duration of the regeneration test would be sufficient to properly define the SO_2 breakthrough curve. In some tests using high SO_2 concentrations the flow rate was reduced to prolong the breakthrough curve, and, near the end of the experimental program the effect of variations in feed rate was studied.

Table 11. Ranges of Reaction Conditions Used in Ce_2O_2S Regeneration Tests

Parameter	Range of Conditions
Temperature, °C	350 – 700
Pressure, atm	1 – 8
Feed Composition	
% SO_2	1 – 20
% N_2	Balance
Total Feed Rate, sccm	100 – 800
Space Velocity, hr^{-1}	925 - 7400

5.3.1. The Effect of Temperature

Preliminary experiments showed that no regeneration occurred at 350°C and that regeneration was rapid and complete at 600°C. In a series of tests the temperature was varied in 50°C intervals from 450°C to 700°C. SO_2 breakthrough curves between 500°C and 700°C are shown in Figure 25. Other reaction conditions for this series are shown on the figure. While some regeneration did occur at 450°C, the rate was quite slow and is not included in the figure.

Regeneration was rapid and complete throughout the 500°C to 700°C range, and the effect of temperature was small. The times, $t_{0.5}$, corresponding to 6% SO_2 in the product gas (50% of the feed concentration) increased slightly from 17.7 minutes at 500°C to a maximum 20.3 minutes at 650°C. Perhaps the most significant difference is that at the two lower temperatures (500 and 550°C), SO_2 first appeared in the product in the third sample, while at higher temperatures, SO_2 first appeared in the product gas in the fourth sample. Regeneration was effectively complete in about 25 minutes. As a result of these tests, 600°C was chosen as the "standard" regeneration temperature, and was used in most of the subsequent regeneration tests.

According to the stoichiometry of the regeneration reaction, the mole fraction of elemental sulfur (considered as S_2) is equal to the difference in the SO_2 mole fraction between the feed and product gases. Thus, for a substantial portion of each run shown in Figure 25, the elemental sulfur content of the product gas was equal to or greater than 11%.

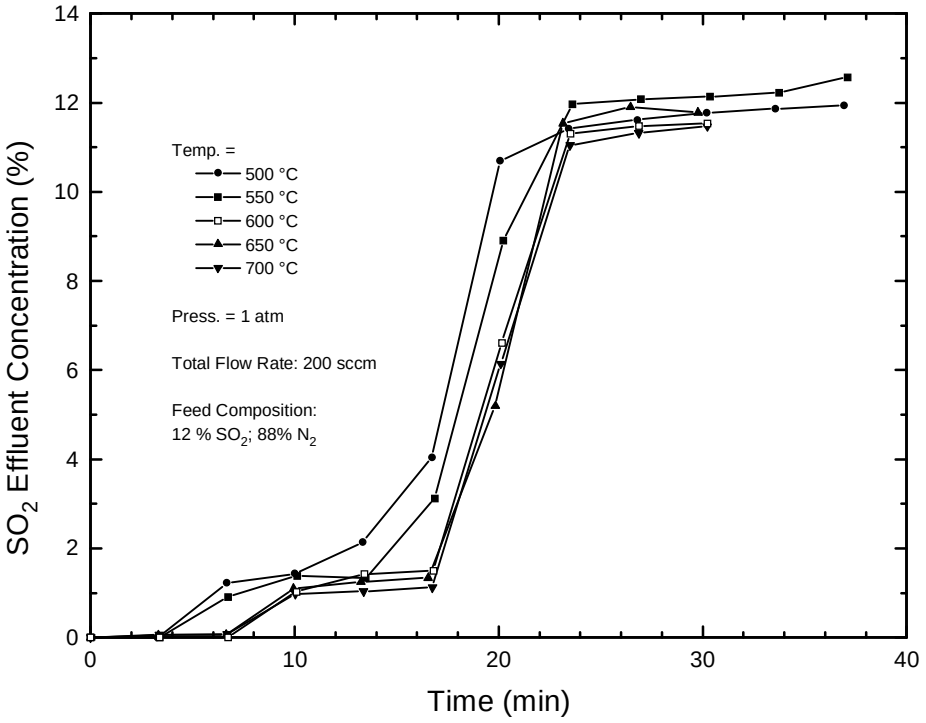

Figure 25. The Effect of Temperature on Ce_2O_2S Regeneration

5.3.2. The Effect of SO_2 Concentration

Regeneration breakthrough curves for a series of tests in which the SO_2 content of the feed gas was varied between 2% and 16% are shown in Figure 26. Other reaction conditions are shown on the figure. The ordinate in this figure is normalized SO_2 concentration, i.e., the ratio of the SO_2 concentrations of the product and feed gases. Therefore, the final normalized concentration from each run is 1.0. An additional test in which the feed gas contained 1% SO_2 was included in this test series. Results are not included since the enlarged time scale would make results from the high concentration tests appear to be almost identical.

The breakthrough curves from each test exhibit the same characteristics. No SO_2 was detected in the product gas during the initial stages of the reaction. This was followed by a SO_2 plateau at a normalized concentration of about 0.1 and then by active breakthrough to the final normalized concentration of 1.0. The duration of the period corresponding to zero SO_2 concentration and the time corresponding to active breakthrough were both roughly inversely proportional to the SO_2 content of the feed gas.

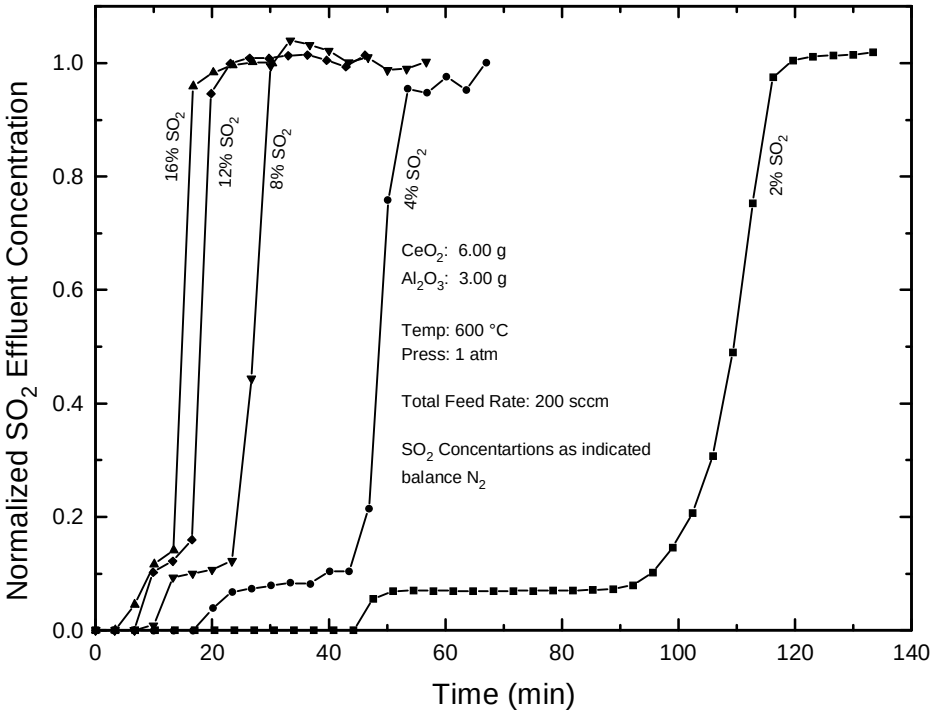

Figure 26. The Effect of SO_2 Concentration (2% ~ 16%) on Ce_2O_2S Regeneration

As the SO_2 concentration increased, the duration of the regeneration run decreased, and at 12% and 16% SO_2 the amount of data collected before complete regeneration was quite limited. Hence, a second series of regeneration runs using a feed rate of 100 sccm (½ the previous feed rate) was carried out. The SO_2 content of the feed was varied from 4% to 20% and the resultant breakthrough curves are shown in Figure 27. The product gas concentration scale is again normalized. The general characteristics of the breakthrough curves are similar to those in Figure 26 except that the initial SO_2 plateau disappeared in the 20% SO_2 test. Also, both the tests using 16% and 20% SO_2 were terminated slightly before completion because elemental sulfur product condensed and plugged the reactor exit lines. However since both tests were almost complete prior to plugging, the essential data were obtained.

Results of the two series of tests are compared in Figure 28 where $t_{0.5}$, the time required for the SO_2 concentration in the product gas to reach 50% of the feed concentration, is plotted as a function of SO_2 feed rate. SO_2 feed rates of 4, 8, and 16 sccm were used in both series of tests; $t_{0.5}$ values were identical in two of the three cases and differed by only 8% in the third.

5.3.3. The Effect of Volumetric Feed Rate

When other parameters, including SO_2 concentration, are constant, the gas residence time in the packed bed is inversely proportional to volumetric feed rate. In addition, the SO_2 feed rate is directly proportional to the total feed rate. An increase in SO_2 feed rate should decrease the breakthrough time while a decrease in residence time should cause initial breakthrough to occur at an earlier time and decrease the slope of the breakthrough curve. These effects are shown in

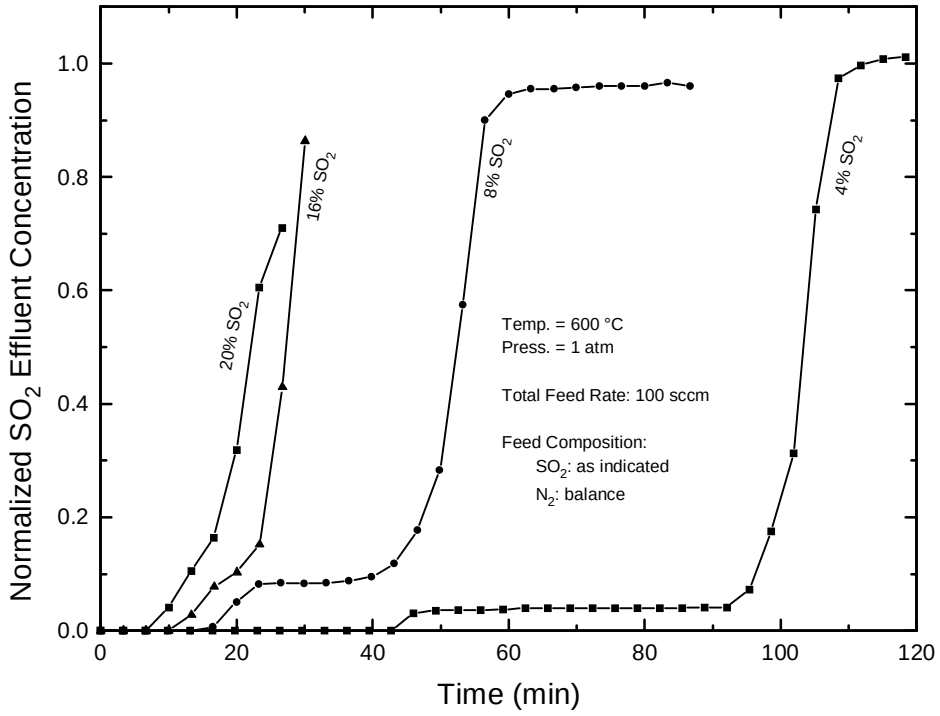

Figure 27. The effect of SO_2 Concentration (4% ~20%) on Ce_2O_2S Regeneration

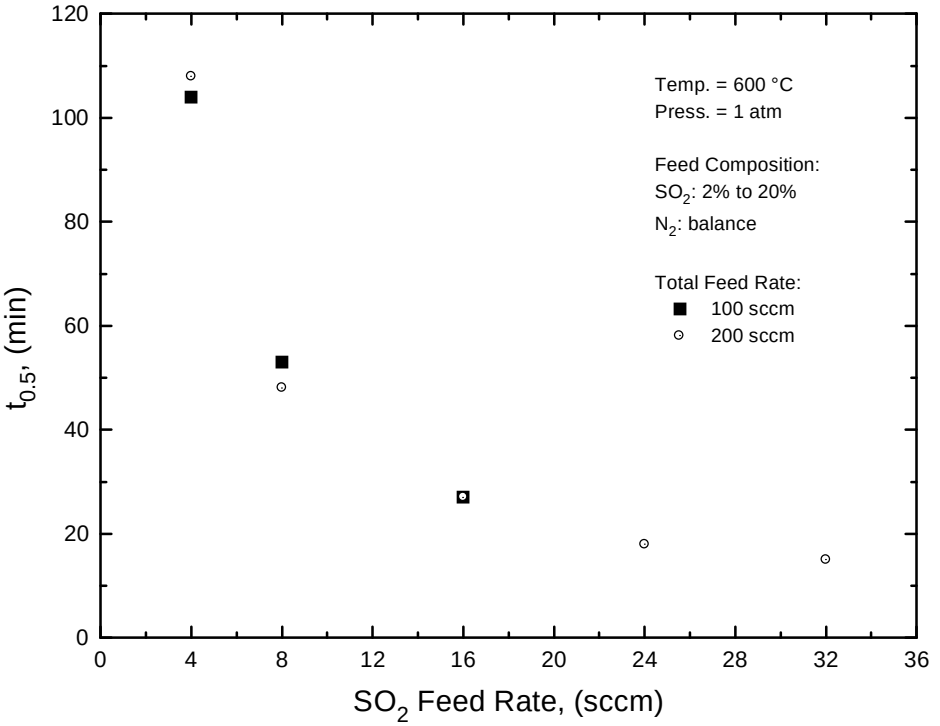

Figure 28. Comparison of $t_{0.5}$ for Ce_2O_2S Regeneration as a Function of SO_2 Feed Rate

Figure 29 for a series of tests using 4% SO_2 at 600°C and 1 atm. $t_{0.5}$ decreased from 103 minutes at a feed rate of 100 sccm to 48 min at 200 sccm and to 29 minutes at 400 sccm. The lack of direct inverse proportionality is due to the delay time between feeding gases to the reactor and the time those gases reached the chromatograph-sampling valve. Delay time corrections were not included in the data of Figure 29. The effect of decreased residence time can be seen from the fact that about 10 minutes were required for the SO_2 product concentration to increase from 20% to 80% of the feed concentration at 400 sccm compared to 7 minutes elapsed time between the same concentrations at 100 sccm.

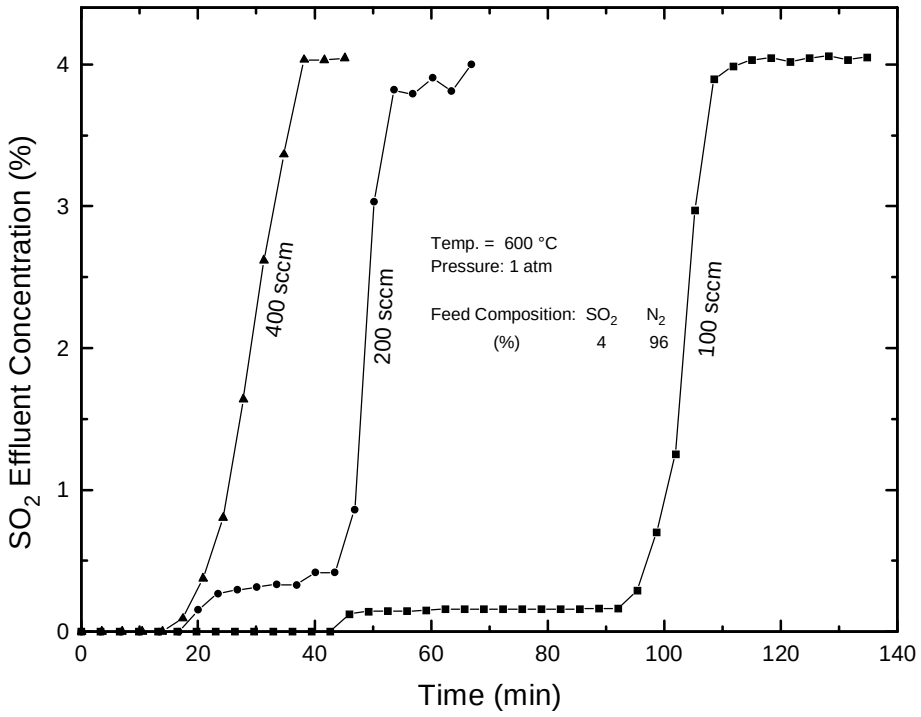

Figure 29. The Effect of Gas Feed Rate on Ce_2O_2S Regeneration

Similar results from other tests using 2% SO_2 at 600°C and 1 atm are shown in Figure 30. Dimensionless time, t*, which in principle accounts for delay time and the change in SO_2 feed rate, is plotted in this figure. Dimensionless time is defined by

$$t^* = \frac{t - t_D}{t_E} \tag{14}$$

where t is the dimensional time, t_D is delay time, and t_E is the theoretical time at which all CeO_2 would be converted to Ce_2O_2S with complete removal of H_2S. By using dimensionless time, breakthrough curves should approximately overlap, with decreased slopes associated with increased residence times being the primary difference. The smaller slope associated with the 800 sccm run is clearly evident and the three breakthrough curves cross at SO_2 product

concentrations of 1%, 1.2%, and 1.6%, respectively, reasonably near the theoretical 1% SO_2 cross-over point.

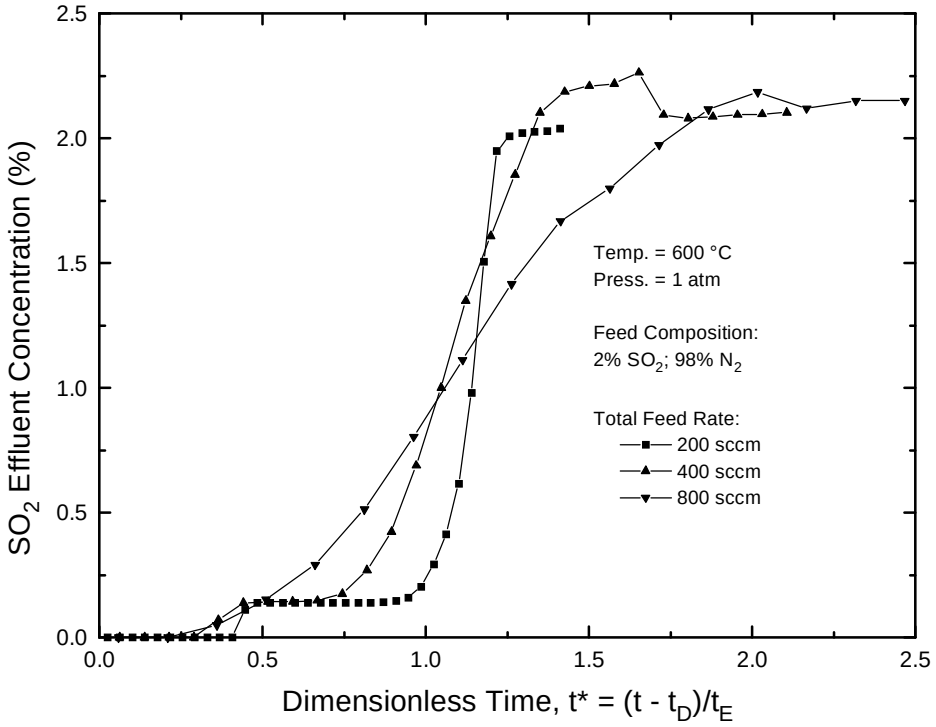

Figure 30. The Effect of Gas Feed Rate on Ce_2O_2S Regeneration: Dimensionless Time Basis

5.3.4. The Effect of Pressure

As previously explained, most regeneration tests were limited to 1 atm because of the low vapor pressure of SO_2. A premixed cylinder containing 12% SO_2 in N_2 was obtained which allowed us to operate at regeneration pressures as large as 8 atm. At a fixed SO_2 concentration, higher total pressure results in increased partial pressure of elemental sulfur in the product gas. This, in turn, increases the tendency for sulfur condensation and plugging. With extra heat tracing and insulation added to the transfer lines between the reactor and condenser, we were able to successfully complete a regeneration test using 4% SO_2 at 600°C and 8 atm. The resulting elemental sulfur partial pressure of 0.32 atm was 60% larger than the maximum sulfur partial pressure in the 1 atm regeneration tests.

Breakthrough curves from the series of regeneration tests using 4% SO_2, 200 sccm feed rate, 600°C and a range of pressures from 1 to 8 atm are shown in Figure 31. All breakthrough curves exhibit the standard shape. No SO_2 was detected in the product gas during the initial stages of the reaction. The length of the zero SO_2 periods ranged from about 17 minutes at 1 atm to 31 minutes at 8 atm. A period in which the SO_2 concentration was approximately constant at 0.4% then followed. Active breakthrough began in the 45 to 50 minute time period and regeneration was complete in all cases by 60 minutes.

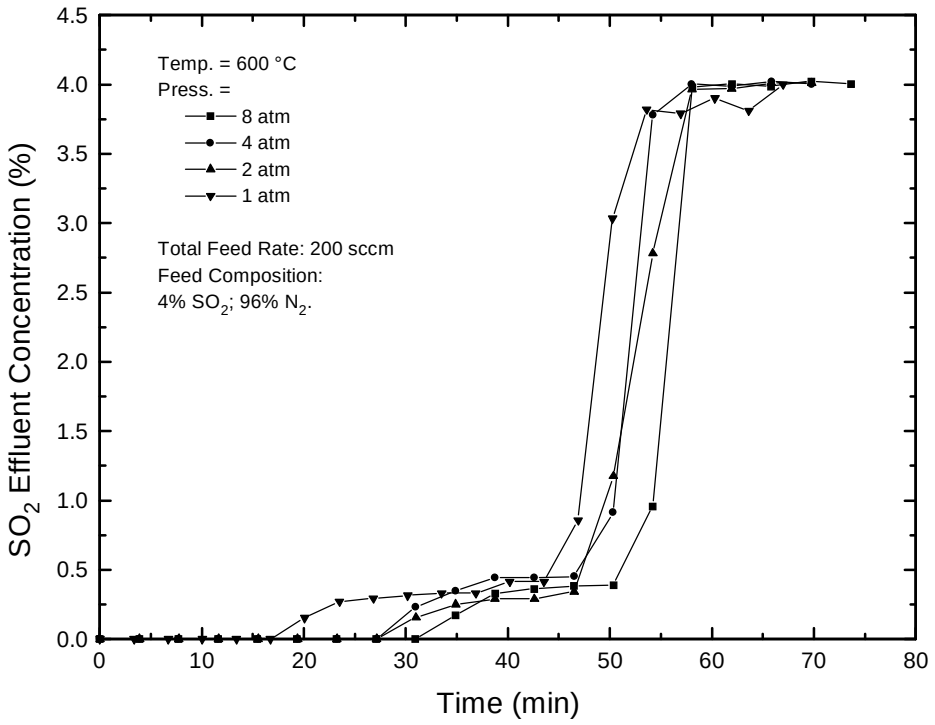

Figure 31. The Effect of Pressure on Ce_2O_2S Regeneration

5.3.5. The Effect of Residence Time

The effect of residence time on the slope of the breakthrough curve was seen earlier in Figure 29 where flow rate was varied at constant SO_2 concentration. In addition, results of a series of tests in which feed rate and SO_2 concentration were varied simultaneously while keeping the SO_2 feed rate constant at 16 sccm is shown in Figure 32. It is clear from this figure that the breakthrough curve having the smallest slope occurred at 800 sccm; about 14 minutes were required for the SO_2 concentration to increase from 20% to 80% of the feed value. At 400 sccm feed rate, the time required to traverse the same concentration interval was reduced to 10 minutes, and only about 5 minutes were required at both 200 and 100 sccm.

5.4 Conclusions

The reaction between Ce_2O_2S and SO_2 was rapid and complete over a wide range of temperatures (500°C to 700°C), feed gas compositions (1% to 20% SO_2), feed gas flow rates (100 to 800 sccm), and pressures (1 to 8 atm). Elemental sulfur concentrations as large as 20% were produced in 1 atm tests, and the maximum elemental sulfur partial pressure of 0.32 atm was produced in an 8 atm test using 4% SO_2 in the feed gas. Regeneration pressures were limited by the low vapor pressure of SO_2, and tests above atmospheric pressure required that a premixed cylinder containing 12% SO_2 in N_2 be used.

Process simulation studies, to be discussed in a later section of this report, indicated an optimum elemental sulfur concentration in the product gas of about 15% at an operating pressure of 15 to 25 atm. This corresponds to elemental sulfur partial pressures from 2.25 to 3.75 atm, or

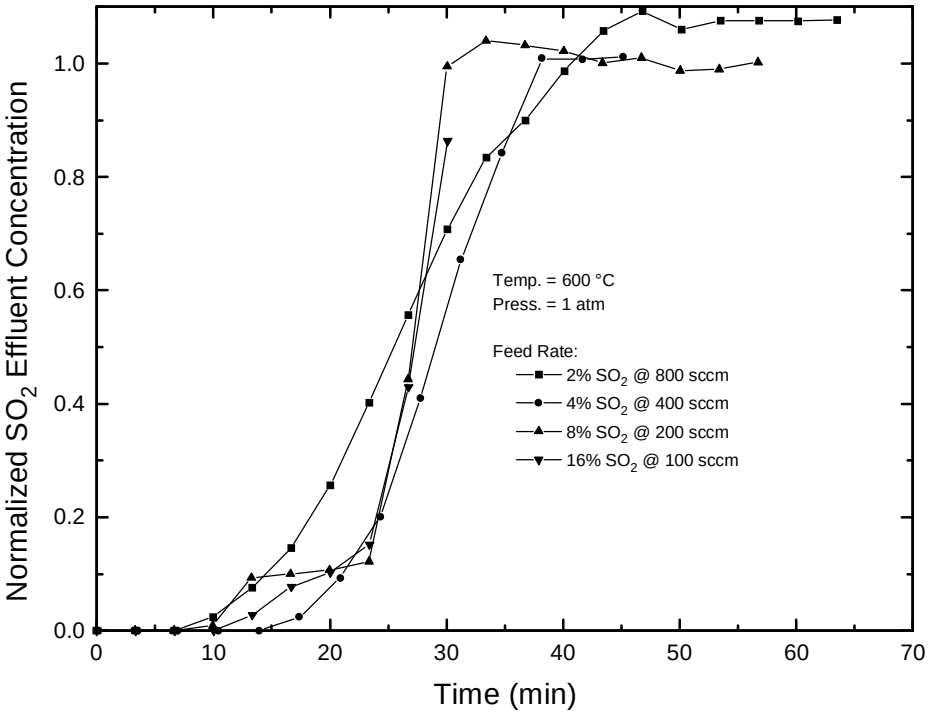

Figure 32. The Effect of Residence Time on Ce_2O_2S Regeneration

about 10 times the maximum achieved in these tests. However, the partial pressure limitations in the experimental study were associated with the low vapor pressure of SO_2 and the strong tendency of the sulfur to condense and plug product lines. Both of these problems should be relatively easy to overcome in a large-scale, continuous commercial operation.

The rate of the regeneration reaction coupled with the large concentration of SO_2 in the feed gas should be sufficient to insure that sorbent regeneration time is small compared to sulfidation time. That is, sorbent circulation rate determined by the sulfidation step could be easily regenerated in the allotted time.

In summary, all results from the Ce_2O_2S-SO_2 regeneration tests were extremely favorable.

CHAPTER 6. REDUCTION AND SULFIDATION OF CERIUM OXIDE

Sulfidation studies were divided into two distinct groups. In the early periods of the research, the regeneration of Ce_2O_2S using SO_2 and the production of elemental sulfur was of primary interest. The purpose of sulfidation runs was primarily to produce Ce_2O_2S for the regeneration studies. Most used the "standard" sulfidation conditions defined in Table 10, and many were carried out before the importance of cleaning the reactor system to remove elemental sulfur deposited during regeneration was discovered. As a consequence, pre-breakthrough concentrations in excess of 0.1% (1000 ppmv) were sometimes measured. After the cleaning procedure was adopted, pre-breakthrough concentrations at or below the TCD detection limit of about 100 ppmv were measured. At about the same time it became apparent that extremely low pre-breakthrough H_2S concentrations could be achieved by the reaction of H_2S with reduced CeO_n ($n<2$).

A flame photometric detector (FPD) capable of measuring H_2S concentrations in the range of 1 to 100 ppmv was then installed in the chromatograph. The TCD and FPD were installed in parallel so that product gas flow could be directed to either detector using a three-way valve. All wetted parts of this valve were of teflon so that no additional contact between product gas and stainless steel surfaces was introduced. The three-way valve could be switched during a run so that the FPD could be used to analyze product gas during early stages of the reaction, and the TCD used when the FPD became saturated. However, this procedure created a data gap lasting about 30 minutes when the gas flow was switched to the TCD. This time was required to enable the TCD to equilibrate after gas flow was established and power was turned on.

Only a small number of runs using both detectors were completed. In most tests where pre-breakthrough sulfidation performance was of primary interest, only the FPD was used and the test was terminated following FPD saturation to minimize sulfur contamination. The regeneration phase was omitted from most of these tests, also to minimize sulfur contamination. When both sulfidation and regeneration phases were included, different product transfer lines were used and all possible stainless steel parts were removed during the sulfidation phase.

This chapter begins with an extension of the literature survey and thermodynamic analysis to include the reduction of CeO_2 to CeO_n ($n<2$) and the subsequent sulfidation of CeO_n. Experimental aspects of the reduction and sulfidation steps are then presented.

6.1. Reduction of CeO_2 to CeO_n ($n<2$)

A more detailed search of cerium oxide literature showed that in a high temperature, highly reducing gas, CeO_2 would be reduced to nonstoichiometric CeO_n ($n<2$) which should have a much greater affinity for H_2S than exhibited by CeO_2.

Bevan and Kordis (1964) published results showing the equilibrium value of n in CeO_n as a function of temperature and pressure. Figure 33 is reproduced from the Bevan and Kordis paper. Results of CHEMQ calculations estimating the equilibrium O_2 pressure in a Shell gas as a

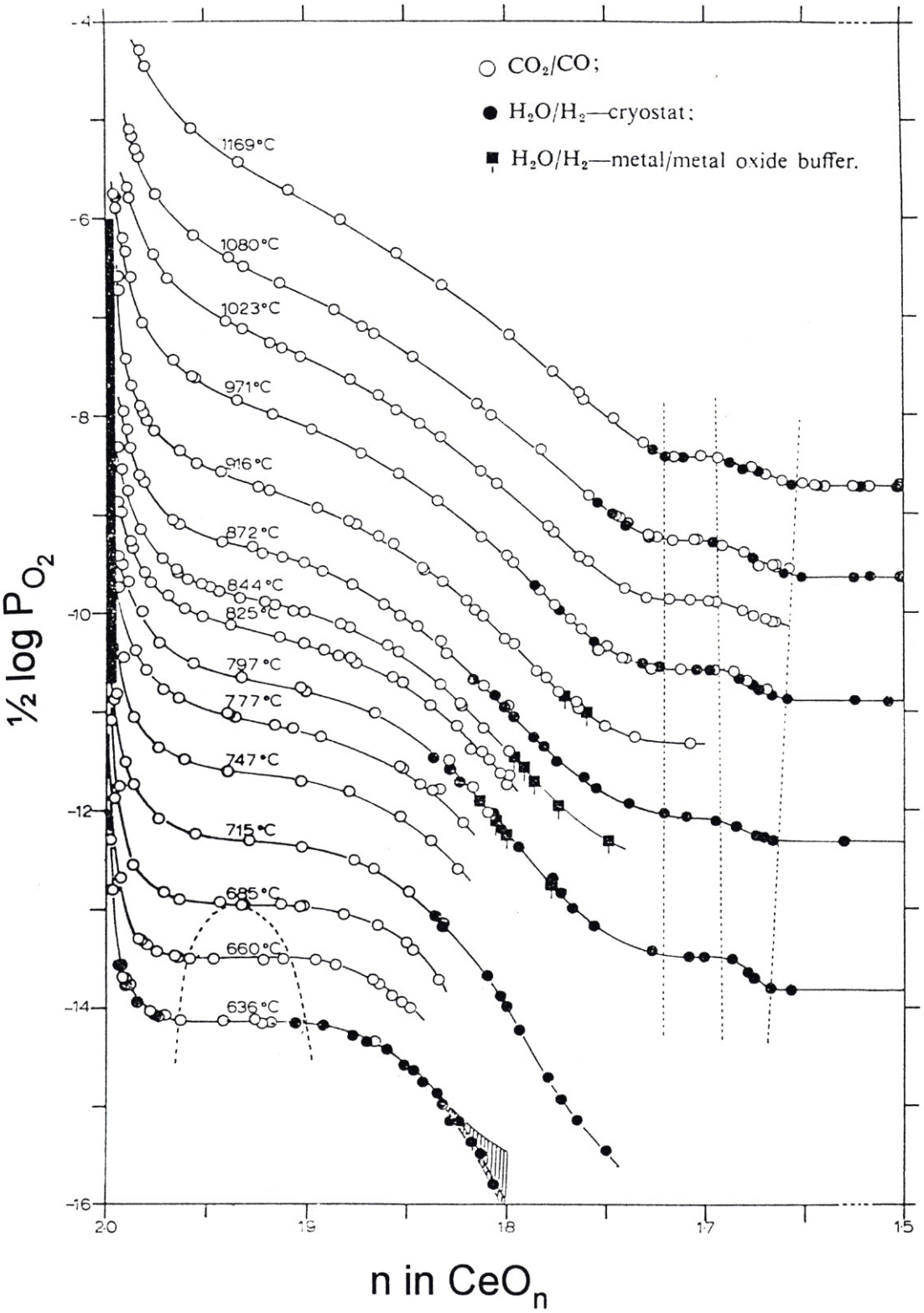

Figure 33. Reduction of CeO_2 to CeO_n as a Function of Oxygen Concentration and Temperature (from Bevan and Kordis, 1964)

function of temperature are shown in Table 12, along with the equilibrium value of n from the Bevan and Kordis study. At the standard sulfidation temperature of 800°C, this calculation suggests an equilibrium product corresponding to $CeO_{1.97}$.

Table 12. Equilibrium Oxygen Pressure and CeO_n Composition in Shell Gas as a Function of Temperature.

Gas Composition, mol%
CO – 60
H_2 – 29
CO_2 – 2
H_2O – 5
H_2S – 1
N_2 – 3

Temperature, °C	P_{O_2}, atm	n in CeO_n
700	$8x10^{-23}$	1.99
750	$5.4x10^{-22}$	1.98
800	$2.8x10^{-21}$	1.97
850	$3.8x10^{-20}$	1.94
900	$4.3x10^{-19}$	1.89
950	$4.0x10^{-18}$	1.88
1000	$3.1x10^{-17}$	1.85

Meng and Kay (1987) published results of cerium oxide sulfidation tests in which H_2S concentration was reduced from 1.2% (12,000 ppmv) in the feed gas to less than 10 ppmv during a 20 minute pre-breakthrough period. Sulfidation temperature was 1145K (872°C) and the feed gas contained 55% CO, 10.8% CO_2, 33.0% H_2, and 1.2% H_2S. Results of these tests are reproduced as Figure 34. The CeO_2 had been pre-reduced at 1145K and 5% H_2/N_2 for 24 hours. Although the composition of the gas used by Meng and Kay was different from the Shell gas, the equilibrium O_2 pressures were sufficiently close so that, to the accuracy with which Figure 33 can be read, the equilibrium values of n are effectively equal.

Reliable thermodynamic data for reduced cerium oxide compounds are not available. An earlier tabulation (Barin et al., 1977) included free energy of formation data for $CeO_{1.83}$ and $CeO_{1.73}$. However, these data were removed from the later tabulation (Barin et al., 1993). In addition, the 1977 data did not appear to be consistent with comparable data for CeO_2 and $CeO_{1.5}$ (Ce_2O_3).

Even without data for CeO_n, it was reasonable to expect, based on the Meng and Kay experimental results as well as the thermodynamic analysis which follows, that reduced CeO_n should be capable of reducing the equilibrium H_2S concentration to values well below those associated with CeO_2. Figure 35 presents the equilibrium H_2S concentration from Shell gas with both CeO_2 and Ce_2O_3 as calculated using thermodynamic data from Barin et al. (1993). At the lower temperatures, the CeO_2-H_2S reaction is exothermic and equilibrium H_2S concentration

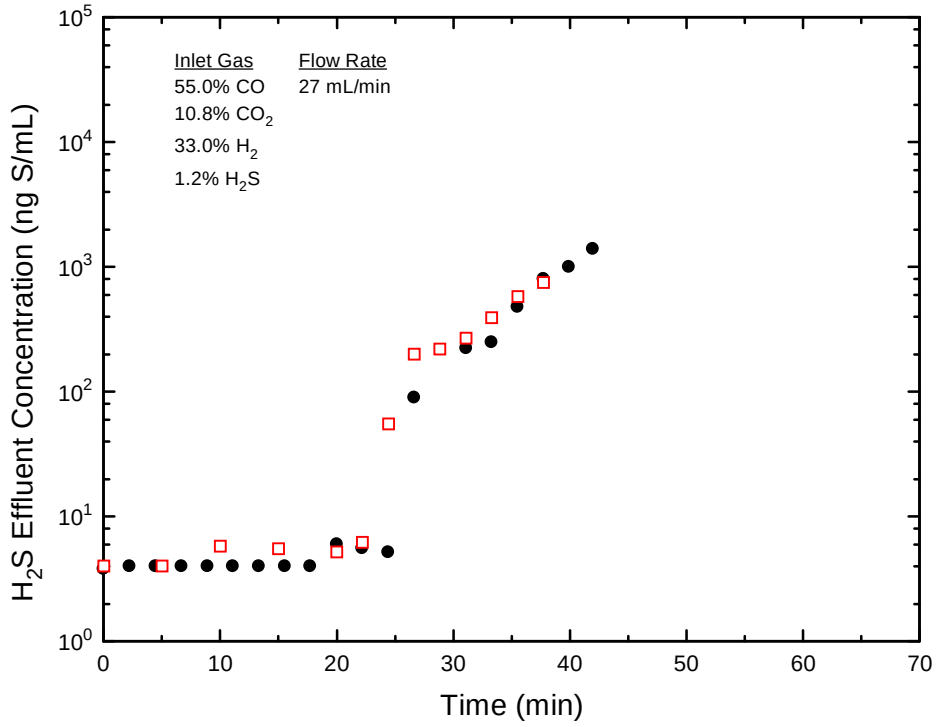

Figure 34. H_2S Breakthrough Curves During Two Sulfidation Cycles of CeO_n (n<2) (Data from Meng and Kay, 1987)

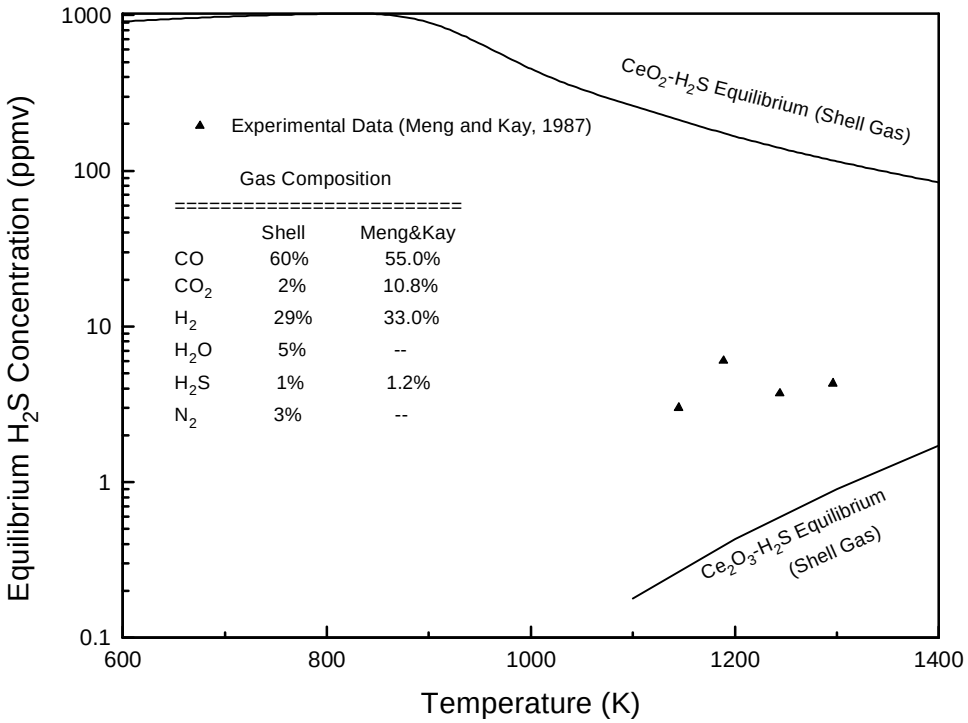

Figure 35. H_2S Equilibrium Concentration With Shell Gas in Contact With CeO_2 and Ce_2O_3

increases with increasing temperature. Above about 600°C, however, the reaction becomes endothermic and potential H_2S removal efficiency increases with increasing temperature. At the standard experimental sulfidation temperature of 800°C, the equilibrium H_2S concentration is about 300 ppmv, well above the IGCC target level of 20 ppmv. Higher operating temperatures result in increased H_2S removal potential, but at 1300°C the equilibrium level of H_2S is still about 50 ppmv.

At high temperature in the Shell gas, however, the reaction would be between CeO_n ($n<2$) and H_2S, and the H_2S removal potential would be increased. The limit of the potential increase is shown by the lower dashed line which represents between Ce_2O_3 ($n=1.5$) and H_2S. This reaction is exothermic throughout and H_2S removal potential decreases with increasing temperature. However, for all temperatures below 1000°C, the equilibrium H_2S concentration is below 1 ppmv. Even at 1300°C, Ce_2O_3 is thermodynamically capable of reducing H_2S to about 5 ppmv.

Experimental results from Meng and Kay (1987) have been added to the figure to illustrate the probable results using partially reduced CeO_n ($1.5<n<2.0$). As previously stated, the gas composition used by Meng and Kay and the Shell gas resulted in similar equilibrium O_2 pressure; thus, it is logical that the equilibrium H_2S concentration should also be similar.

A CeO_2 reduction experiment was carried out to compare experimental results with theory. An atmospheric pressure electrobalance reactor was used to monitor solid mass as a function of temperature. The temperature range covered was 600°C to 1000°C and the feed gas contained 3.5% CO_2 and 40% H_2 in helium. Helium was used as the inert gas instead of nitrogen as it produced less aerodynamic drag and resulted in increased electrobalance sensitivity. The CO_2 and H_2 concentrations were chosen to provide an approximate match to the equilibrium O_2 pressure of Shell gas while avoiding the complication of feeding steam to the reactor. CeO_2 was heated to 600°C in helium and held at that temperature until the weight was constant. H_2 and CO_2 were then introduced and the temperature was increased in 50°C or 100°C increments to 1000°C. The temperature was held constant at each increment until the weight was constant.

The equilibrium valve of n in CeO_n was calculated from the measured weight loss and the assumption that the sorbent following heat treatment at 600°C was pure CeO_2. Experimental results are compared in Figure 36 to predicted results based on calculated equilibrium oxygen pressures for the Shell gas coupled with the results from Bevan and Kordis. Duplicate experimental tests were carried out, and, as seen in the figure, the results were quite reproducible. The experimental results also were in close agreement with theory. At 800°C the experimental and theoretical values of n were both 1.97. At 1000°C, the experimental value of n=1.86 being was marginally larger than the theoretical value of n=1.83.

6.2. Sulfidation of CeO_n ($n<2$) to Ce_2O_2S

The emphasis in this series of tests was to determine pre-breakthrough concentrations for the CeO_n-H_2S reaction. Product gas analysis was accomplished using the FPD and most runs were terminated when the FPD became saturated at about 100 ppmv. The effects of temperature

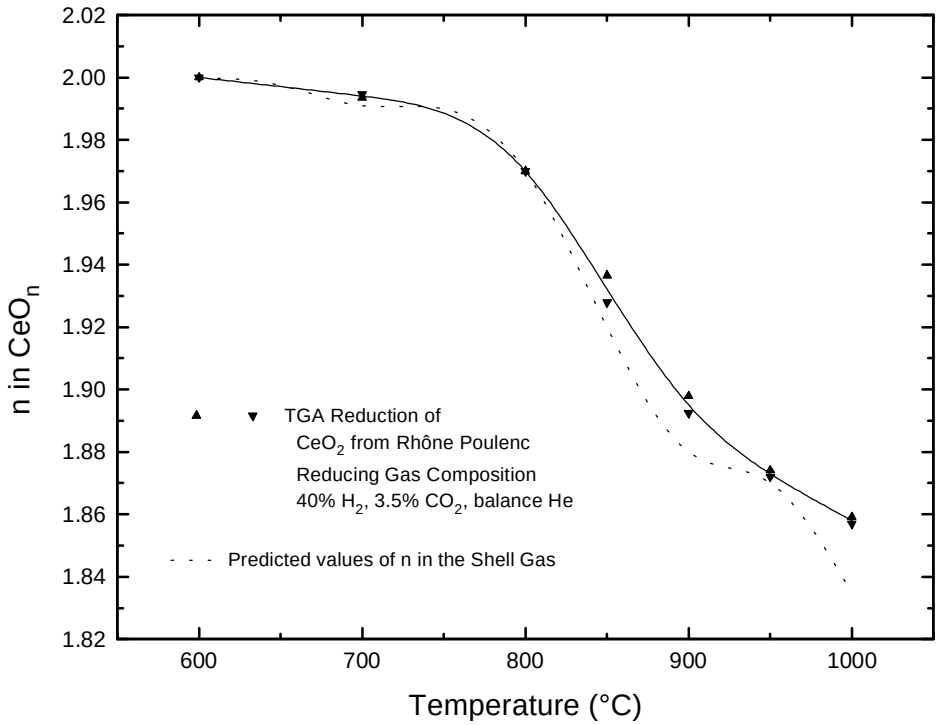

Figure 36. Reduction of CeO_2 in 40%H_2/3.5%CO_2/He

(600°C to 850°C), pressure (5 to 15 atm), gas feed rate (200 to 800 sccm), and feed gas composition (including the addition of H_2O) were investigated. In most tests the sorbent was pre-reduced in 10% H_2/N_2 at the temperature and pressure of the subsequent sulfidation. This ensured that the entire sorbent bed was fully reduced to CeO_n before exposure to H_2S. No pre-reduction step was included in other runs in which case reduction and sulfidation occurred simultaneously. Initial tests used the standard sulfidation feed gas composition of 1% H_2S/10% H_2/balance N_2. At these conditions FDP saturation occurred after about 25 minutes and the H_2S concentration increased from quite low levels to above the FPD saturation limit in a single sample interval. In order to increase the amount of data which was obtained prior to FPD saturation, the H_2S feed concentration was decreased to 0.25% in later tests. Finally, varying concentrations of steam were added to the feed gas in an effort to more closely simulate a Shell gas atmosphere. Completely matching the composition of the Shell gas in the laboratory tests was impractical because of the strong tendency for carbon deposition during feed gas preheating.

All results at the standard sulfidation pressure of 5 atm were in agreement with expectation and theory. However, results of higher-pressure tests at both 10 and 15 atm were sometimes inconsistent and counter to expectation and theory. The reasons for this are not clear. However, it may have been associated with the relatively close approach of the reaction pressure to the vapor pressure of H_2S which is about 20 atm at room temperature. As the pressure difference across the control valves on the mass flow controllers decreases, their accuracy decreases. In any event, the apparent problems were associated with breakthrough time; pre-breakthrough H_2S concentration results were consistent throughout.

6.2.1. The Effect of Temperature

The first series of sulfidation tests using the FPD and reactor system which minimized contact between the product gas and stainless steel examined the effect of temperature. Reaction pressure was 5 atm and the feed gas contained 1% H_2S and 10% H_2 in N_2. The sorbent was pre-reduced in 10% H_2 in N_2 at 5 atm and the sulfidation temperature prior to introducing H_2S. The temperature range investigated was from 600°C to 850°C. Results from tests at 650°C and higher are shown in Figure 37. All pre-breakthrough H_2S concentrations were below 10 ppmv. The concentrations decreased with decreasing temperature from about 6 ppmv at 850°C to less than 1 ppmv at both 650°C and 700°C. In each case the H_2S concentration in the next sample exceeded the FPD saturation limit of ~100 ppmv. These results are consistent with the sulfidation reaction being exothermic and equilibrium being closely approached. In the 600°C test (not shown) the H_2S concentration in all samples exceeded the FPD saturation limit, presumably because the kinetics of the reaction becomes too slow for equilibrium to be approached. The sub-1 ppmv concentrations reported at 650°C and 700°C should be treated with suspicion since the limit of reliable analysis using the FPD is about 1 ppmv and the ultimate detection limit is about 0.3 ppmv. Nevertheless, it is certain that pre-breakthrough concentrations in the range of 1 ppmv were achieved.

It is of interest to note that the pre-breakthrough concentrations shown in Figure 37 compare quite well to the previously published results of Meng and Kay (1987) at higher temperature. This is illustrated in Figure 38 where H_2S concentrations from the third sample of each of the Figure 37 tests have been added to the Meng and Kay data. While the feed gas compositions used by Meng and Kay and in this study are different, and both are different from the Shell gas composition used to establish the thermodynamic limits, the results are quite similar. The results of this series of tests clearly show that IGCC target limits of less than 20 ppmv H_2S can be achieved by the reaction of CeO_n ($n<2$) with H_2S.

6.2.2. The Effect of H_2S Concentration

FPD saturation occurred in about 25 minutes after only four or five samples when the feed gas contained 1% H_2S. In order to extend the duration of the pre-breakthrough period and obtain more data prior to breakthrough, the concentration of H_2S in the feed gas was reduced to 0.25%. At the same time the standard reduction-sulfidation temperature was reduced from 800°C to 700°C to take advantage of the lower pre-breakthrough concentration shown in Figure 37.

Results of duplicate tests at these new conditions are shown in Figure 39. Pre-breakthrough H_2S concentrations of 1 ppmv or less were achieved in both tests for about the first 120 minutes. Concentrations then increased rapidly to about 100 ppmv with an apparent secondary plateau in the 100 to 200 ppmv region until the runs were terminated.

Run Ce-215s01 was one of the few tests in which product gas flow was shifted to the TCD once FPD saturation was reached. The complete breakthrough curve for this run shown in Figure 40 confirms the existence of a second plateau in the 100 to 300 ppmv region which lasted until about 400 minutes when final breakthrough to the 2500 ppmv feed concentration occurred.

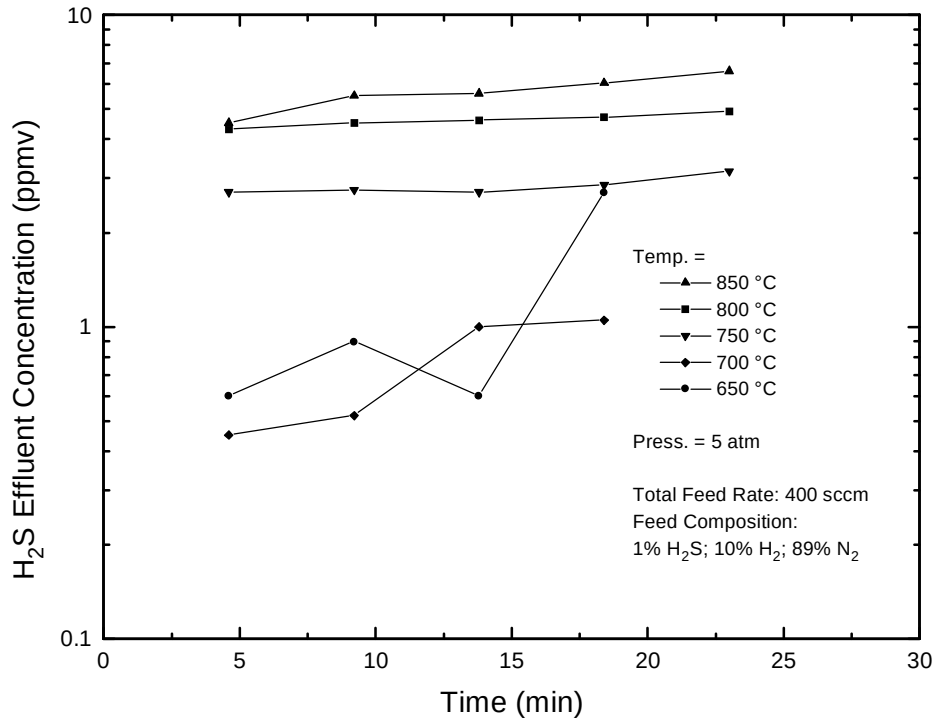

Figure 37. The Effect of Temperature on Prebreakthrough H_2S Concentration

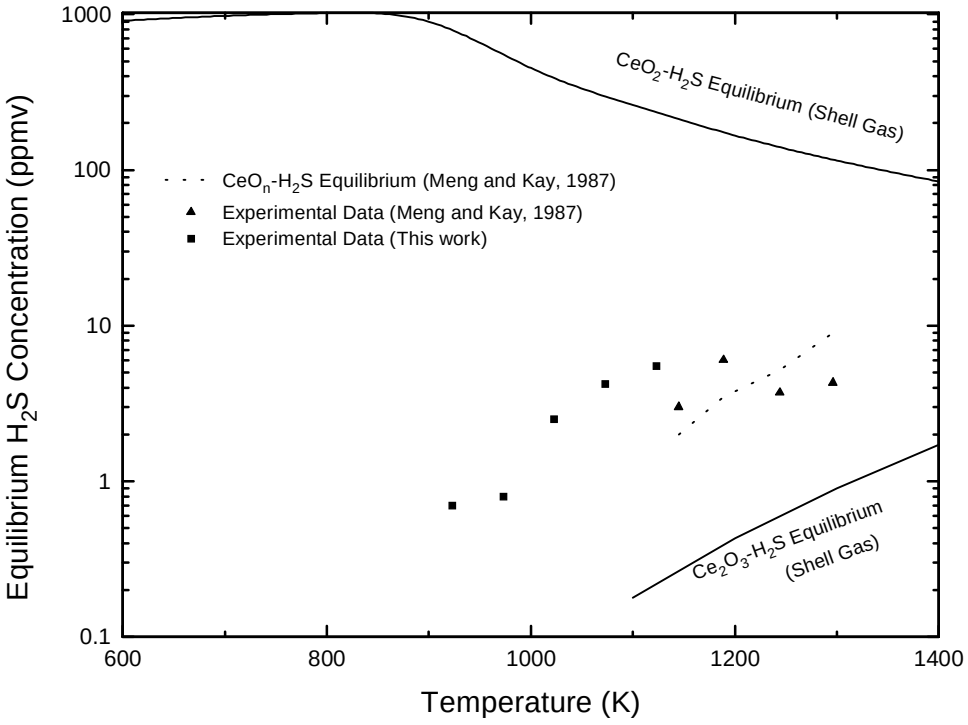

Figure 38. Comparison of Prebreakthrough H_2S Concentrations from This Work With Results from Meng and Kay (1987)

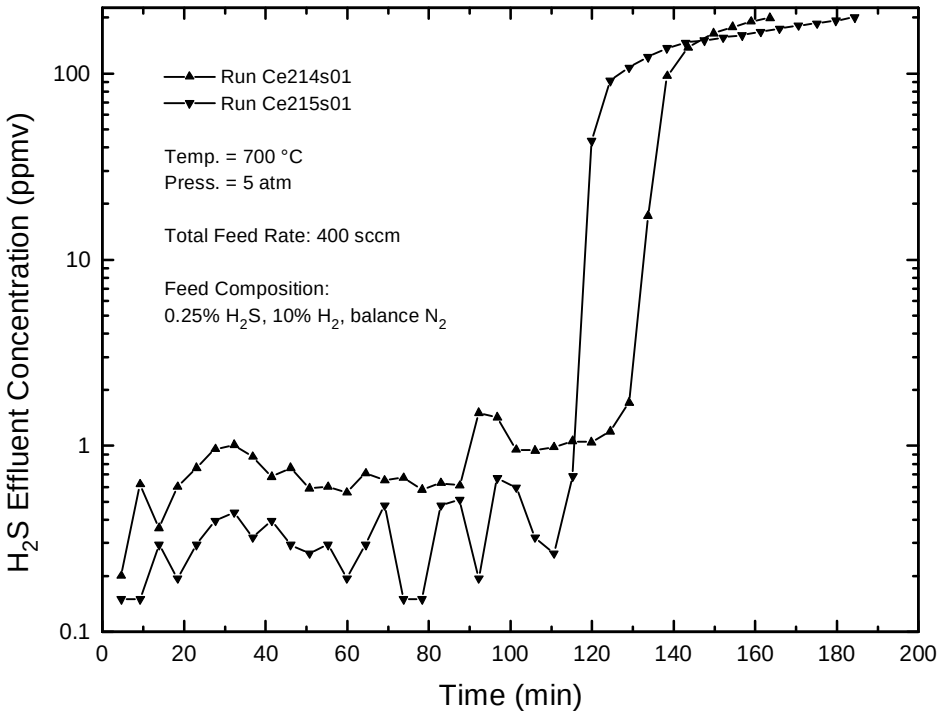

Figure 39. H_2S Breakthrough Curves With 0.25% H_2S in the Feed Gas

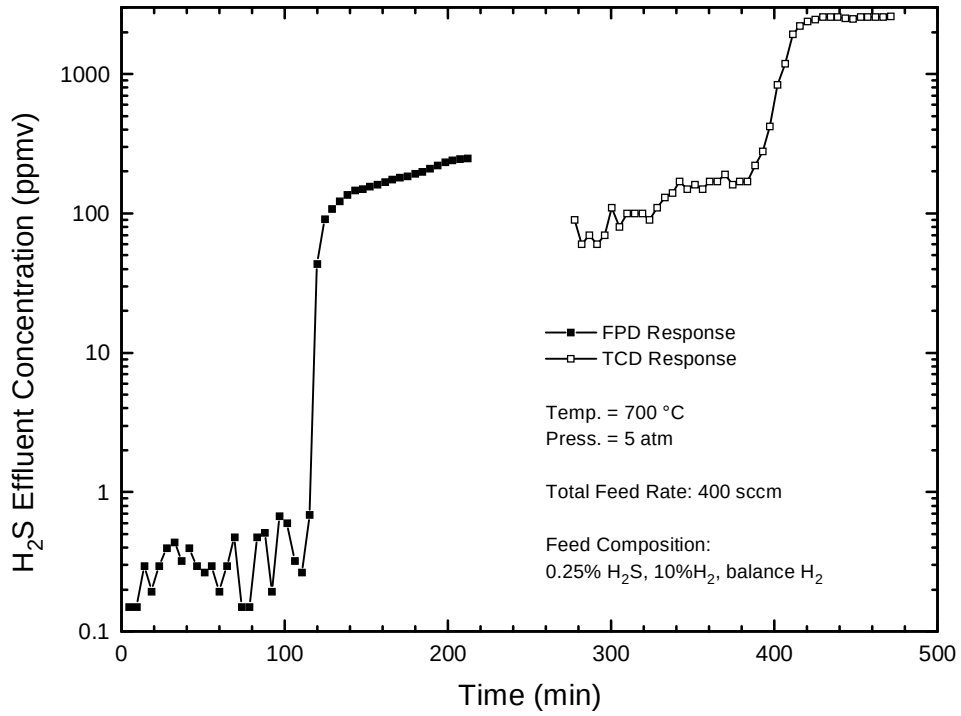

Figure 40. Complete H_2S Breakthorugh Curve Using Both the FPD and TCD

It must be stressed that concentrations near 100 ppmv from both the FPD and TCD should be treated with caution since 100 ppmv is near the saturation limit of the FPD and also near the lower detection limit of the TCD. Thus the apparent decrease in H_2S concentration following switching detectors may be attributed to analytical uncertainty.

6.2.3. The Effect of Volumetric Feed Rate

The effect of volumetric feed rate at 200, 400, and 800 sccm (SV = 1850, 3700, 7400 hr^{-1}) was investigated at 700°C and 5 atm using 0.25% in the feed gas. In addition, nonreacting tracer tests were carried out at the same conditions so that delay time corrections could be applied to the concentration-time data. Delay time is defined as the time interval between opening the valve to feed reactive gases and those gases reaching the chromatograph-sampling valve.

FPD results are shown in Figure 41 as a function of dimensionless time, t*. When H_2S removal is essentially complete, as it is in all of the pre-breakthrough data of Figure 41, t* is also equal to the fractional conversion of CeO_n to Ce_2O_2S. Thus we see that pre-breakthrough concentrations of about 1 ppmv were achieved at all flow rates, and that FPD breakthrough began at t* ~ 0.17 at 800 sccm, 0.31 at 400 sccm, and 0.32 at 200 sccm. However, at 200 sccm the H_2S concentration remained below 10 ppmv until t* ~ 0.41.

Results of similar tests to determine the effect of volumetric feed rate at 10 atm pressure were less satisfactory. Non-reacting tracer tests were also carried out at the higher pressure so that FPD breakthrough curves could be plotted as a function of dimensionless time. Five tests were made in this series with duplicate tests at both 400 and 800 sccm. Results are shown in Figure 42. Once again, all pre-breakthrough concentrations were below 5 ppmv and most were about 1 ppmv. However, the difference between presumably duplicate runs was greater than expected, and the effect of feed rate on breakthrough time agreed with expectation in only a qualitative way. FPD breakthrough began at t* ~ 0.39 at 200 sccm, at t* ~ 0.24 and 0.32 at 400 sccm, and t* ~ 0.22 and 0.35 at 800 sccm. In addition to the difference in duplicate runs, comparison of Figures 41 and 42 shows a much smaller effect of feed rate on initial breakthrough time. In particular, the effect of a feed rate change from 400 to 800 sccm was much smaller at 10 atm than at 5 atm.

In another pair of tests at constant temperature and pressure, the feed gas rate and H_2S concentration were varied simultaneously to produce constant H_2S feed rate with variable residence time. Reaction conditions for these tests were 700°C and 5 atm, with a feed rate of 800 sccm using 0.25% H_2S and 200 sccm using 1% H_2S. The reduced residence time provides less opportunity for the H_2S to react and should result in earlier breakthrough. FPD breakthrough curves from the tests on a dimensionless time basis are compared in Figure 43. At the small residence time (large feed rate) initial breakthrough occurred at t* ~ 0.17 and the FPD was saturated at t* ~ 0.20. With a four-fold increase in residence time (small feed rate) FPD breakthrough occurred at t* ~ 0.31. This result confirms that the sorbent can be more effectively utilized at the residence time increases.

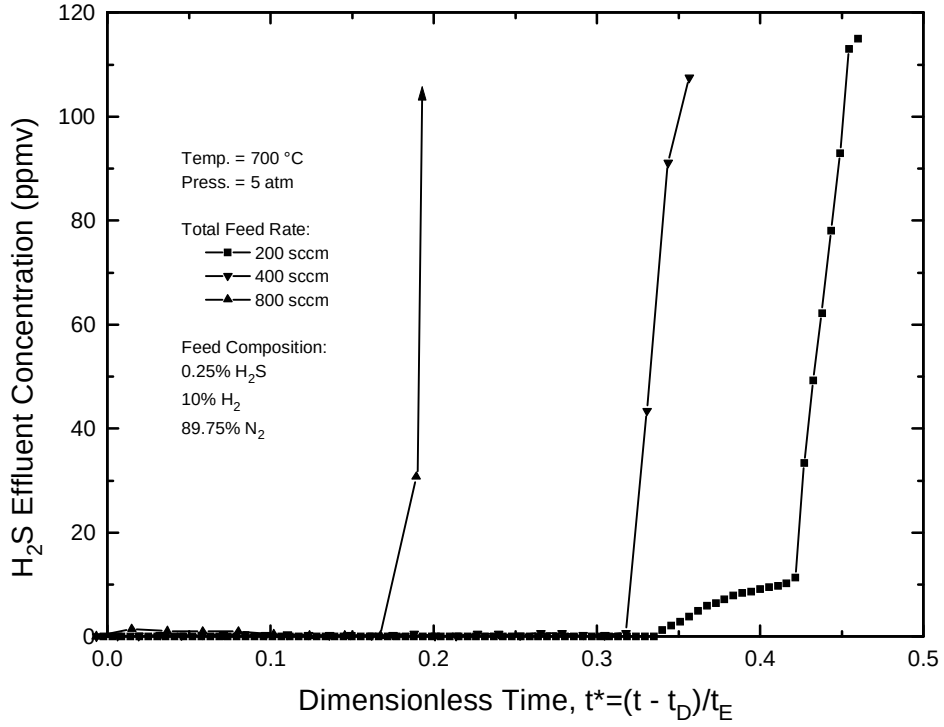

Figure 41. H_2S FPD Breakthrough Curves as a Function of Feed Rate: Dimensionless Time Basis

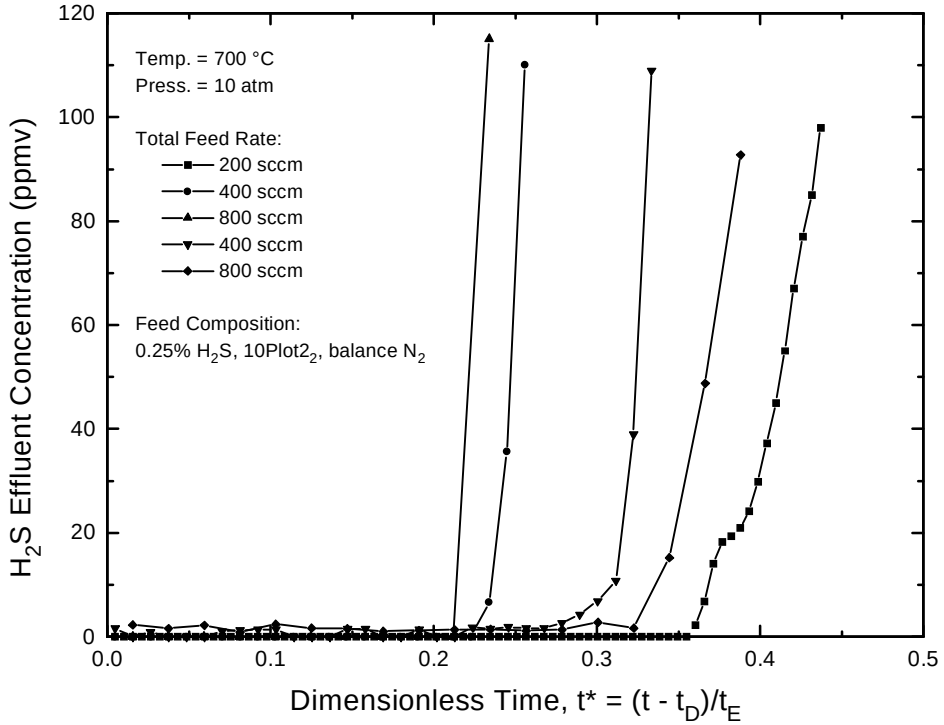

Figure 42. The Effect of Feed Rate at 10 atm Sulfidation Pressure: Dimensionless Time Basis

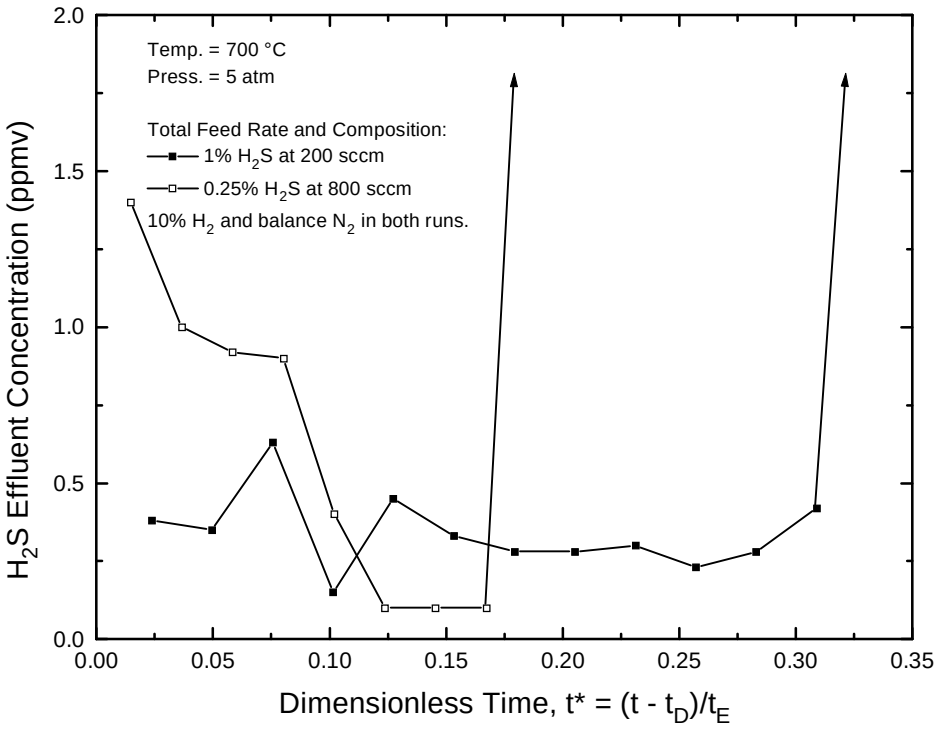

Figure 43. The Effect of Residence Time: Dimensionless Time Basis

6.2.4. The Effect of Pressure

The effect of pressure was studied in a series of tests at 700°C using 400 sccm of feed gas containing 0.25% H_2S. When the feed rate and temperature are constant, the H_2S feed rate is also constant and both the residence time in the sorbent bed and the H_2S concentration (mole/volume) are directly proportional to pressure. Delay time should increase with increasing pressure, but otherwise pressure should have little effect on initial breakthrough time. Experimental results did not agree, however, as shown in Figure 44 for tests at 5, 10, and 15 atm. Breakthrough at 5 and 10 atm both occurred after about 120 minutes, but the 200 minutes breakthrough time was totally different. As discussed in the introduction to this chapter, high pressure results, particularly at 15 atm, were often questionable. Malfunction of the mass flow controller valves because of the relatively small difference between the vapor pressure of H_2S and reactor pressure was suggested as a possible cause, but without proof. However, the results in Figure 44 suggest that the H_2S flow rate at 15 atm may have been less than intended.

6.2.5. Comparison of Results With and Without Pre-reduction

A separate reduction step preceding sulfidation was used in all FPD sulfidation runs described to this point. However, in a commercial system, this separate step would add to both the complexity and cost of a desulfurization process. Results of tests with and without prereduction, but otherwise the same reaction conditions, are compared in Figure 45. With prereduction the H_2S concentration remained near the 1 ppmv level for 115 minutes. Without

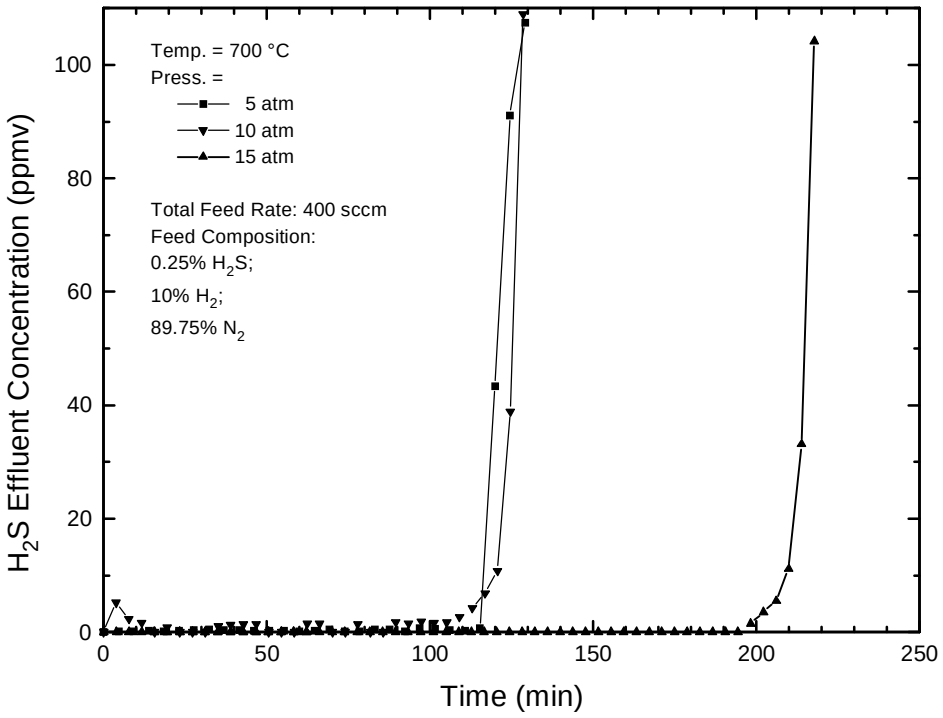

Figure 44. The Effect of Pressure at Constant Feed Rate

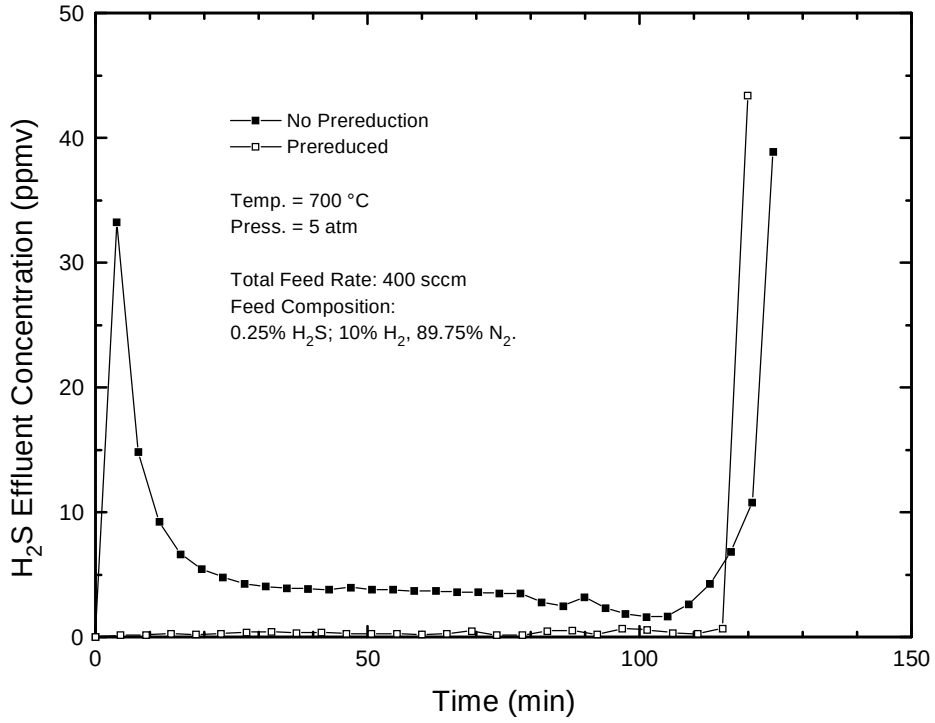

Figure 45. Comparison of Sulfidation Results With and Without Prereduction

prereduction, there was an early H_2S concentration peak at about 33 ppmv followed by a decrease to less than 5 ppmv between 23 and 115 minutes. FPD breakthrough occurred in both tests at about 120 minutes.

The following explanation is proposed to describe the difference in performance. With pre-reduction the entire bed consists of CeO_n ($n<2$) before being exposed to H_2S. The value of n depends on the temperature and H_2 concentration during reduction. Without pre-reduction, the entire bed is CeO_2 at the beginning of the test and reduction and sulfidation occur simultaneously. The early H_2S peak is associated with incomplete reduction. Because of the large ratio of H_2 to H_2S, reduction occurs downstream of the sulfidation reaction front and the subsequent reaction is between H_2S and CeO_m ($m<2$). We expect m to be larger than n which accounts for the reduced H_2S removal (5 ppmv vs 1 ppmv). With pre-reduction all CeO_2 is exposed to the full concentration of H_2 with no H_2O present. Without pre-reduction, the upstream reaction of H_2S consumes a small amount of H_2 and, more importantly, produces H_2O so that the reducing power of gas is decreased so that $m>n$. Even though sulfidation performance suffered somewhat without pre-reduction, the H_2S concentration was below the 20 ppmv IGCC target level during most of the pre-breakthrough period.

6.2.6. The Effect of Steam in the Feed Gas

In the final series of sulfidation tests, steam of varying concentrations was added to the reactor feed gas. Steam is expected to affect sulfidation performance in two ways - - first as a product of the sulfidation reaction and secondly by altering the reducing power of the gas. Three different feed gas compositions shown in Table 13 were used. The composition of the standard steam-free feed gas is also included for comparison. Compositions A and B were chosen to produce an equilibrium O_2 pressure approximately equal to that of Shell gas, and in composition C the H_2O and H_2 contents match those of Shell gas. However, no CO or CO_2 were included in composition C to avoid problems with carbon deposition. The product gas composition listed in Table 13 was calculated by assuming complete removal of H_2S with the corresponding changes in H_2 and H_2O. Equilibrium O_2 pressure was then calculated from the product gas composition using CHEMQ.

The equilibrium O_2 pressure at 700°C varied by a factor of approximately 20, with a minimum of 0.62×10^{-21} atm in composition A and a maximum of 12×10^{-21} atm in composition C. Note that the equilibrium pressure of O_2 in the standard feed gas is greater than in either compositions A or B. The increased H_2 in gases A and B more than compensated for the relatively small steam content of these gases. No pre-reduction step was included in any of the tests.

Results from sulfidation tests using gas compositions A and B are compared to results using the standard feed gas composition in Figure 46. The addition of H_2O at these levels had no negative impact. In both tests, the early H_2S peak was absent, pre-breakthrough H_2S concentrations were slightly smaller (~2 ppmv compared to ~5 ppmv), and the FPD breakthrough time was extended to 195 minutes from 120 minutes. All of the factors are attributed to the reduced O_2 pressure, i.e., the increased reducing power of the sulfidation gas.

Table 13. Composition and Equilibrium Oxygen Pressure at 700°C of Experimental Gases

	Experimental Gases			
	Ce232s01 Standard	Ce237s01 A	Ce238s01 B	Ce239s01 C
	Feed Comp., mol %			
H_2S	0.25	0.25	0.25	0.25
H_2O	0	2.5	3.5	6.5
H_2	10	50.25	50.25	28.25
CO	0	0	0	0
CO_2	0	0	0	0
N_2	89.75	47	46	65
	Product Comp., mol %			
H_2S	0	0	0	0
H_2O	0.5	3.0	4.0	7.0
H_2	9.75	50	50	28
CO	0	0	0	0
CO_2	0	0	0	0
N_2	89.75	47	46	65
Product, H_2/H_2O Ratio	19.5	16.7	12.5	4
Equil. O_2 Press, atm (at 700°C and 5 atm)	$8.5x10^{-21}$	$0.62x10^{-21}$	$1.1x10^{-21}$	$12x10^{-21}$

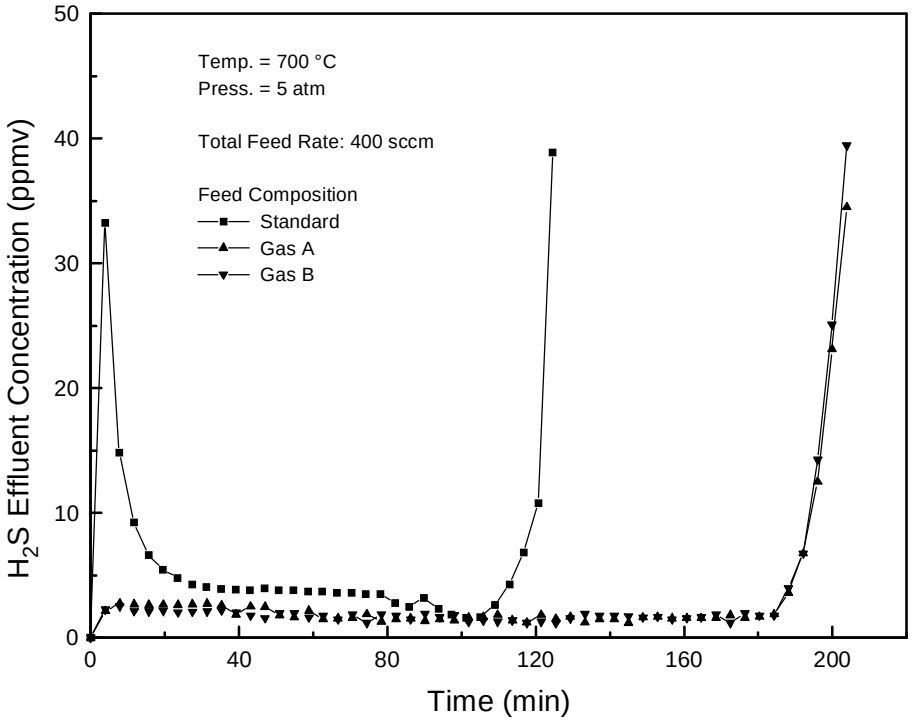

Figure 46. The Effect of Steam on Sulfidation Performance: Large H_2-to-H_2O Ratio

Gas composition C was fixed so that the H_2O and H_2 contents were approximately equal to the Shell gas. However, without CO and CO_2 in the gas, the equilibrium O_2 pressure was larger than that of the Shell gas. The relatively poor sulfidation results shown in Figure 47, in which the prebreakthrough H_2S concentration of about 70 ppmv lasted for only 20 minutes, may be attributed to the lower reducing power (higher O_2 pressure) of the experimental gas.

Two additional sulfidation tests, one at 700°C and the other 800°C were carried out using feed gas composition C. Both the FPD and TCD were used in these tests so that sulfidation was carried out to completion. Results are shown in Figure 48. The FPD became saturated after about 25 minutes in each test and the ensuing data gap is associated with the time required for the TCD to equilibrate after flow was switched from the FPD. During the early portions of the tests, the higher temperature (800°C) produced lower H_2S concentrations, about 10 ppmv versus 70 ppmv, but for a shorter time, 20 minutes versus 40 minutes. The concentration plateau following FPD breakthrough at 300-400 ppmv was clearly present in both runs. Finally, the TCD breakthrough time was effectively identical at 450 minutes in each test. Material balance closure in both tests was quite good with the amount of sulfur removed equal to 99% and 101% of stoichiometric at 700°C and 800°C, respectively.

6.3. Conclusions

The key to high efficiency desulfurization using cerium sorbent is high temperature and a highly reducing gas such as produced in the Shell gasification process. Under these conditions CeO_2 is reduced to CeO_n ($n<2$) which is capable of removing H_2S to concentrations which meet IGCC specifications. The temperature and gas composition which are required for high efficiency H_2S removal using cerium are outside the permissible operating window for zinc-based sorbents. In a Shell gas, ZnO would be reduced to volatile zinc vapor at temperature below the 700-800°C level used in the cerium sorbent desulfurization tests.

At 700°C using pre-reduced CeO_n, approximately 30% cerium conversion was achieved with H_2S concentrations in the product gas remaining near the 1 ppmv level. An intermediate H_2S concentration plateau near 300 ppmv, which is characteristic of the CeO_2-H_2S reaction, was then observed before final H_2S breakthrough occurred with cerium conversions approaching 100%. Similar results, except for slightly higher initial H_2S concentrations of about 5 ppmv, were observed when the sorbent was not pre-reduced, i.e., when reduction and sulfidation occurred simultaneously. Even though pre-reduction results in lower prebreakthrough H_2S levels, 5 ppmv H_2S is still within IGCC specifications, and pre-reduction may not be necessary.

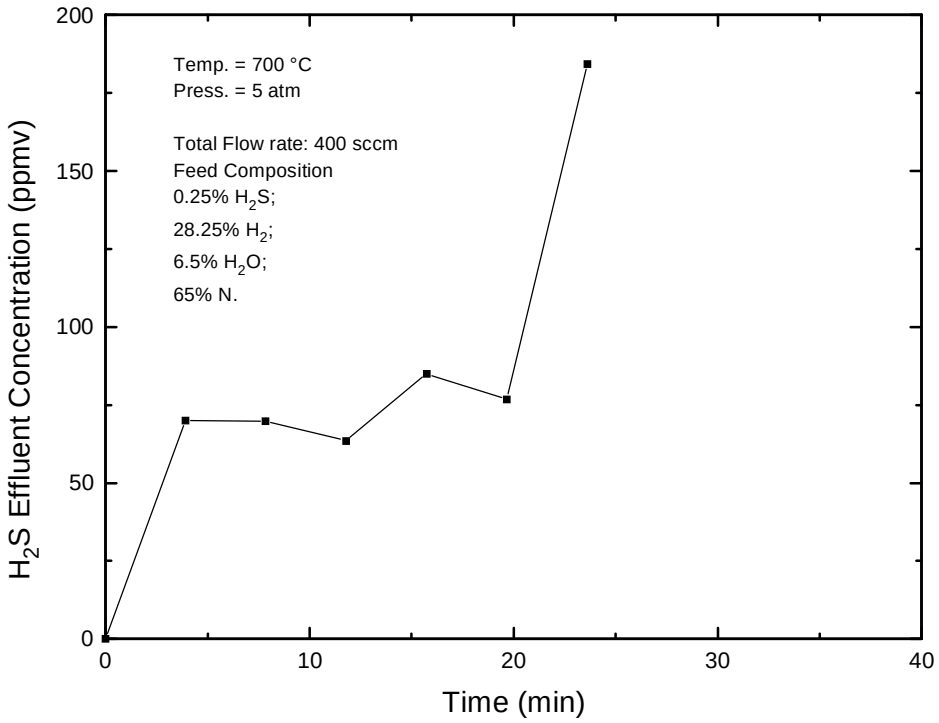

Figure 47. Sulfidation Breakthrough Curve Using Feed Gas Composition C

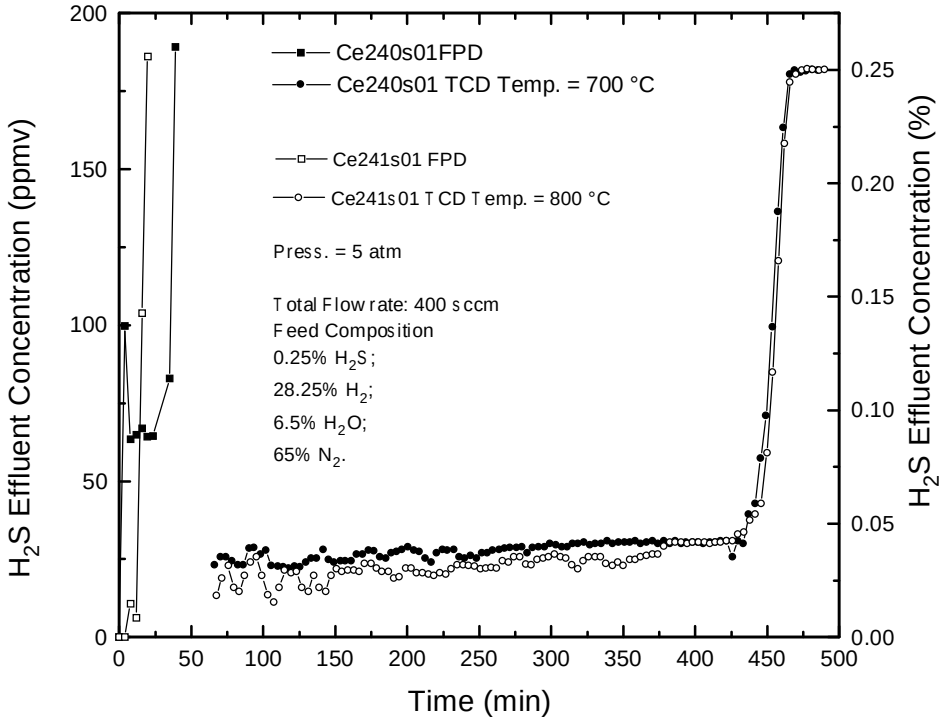

Figure 48. Complete (FPD + TCD) Sulfidation Breakthrough Curves Using Feed Gas Composition C

CHAPTER 7. MULTICYCLE TEST RESULTS

Two extended duration tests consisting of ten and twenty-five sulfidation-regeneration cycles were carried out to provide preliminary data on sorbent durability. In each test the sorbent charge consisted of 6.0g of Rhône Poulenc CeO_2, which had been pressed into tablets, crushed, and sieved. The CeO_2 was then mixed with 3.0g of Al_2O_3 and added to the reactor. Product gas analysis during the sulfidation phase of each cycle was achieved using the thermal conductivity detector (TCD). No effort was made to determine minimum pre-breakthrough H_2S concentrations using the flame photometric detector (FPD) since long-term trends in the overall sulfidation and regeneration breakthrough curves were of primary interest. Standard conditions shown in Table 14 were used in each cycle of all these tests.

Table 14. Sulfidation and Regeneration Reaction Conditions in Multicycle Tests Ce-116 and Ce-204

Sulfidation		Regeneration	
T, °C	800	T, °C	600
P, atm	5	P, atm	1
Feed Composition		Feed Composition	
% H_2S	1	% SO_2	12
% H_2	10	% N_2	88
% N_2	89		
Feed Rate, sccm	400	Feed Rate, sccm	200
Space Velocity, hr^{-1}	3700	Space Velocity, hr^{-1}	1850

7.1. Test Ce-116 (Cycles 01 through 10)

This multicycle test came early during the test program and provided the first indication of the durability of the cerium sorbent. It was during this test that reaction between H_2 in the sulfidation product gas with elemental sulfur deposited downstream of the sorbent bed in previous regeneration tests was discovered. Previously described cleaning procedures between regeneration and sulfidation phases were adopted during this multicycle test.

H_2S breakthrough curves for nine of the ten-sulfidation cycles are shown in Figures 49 and 50. An error was made in the sulfidation gas feed rate in cycle 01, and results from this cycle are not shown. Figure 49 shows the entire breakthrough curves while in Figure 50 the concentration scale has been expanded to emphasize H_2S concentration during the pre-breakthrough period. In sulfidation cycle 08 the H_2S mass flow controller failed after 175 minutes causing the H_2S feed rate to decrease which resulted in decreasing H_2S concentrations; the failure of the controller may have begun at an earlier time which would explain the earlier deviation of the cycle 08 breakthrough curve from the norm.

There was a wide variation in pre-breakthrough behavior, which is particularly evident in Figure 50. The pre-breakthrough H_2S concentration in cycle 02 of about 0.1% H_2S (1000 ppmv) corresponds to only 90% H_2S removal. However, in all other cycles the initial H_2S

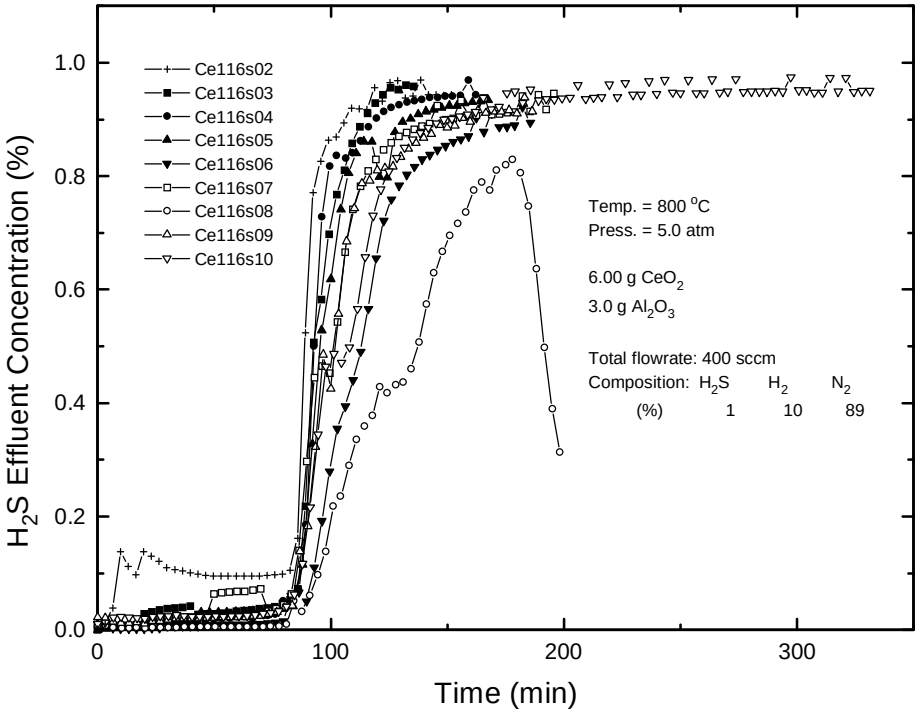

Figure 49. H_2S Breakthrough Curves from Test Ce-116 (Nine Cycles)

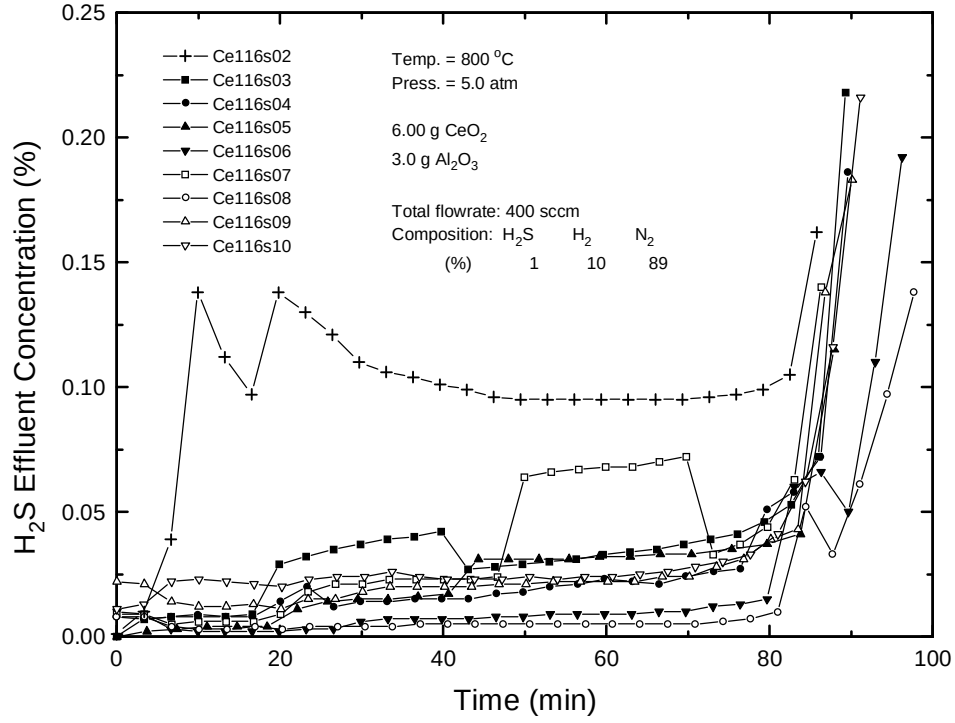

Figure 50. The Prebreakthrough Periods of Test Ce-116 (Nine Cycles)

concentrations were equal to or less than 0.025% (250 ppmv), and, with the exception of the unexplained upset in cycle 07 in the 50 to 70 minute period, the H_2S concentrations remained below 0.05% (500 ppmv, 95% removal) for about 80 minutes in each cycle. Of particular interest, the H_2S concentration in cycles 06 and 08 were below 150 ppmv for the first 80 minutes of the test.

The reaction between H_2 in the sulfidation product gas and sulfur deposited in the product lines during the previous regeneration cycle was discovered between cycles 02 and 03, and cleaning procedures were adopted at that time. It is clear from Figure 50 that the pre-breakthrough H_2S concentrations decreased significantly at that point.

The ten regeneration cycles used the same regeneration conditions (see Table 14). SO_2 breakthrough curves for all cycles are shown in Figure 51. With the exception of two samples - the first at 17 minutes in cycle 03 and the second at 10 minutes in cycle 10 - the results were effectively identical. The first measurable concentration of SO_2, about 1%, was detected after 10 minutes, and by 23 minutes regeneration was effectively complete. The steady-state SO_2 content of the product gas ranged from 11.8% to 12.2%, or within about 2% of the nominal feed concentration of 12.0%.

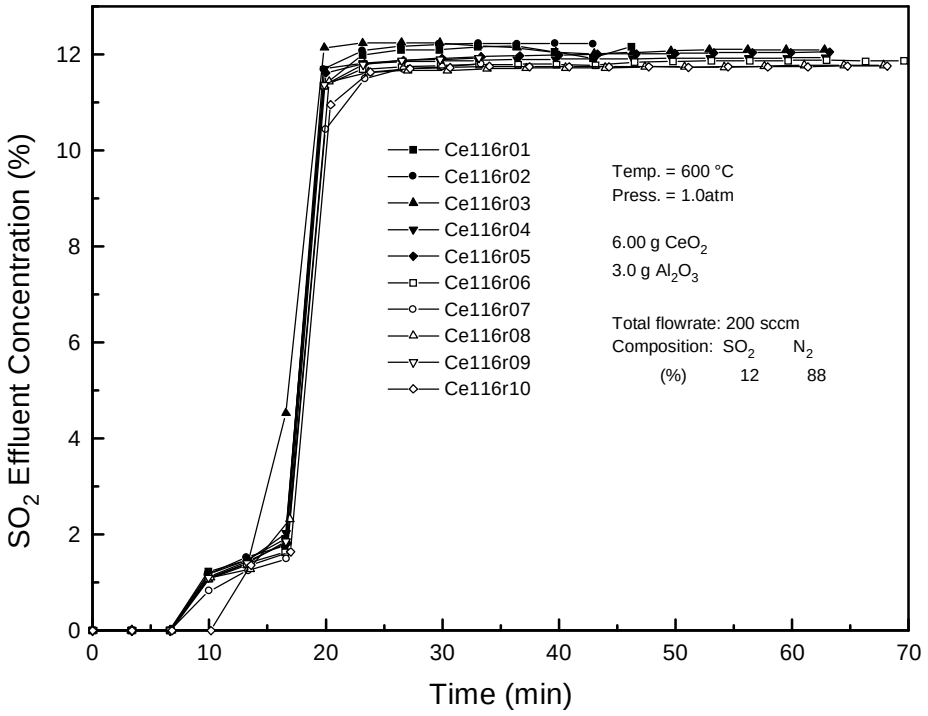

Figure 51. SO_2 Breakthrough Curves for the Ten Regeneration Cycles of Test Ce-116

Sulfur material balance results, expressed as percent of stoichiometric sulfur removed during sulfidation and liberated during regeneration, are presented as a function of cycle number in Figure 52. Sulfur removal ranged from a minimum of 82% of stoichiometric in cycle 02 to a maximum of 106% in cycle 10. The eight-cycle average was 96% of stoichiometric. Results from sulfidation cycles 01 and 08 are omitted because of the previously described problems with flow rates in those cycles. Results from the ten regeneration cycles ranged from a low of 95% of stoichiometric in cycle 03 to a maximum of 102% in cycle 10, and the ten-cycle average was 101%. There was no apparent decrease in sulfur removal or liberation as the number of cycles increased.

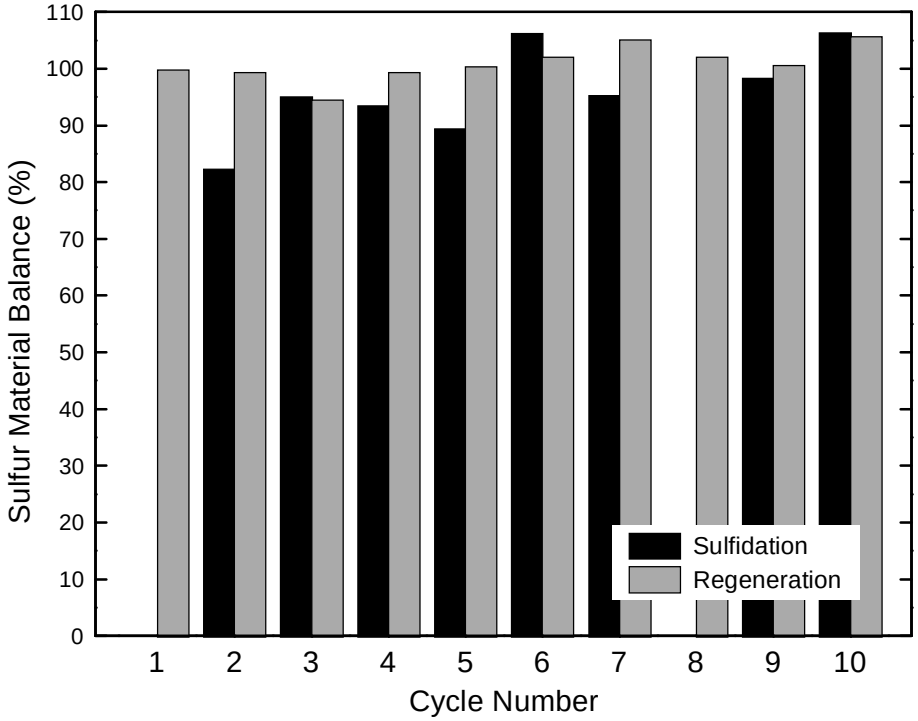

Figure 52. Percent Sulfur Removed During Sulfidation and Liberated During Regeneration: Test Ce-116

The overall results from this first multicycle test were quite favorable. The relatively constant slopes of the sulfidation and regeneration breakthrough curves, the minimal variation in $t_{0.5}$ with cycle number, and the good sulfur material balance closure during sulfidation and regeneration all suggested that little, if any, sorbent deterioration occurred.

7.2. Test Ce-204 (Cycles 01 through 25)

This twenty-five cycle test, which occurred near the end of the experimental program, used "standard" sulfidation and regeneration conditions (see Table 14) in each cycle. In addition, the sorbent was pre-reduced before each sulfidation cycle and the reactor was carefully cleaned after each regeneration. The overall procedure was as follows:

1. Reduction at 800°C and 5 atm. In cycles 01 through 15 the reduction gas contained 10% H_2 in N_2 at a flow rate of 400 sccm. In the remaining cycles, reduction was carried out in 100% H_2 at a flow rate of 50 sccm. Reduction was generally carried out overnight.

2. Each sulfidation cycle was carried out to completion and typically required about 2 hours. Contact between the product gas and stainless steel was minimized by using the teflon-lined transfer line and eliminating the condenser and all but one of the filters upstream of the back pressure regulator. Teflon tubing was used between the back pressure regulator and the chromatograph sampling valve. Stainless steel in contact with the sulfidation product gas consisted of three fittings, one filter, the backpressure regulator, the chromatograph sampling valve, and the housing of the TCD, which was used for all gas analysis. Only two of the fittings were at high temperature.

3. The bed temperature was decreased to 600°C under nitrogen. During this time the teflon-lined product line was removed and replaced with the heat-traced stainless steel line, condenser, and series of filters.

4. Regeneration was continued until the SO_2 content of the product gas reached 12%, typically about 30 minutes. The backpressure regulator was removed during the atmospheric pressure regenerator tests so that it would not be contaminated with sulfur during the next sulfidation cycle. The only stainless steel parts exposed to both sulfidation and regeneration product gases were one fitting, the sampling valve, and the TCD housing.

5. Cleaning with the reactor at 800°C and the product line at 350°C, both at 5 atm, using air at 50 sccm. The purpose of this oxidation step was to remove, to the extent possible, all sulfur species deposited downstream of the sorbent bed.

Complete H_2S breakthrough curves for the 25 sulfidation cycles as shown in Figure 53. Results of a nonreacting H_2S tracer test at the same conditions are shown for comparison. All concentration-time curves were similar except for the following. In the 20 to 90 minute range the H_2S concentration in cycle 01 was clearly larger than in any of the remaining cycles. In the same time range the H_2S concentrations in cycles 02 through 15 were closely bunched at an intermediate level, while in cycles 16 through 25 the H_2S concentration was below the TCD detection limit for the first 80 minutes. These features are more clearly shown in Figure 54 where the concentration scale is expanded to emphasize results during the early reaction period. The improvement between cycles 15 and 16 is due to the switch from 10% H_2 to 100% H_2 during the reduction step. However, it is not clear whether the decreased pre-breakthrough concentration resulted from improved reactor cleaning or from increased reduction of CeO_2 or a combination of both.

The time, $t_{0.5}$, required for the product H_2S concentration to reach one-half of the feed concentration is shown as a function of cycle number in Figure 55. Results from cycle 16 are omitted because of mass flow controller problems experienced in that cycle. $t_{0.5}$ ranged from 97

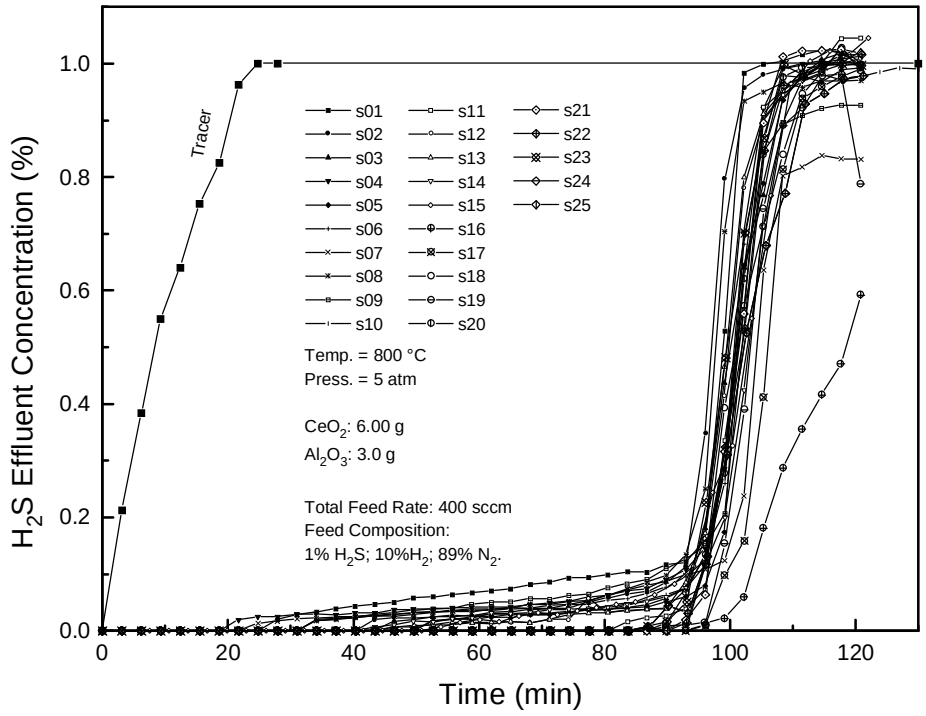

Figure 53. Sulfidation Breakthrough Curves for the Twenty-Five Cycles of Test Ce-204

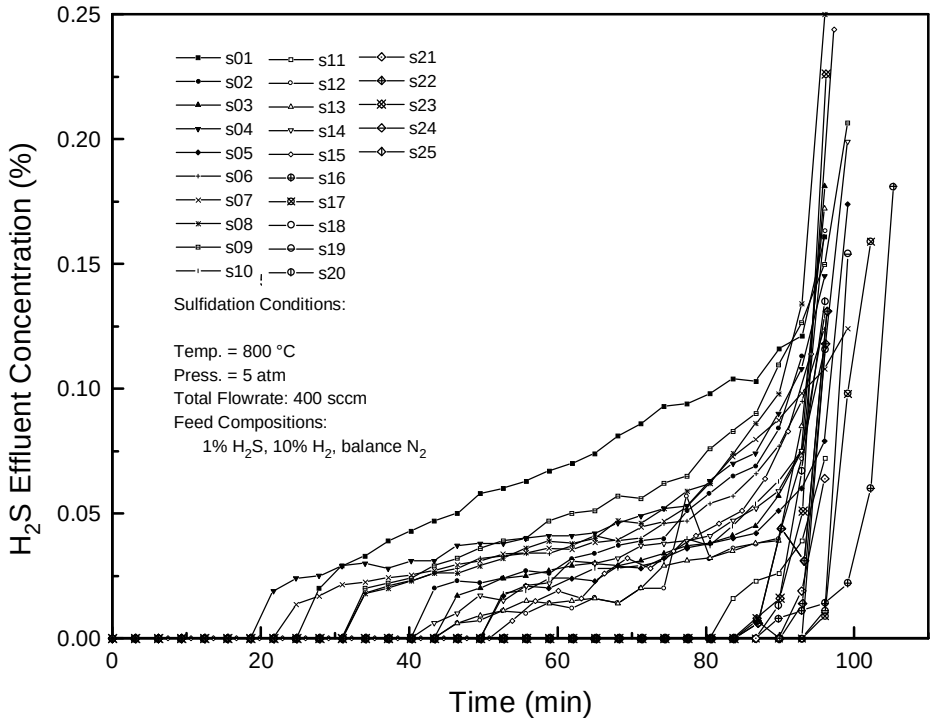

Figure 54. Sulfidation Prebreakthrough Curves for the Twenty-Five Cycles of Test Ce-204

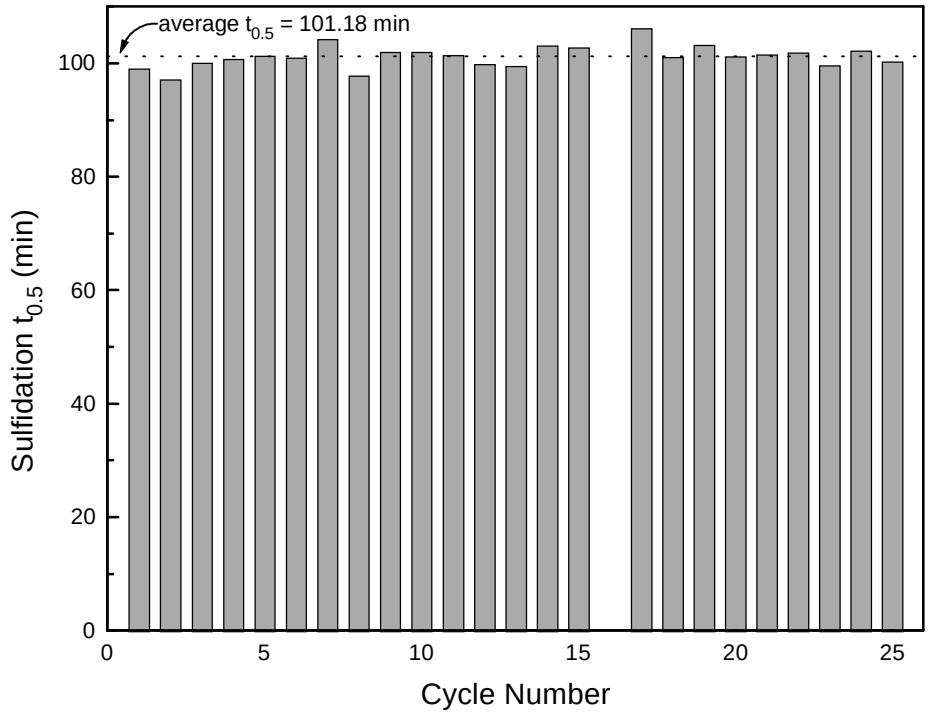

Figure 55. $t_{0.5}$ Versus Cycle Number for the Twenty-Five Sulfidation Cycles of Test Ce-204

minutes in cycle 02 to 110 minutes in cycle 17. The 24-cycle average was 101 minutes and there was no indication of a decrease in $t_{0.5}$ with increasing cycle number.

Numerical integration of the area between the H_2S breakthrough curves and the nonreacting tracer result shown in Figure 53 was used to calculate the overall percent conversion of the sorbent to Ce_2O_2S at the conclusion of each sulfidation cycle. These results are presented in Figure 56. The smallest conversion, 95% of stoichiometric, occurred in cycle 01 while the largest (omitting cycle 16), 108% of stoichiometric, occurred in cycle 17. The 25-cycle average was 101.9% of stoichiometric.

Regeneration conditions were constant in each cycle at the standard conditions shown in Table 14. SO_2 breakthrough curves from each regeneration cycle along with results from a nonreacting tracer test are shown in Figure 57. Results from cycle 08 are omitted because of elemental sulfur plugging problems. Complete regeneration was achieved in that cycle, however, as shown by the cycle 09 sulfidation results. Plugging also occurred near the end of cycles 06 and 10, but results from these cycles are included because regeneration was effectively complete before the problem occurred. $t_{0.5}$ corresponding to 6% SO_2 in the regeneration product gas is shown for each cycle in Figure 58. Results from cycle 08 are omitted. $t_{0.5}$ varied from 20.6 minutes in cycle 01 to 23.0 minutes in cycle 06. The 24-cycle average was 21.9 minutes and, once again, there was no evidence of performance deterioration in the latter cycles.

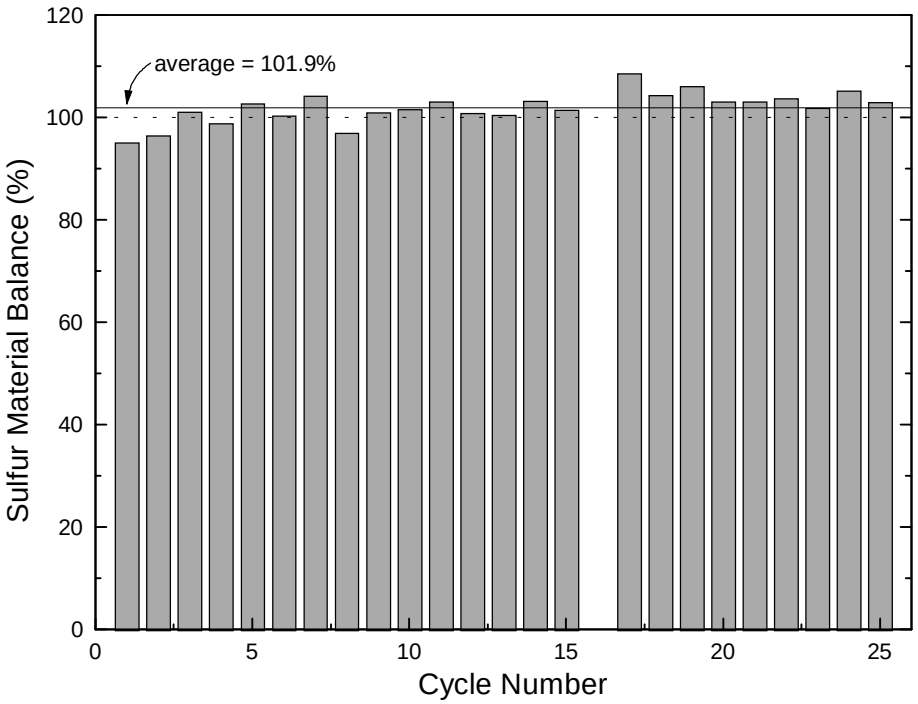

Figure 56. Percent Conversion of Sorbent to Ce_2O_2S in the Twenty-Five Sulfidation Cycles of Test Ce-204

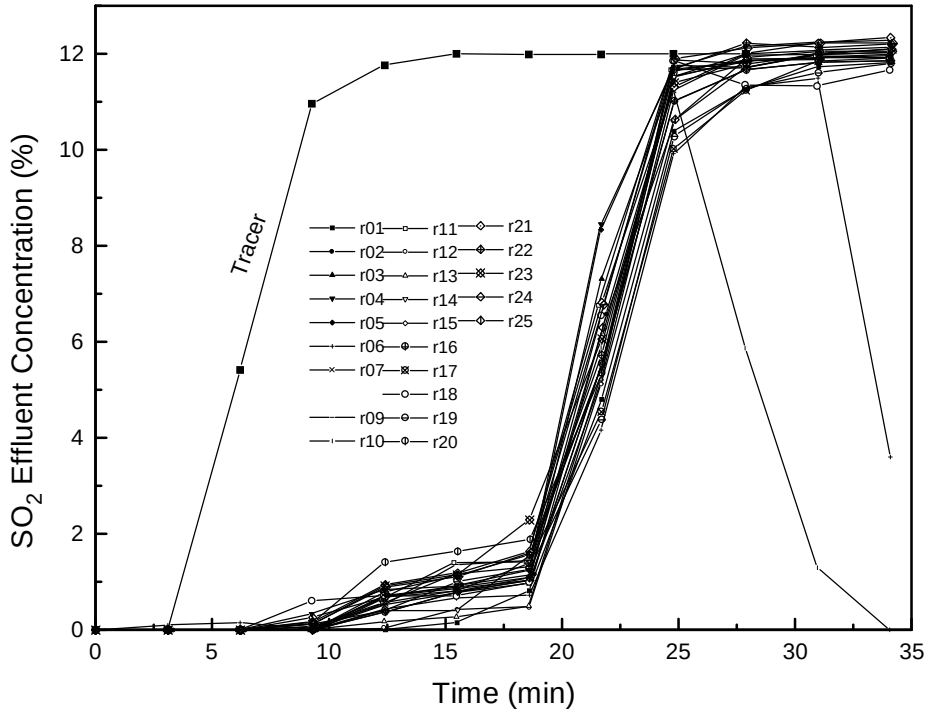

Figure 57. Regeneration Breakthrough Curves for the Twenty-Four Cycles of Test Ce-204

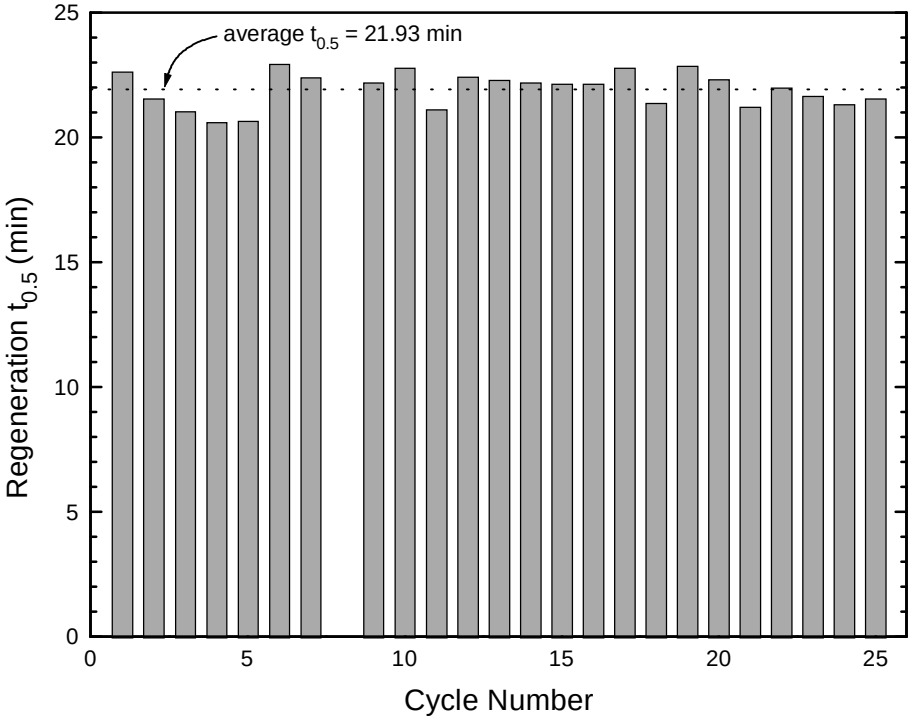

Figure 58. $t_{0.5}$ Versus Cycle Number for the Twenty-Five Regeneration Cycles of Test Ce-204

Percent conversion of Ce_2O_2S to CeO_2 for each cycle based on numerical integration is shown in Figure 59. Results ranged from 91% in cycle 05 to 109% in cycle 06 with a 24-cycle average of 98%. The scatter in the regeneration results is somewhat larger than in sulfidation because only 9 or 10 data points were collected during a regeneration cycle compared to about 40 data points during sulfidation. Nevertheless, the agreement between the sulfidation and regeneration results is felt to be quite good.

7.3 Conclusions

Two sorbent durability tests, the first consisting of ten sulfidation-regeneration cycles and the second of twenty-five cycles, showed exceptional reproducibility during sulfidation and regeneration. There was no apparent decrease in sorbent activity as measured by either breakthrough time or sulfur capacity. Cycle-to-cycle variation appeared to be random.

Particularly impressive were the results from the twenty-five-cycle test. This test extended over fifty-eight days, during which the sorbent was continually exposed to a temperature of at least 600°C with the temperature being 800°C for approximately 90% of that time. The sorbent was alternately exposed a H_2/N_2 atmosphere during reduction, $H_2S/H_2/N_2$ during sulfidation, SO_2/N_2 during regeneration, air during cleaning, and N_2 purge between each phase.

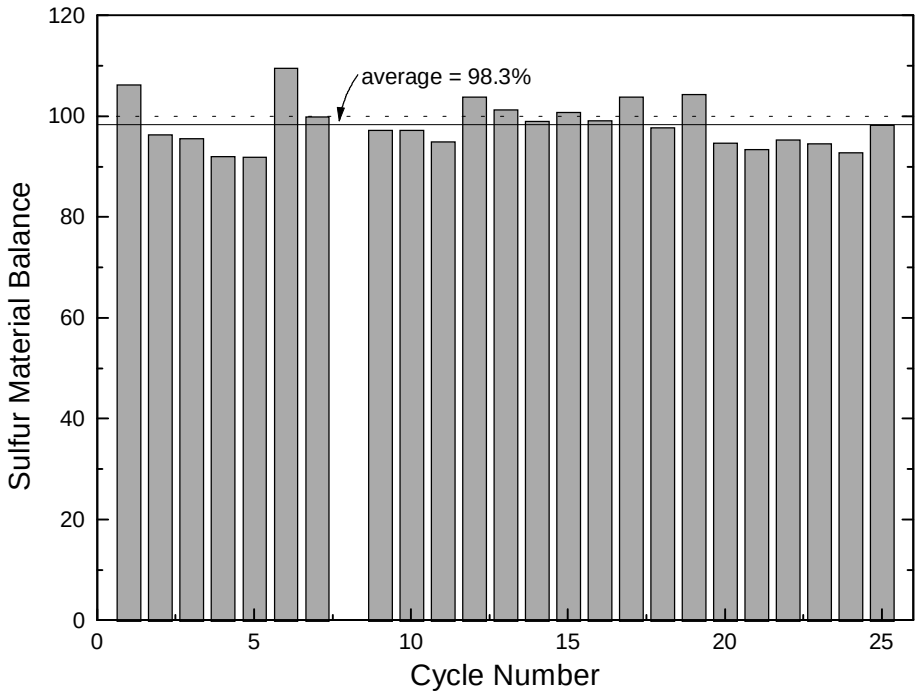

Figure 59. Percent Conversion of Ce_2O_2S to CeO_2 in the Twenty-Five regeneration Cycles of Test Ce-204

This durability was achieved using a physical mixture of CeO_2 and Al_2O_2 without the addition of binders or surface area enhancers. Pretreatment consisted only of hydraulically pressing the CeO_2 into tablets, and subsequently crushing and sieving the tablets for particle size control. This step was required only because the extremely small particle size of the as-received CeO_2 resulted in excessive pressure drop across the sorbent bed. These initial durability results stand in stark contrast to the years of sorbent development research required to develop a zinc-based sorbent having satisfactory durability.

CHAPTER 8. RESULTS USING OTHER CeO_2 SOURCES

Five additional sources of CeO_2 were tested to compare results with the standard Rhône Poulenc CeO_2, which had been used in all tests described to this point. Brief descriptions of the alternate CeO_2 sorbents are found in Table 15. Two of the alternate sorbents, designated MC and MCC, were obtained from Molycorp while the remaining three, WGW1, WGW2, and WGW3, were obtained from Gas Desulfurization Corporation and were prepared by Engelhard by depositing CeO_2, or CeO_2 + La_2O_3, on porous Al_2O_3 spheres of approximately 1/8 inch diameter. These spherical pellets were crushed and sieved to 150 to 300 microns, the same particle size as used in the Rhône Poulenc CeO_2 tests. While no surface area data are available on the WGW sorbents, we expect relatively high surface areas to be associated with the Al_2O_3 support. Sorbent MC was 96% CeO_2 which was tableted, crushed, sieved and then mixed with Al_2O_3 using the same procedure as used with the Rhône Poulenc CeO_2. However, as noted in Table 15, the specific surface area was less than 10% of the Rhône Poulenc CeO_2. Sorbent MCC consisted of $Ce_2(CO_3)_3$ which was calcined to CeO_2 prior to sulfidation. In one test the carbonate was calcined externally in a tube furnace and then mixed with Al_2O_3 and charged to the reactor. In another test, the carbonate was calcined in the reactor after being mixed with Al_2O_3. While no data are available on the surface areas of either the carbonate precursor or the oxide product, we hoped that calcination would produce high surface area CeO_2.

MC sorbent was used in one four-cycle tests in the early phases of the test program when sorbent regeneration performance was of primary interest; the TCD was used for product gas analysis during sulfidation and regeneration cycles. Results of this multicycle test are presented in the following section of this chapter. Other tests using the alternate sorbents were carried out in the latter stages of the test program when the FPD was used for product gas analysis and minimum pre-breakthrough H_2S concentrations were of primary interest. Results from these tests are combined into a single section within this chapter.

8.1. Results From Test Ce-123 Using MC Sorbent

Standard sulfidation and regeneration reaction conditions were used in this four-cycle test. The TCD was used for product gas analysis during both the sulfidation and regeneration cycles.

Figure 60 compares the early portions of the sulfidation breakthrough curve from the first cycle of Ce-123 with data from a test using Rhône Poulenc sorbent at the same reaction conditions. Similar cleaning procedures were followed prior to each test to minimize H_2S formed by reaction of H_2 with elemental sulfur deposited during the previous regeneration test. H_2S concentrations were equal to or less than 200 ppmv for the first 30 minutes of each test. Thereafter, the H_2S concentration in test Ce-123 increased rapidly while the concentration remained below 300 ppmv for 80 minutes using Rhône Poulenc sorbent. By the time active breakthrough began with Rhône Poulenc CeO_2, the H_2S concentration had increased to about 1500 ppmv using Molycorp CeO_2.

Table 15. Alternate CeO_2 Sorbents

Designation	Description
RP	CeO_2 from Rhone Poulenc was used in all tests prior to those described in this chapter. Electrobalance tests showed that this sorbent contained 9% volatiles. The powder was hydraulically pressed into tablets at 20,000 psi, and the tablets were subsequently crushed and sieved with the 150-300 micron particles used in reaction tests. The surface area of the fresh sorbent (after tableting, crushing, and sieving) was 156 m^2/g.
MC	96% CeO_2 from Molycorp. This sorbent was pressed into tablets which were subsequently crushed and sieved in a manner similar to that used for Rhone Poulenc sorbent. However, the surface area after tabletting, crushing, and sieving was only 11 m^2/g.
MCC	Cerium carbonate, $Ce_2(CO_3)_3$, from Molycorp served as the CeO_2 precursor in two tests. In one test (Ce-235) 10g of the as-received $Ce_2(CO_3)_3$ was mixed with 3.0 g of Al_2O_3 and the mixture was calcined inside the reactor at 700EC in N_2. The 6.6g of CeO_2 shown in Table 17 for this run is based on measured weight loss at 200°C (presumably H_2O) followed by the presumption of complete calcination of pure $Ce_2(CO_3)_3$ to $2CeO_2$. In test Ce-236, $Ce_2(CO_3)_3$ was calcined at 750°C in air in a tube furnace outside the reactor. 6.0g of the calcined product was then mixed with 3.0g of Al_2O_3 and added to the reactor.
WGW1	This sorbent was supplied by Gas Desulfurization Corp. and consisted of 22% (wt) CeO_2 deposited on Al_2O_3 substrate. The as-received sorbent was in the form of 1/8-inch diameter spheres which were crushed and sieved for use in tests Ce-226 and Ce-228.
WGW2	This sorbent was also obtained from Gas Desulfurization Corp. and was similar to WGW1 except that La_2O_3 as well as CeO_2 was deposited on the Al_2O_3 substrate. The composition (wt.%) was reported to be 18.2% CeO_2, 3.8% La_2O_3, and 78% Al_2O_3. This sorbent was also in the form of 1/8-inch diameter spheres, and was treated in the same manner as WGW1.
WGW3	This sorbent was similar to WGW1 except for a high loading of 50% CeO_2. This sorbent was received as 1/8-inch diameter spheres and was handled in the same manner as the other sorbents from Gas Desulfurization Corp. It was used in test Ce-231.

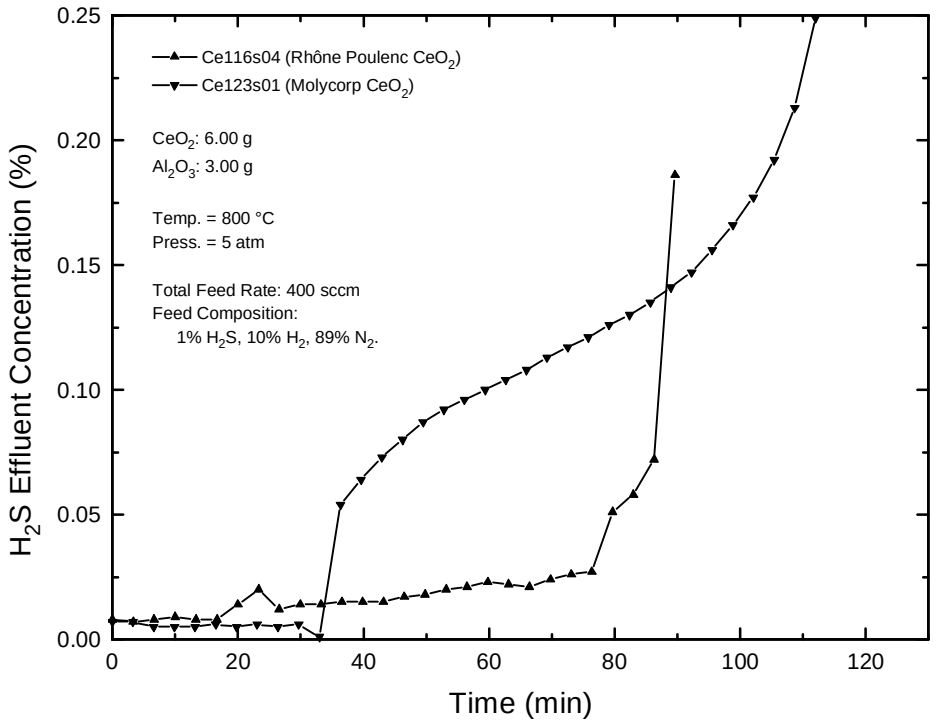

Figure 60. Comparison of Prebreakthrough Periods of Sulfidation Tests Using CeO_2 from Rhône Poulenc and Molycorp

The complete H_2S breakthrough curves for the four sulfidation cycles of test Ce-123 are compared in Figure 61. All show the same general characteristics with H_2S concentrations near the 100 ppmv level for about 30 minutes, followed by a plateau at the 1000 to 2000 ppmv level between 30 and 100 minutes, and then final breakthrough to complete sulfidation after about 150 minutes. Significantly, the slope of the curve during the active breakthrough period was considerably smaller using MC sorbent. The duration of the active breakthrough period was about 50 minutes using Molycorp sorbent compared to about 30 minutes using Rhône Poulenc sorbent. There is also an indication of minor performance deterioration over the four cycles. Active breakthrough occurred about 10 minutes earlier in cycle 04 than in cycle 01. In addition the quantity of sulfur removed decreased by about 6% from cycle 01 to cycle 04.

Figure 62 compares the regeneration breakthrough curves from cycle 01 of test Ce-123 with a regeneration curve at the same reaction conditions using Rhône Poulenc sorbent. The results were similar. No SO_2 was detected in the first two samples of both tests. However, the slope of the SO_2 breakthrough curve was somewhat smaller using Molycorp sorbent. Results from three of the four regeneration cycles of test Ce-123 are presented in Figure 63. No results for the third cycle are included because of mass flow controller problems. The regeneration results were effectively equal with no SO_2 detected in the first two samples, about 2% SO_2 in samples three through five, and complete regeneration by sample 8 after 27 minutes. Sulfur material balance results in the three cycles were quite reproducible and were in reasonable agreement with the sulfidation cycles of this test.

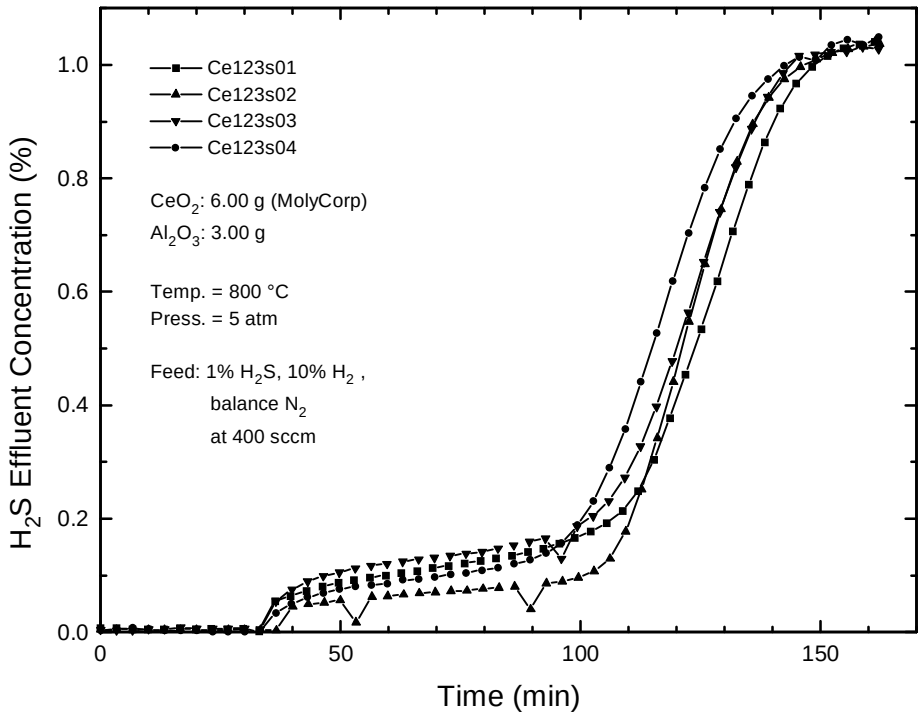

Figure 61. Sulfidation Breakthrough Curves from the Four Cycles of Test Ce-123 (Molycorp CeO_2)

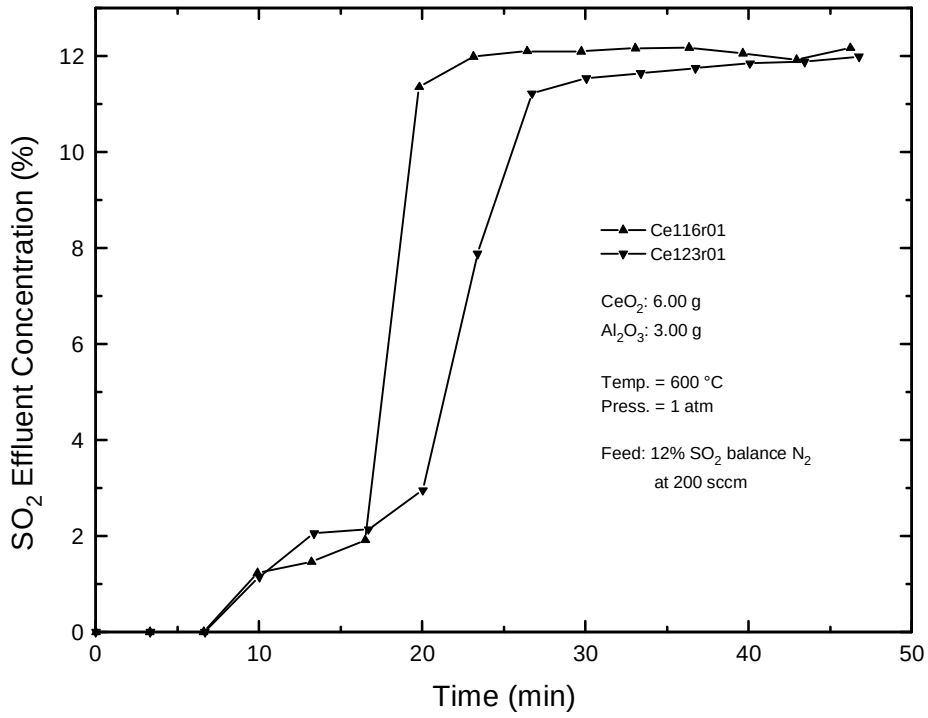

Figure 62. Comparison of the Regeneration Breakthrough Curves Using CeO_2 from Rhône Poulenc and Molycorp

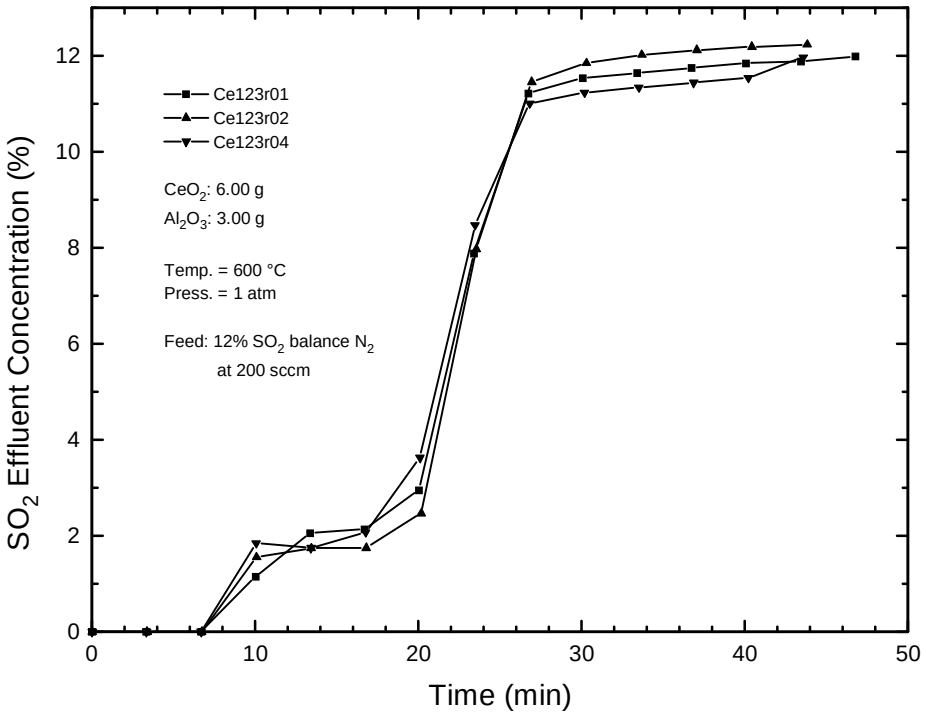

Figure 63. Regeneration Breakthrough Curves from Three of the Four Cycles of Test Ce-123 (Molycorp CeO_2)

Although the performance of the Molycorp CeO_2 in this multicycle test was reasonably good, it was somewhat inferior to the performance of Rhône Poulenc CeO_2. The initial breakthrough during sulfidation occurred at an earlier time and the slope of the active breakthrough curve was somewhat smaller during sulfidation and regeneration. The probable explanation is the difference in surface areas of the two sorbents. The surface area of as-received Rhône Poulenc sorbent was 220 m^2/g compared to 9.6 m^2/g for as-received Molycorp CeO_2. The surface area of the CeO_2-Al_2O_3 mixture charged to the reactor was 156 m^2/g for Rhône Poulenc compared to only 11.2 m^2/g for Molycorp.

8.2. Sulfidation Test Results Using Other CeO_2 Sorbents

The remaining tests using the other CeO_2 sorbent materials were performed during the latter stages of the test program when determination of the minimum pre-breakthrough H_2S concentration was of primary interest. No regeneration tests were included and the sulfidation tests were terminated when the FPD became saturated. The sorbent used and reaction conditions for each test are presented in Table 16. A pre-reduction step was included in only two of the nine tests (Ce-228 using WGW1 sorbent and Ce-229 using WGW2 sorbent). Sulfidation and, when appropriate, pre-reduction temperature was 700°C except in Ce-243 where the temperature was 800°C. The feed gas contained 0.25% H_2S/10% H_2/balance N_2 except in test Ce-243 where the feed contained H_2 and H_2O in proportions equal to those found in Shell gas. The feed gas flow rate was either 200 sccm or 400 sccm. The quantity of CeO_2 was variable in each test, and, particularly with sorbents WGW1 and WGW2, was significantly less than the standard quantity of 6.0g used in tests with Rhône Poulenc CeO_2.

Table 16. Summary of Reduction-Sulfidation Conditions Using Alternate CeO_2 Sorbents

Test	Ce-226	Ce-227	Ce-228	Ce-229	Ce-230
Sorbent, g	WGW1	WGW2	WGW1	WGW2	WGW3
CeO_2	2.2	1.8	2.2	1.8	5.0
La_2O_3	–	0.4	–	0.4	–
Al_2O_3	7.8	7.8	7.8	7.8	5.0
Pre-Reduction	None	None	Yes	Yes	None
Temp., °C	–	–	700	700	–
Press., atm	–	–	5	5	–
Gas Comp., $\%H_2$	–	–	10	10	–
$\% N_2$	–	–	90	90	–
Sulfidation					
Temp., °C	700	700	700	700	700
Press., atm	5	5	5	5	5
Gas Comp., $\%H_2S$	0.25	0.25	0.25	0.25	0.25
$\% H_2$	10	10	10	10	10
$\% H_2O$	0	0	0	0	0
$\% N_2$	89.75	89.75	89.75	89.75	89.75
Feed Rate, sccm	200	200	400	400	400
Space Velocity, hr^{-1}	1850	1850	3700	3700	3700

Test	Ce-231	Ce-235	Ce-236	Ce-243
Sorbent, g	MC	MCC	MCC	WGW2
CeO_2	6.0	6.6	6.0	1.8
La_2O_3	–	–	–	0.4
Al_2O_3	3.0	3.0	3.0	7.8
Pre-Reduction	None	None	None	None
Temp., °C	–	–	–	–
Press., atm	–	–	–	–
Gas Comp., $\%H_2$	–	–	–	–
$\% N_2$	–	–	–	–
Sulfidation				
Temp., °C	700	700	700	800
Press., atm	5	5	5	5
Gas Comp., $\%H_2S$	0.25	0.25	0.25	0.25
$\% H_2$	10	10	10	28.25
$\% H_2O$	0	0	0	6.5
$\% N_2$	89.75	89.75	89.75	65
Feed Rate, sccm	400	400	400	400
Space Velocity, hr^{-1}	3700	3700	3700	3700

Results from two tests using WGW1 sorbent are compared in Figure 64. No pre-reduction step was included in test Ce-226 and the feed rate was 200 sccm. Pre-reduction was included in Ce-228 and the feed rate was doubled to 400 sccm. Without pre-reduction, an early peak in the H_2S concentration at 15 ppmv was followed by a decrease to about 5 ppmv before FPD breakthrough occurred at 150 minutes. With pre-reduction the early H_2S peak was absent and the H_2S concentration was near zero for 23 minutes before increasing to about 5 ppmv before FPD breakthrough occurred at 55 minutes. Much of the difference in FPD breakthrough times may be attributed to the difference in feed rates.

The general shapes of the breakthrough curves are quite similar to those shown in Figure 45 where results using Rhône Poulenc sorbent with and without pre-reduction were compared. Without pre-reduction, an early H_2S peak was followed by a decrease to 5 ppmv with both sorbents. Pre-reduction eliminated the early peak and produced H_2S concentrations near 1 ppmv during the early stages of the run. The difference in FPD breakthrough times is due to the different feed rates and different quantities of CeO_2 in the sorbent charge. With 6.0 g of Rhône Poulenc sorbent, FPD breakthrough at the reaction conditions of Ce-228 occurred in about 90 minutes. The ratio of breakthrough times (90/60 = 1.5) is considerably smaller than the ratio of quantities of CeO_2 ($6.0 \times 0.91/2.2 = 2.5$) which suggests more efficient utilization of CeO_2 in WGW1 sorbent prior to FPD breakthrough. This result is reasonable since improved dispersion is expected when the CeO_2 is deposited on the surface of the Al_2O_3 support.

Similar results for sorbent WGW2 with and without pre-reduction are illustrated in Figure 65. Once again, different feed rates of 200 sccm and 400 sccm were used, which accounted for the difference in breakthrough times. With no pre-reduction the early H_2S peak was followed by an extended period during which the H_2S concentration was about 5 ppmv. Pre-reduction eliminated the early peak and the initial H_2S concentration was about 1 ppmv. Comparison of results from Figure 64 and 65 suggests that the addition of La_2O_3 had no major effect either with or without pre-reduction.

The sulfidation responses of three alternate CeO_2 sorbents — WGW1, WGW3, and MC — are compared to the standard Rhône Poulenc sorbent response in Figure 66. No pre-reduction step was included and the familiar early H_2S peak was present in each of the tests. This early peak was followed by a H_2S plateau ranging from 1 ppmv to about 20 ppmv for times ranging between 70 and 150 minutes. The poorest pre-breakthrough performance was associated with sorbent WGW3 with a H_2S plateau of 20 ppmv. The lowest pre-breakthrough concentration of 1 ppmv occurred using sorbent MC. FPD breakthrough times should not be directly compared because of the variable quantities of CeO_2 in each test, ranging from 2.2 g in WGW1 to 6.0 g in both MC and RP sorbents. Dividing the FPD breakthrough time by the mass of CeO_2 provides a more realistic basis for comparison. On this basis sorbent WGW1 is clearly superior (150/2.2 =68 min/g CeO_2) followed, in order, by WGW3 (140/5 = 28 min/g CeO_2), RP ($120/6.0 \times 0.91$ = 22 min/g CeO_2) and MC (70/6 = 11.7 min/g CeO_2). These results correlate with the accessibility of CeO_2, with the CeO_2 on Al_2O_3 sorbents showing best performance followed by high surface area RP sorbent and with MC sorbent, which had relatively low surface area, exhibiting the poorest performance.

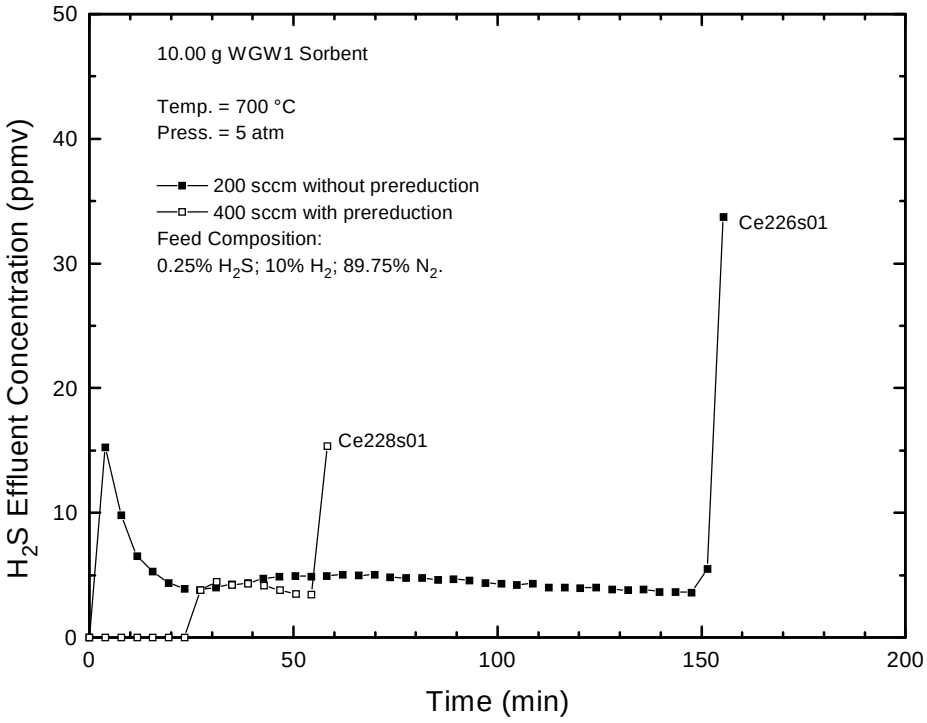

Figure 64. H_2S Breakthrough Curves Using WGW1 Sorbent

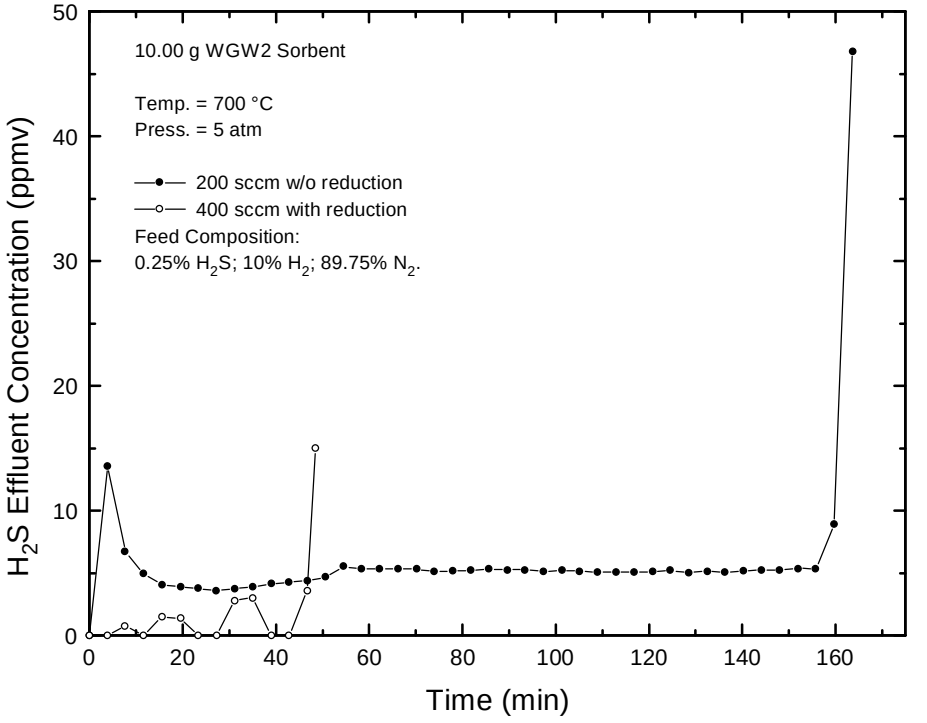

Figure 65. H_2S Breakthrough Curves Using WGW2 Sorbent

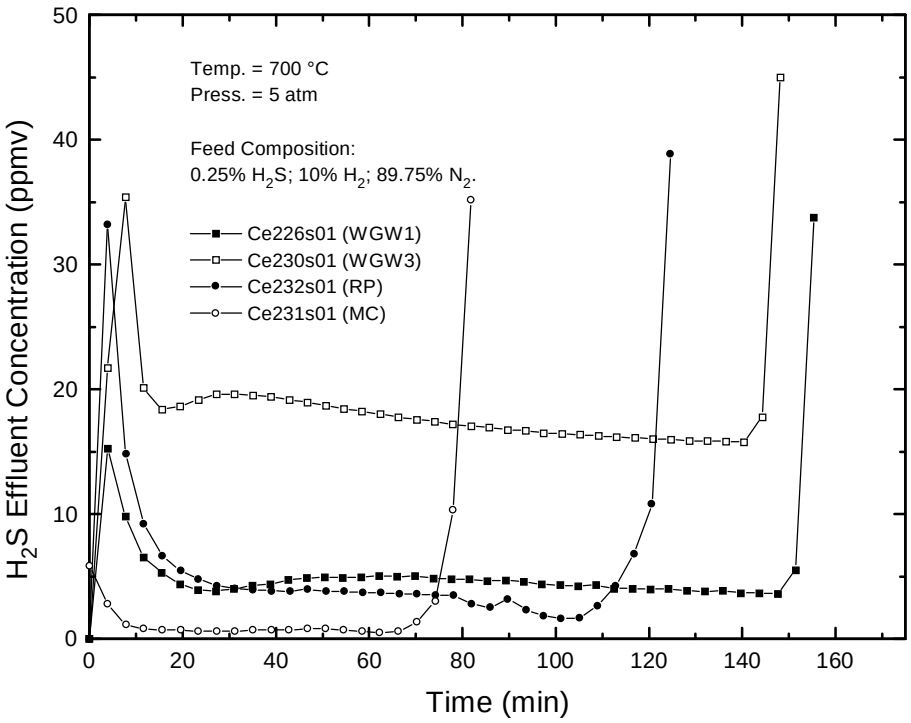

Figure 66. Comparison of H_2S Breakthrough Curves Using Four Cerium-Based Sorbents

Two tests were performed using $Ce_2(CO_3)_3$ as the sorbent precursor (sorbent MCC). In one test, 10 g of $Ce_2(CO_3)_3$ was mixed with 3.0 g of Al_2O_3, the mixture was added to the reactor, and calcination occurred at 700°C in N_2. The 6.6 g CeO_2 shown for test Ce-235 in Table 16, was based on measured weight loss at 200°C (presumably water) and the assumption of complete calcination of pure $Ce_2(CO_3)_3$ to $2CeO_2$. In the second test (Ce-236), $Ce_2(CO_3)_3$ was calcined at 750°C in air using a tube furnace. 6.0 g of calcined product was then mixed with 3.0 g of Al_2O_3 and added to the reactor. No pre-reduction step was included and "standard" sulfidation conditions were used.

Sulfidation results shown in Figure 67 were quite similar except for FPD breakthrough time. An initial small H_2S peak was followed by an extended pre-breakthrough period when the H_2S concentration was about 1 ppmv. FPD breakthrough occurred after about 105 minutes in Ce-235 and about 80 minutes in Ce-236. The ratio of breakthrough times to sorbent masses (105/6.6 = 16 min/g) and (80/6.0 = 13 min/g) suggests that calcination within the reactor increased cerium accessibility and produced somewhat better results.

The only test using an alternate sorbents with steam added to the feed gas was Ce-243. WGW2 sorbent was used and the steam and hydrogen contents of the feed gas approximated the levels found in Shell gas. The H_2S content of all samples was above the FPD saturation limit and no useful results were obtained. Results of a test using the standard Rhône Poulenc sorbents at the same reaction conditions were presented in Figure 47. In that test the initial H_2S concentration was about 70 ppmv and the FPD saturation limit was exceed in about 25 minutes. While the results of Ce-243 using WGW2 sorbent were somewhat poorer, this result may have been due to the small amount of CeO_2 in the WGW2 sorbent charge.

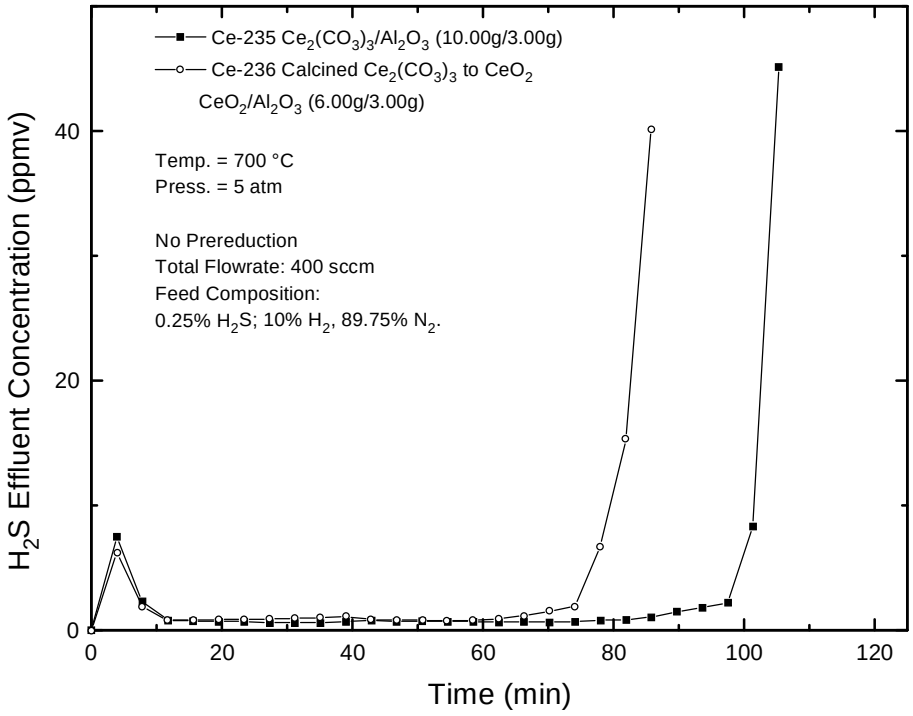

Figure 67. Sulfidation Using $Ce_2(CO_3)_3$ as the Sorbent Precursor (Sorbent MCC)

8.3. Conclusions

All alternate sorbents performed well in the limited sulfidation tests. With the exception of sorbent WGW3 all were successful in reducing pre-breakthrough H_2S concentrations to the 5 ppmv level. The pre-breakthrough concentration in the single test using WGW3 sorbent was about 20 ppmv. Variable H_2S breakthrough times and different slopes during the active breakthrough period may be attributed to the large differences in the mass of initial CeO_2 and to the different structural properties of the sorbents. The addition of La_2O_3 in sorbent WGW2 did not seem to alter the sorbent performance to any significant degree. In the single multicycle test, a four-cycle test using sorbent MC, there was evidence of minor deterioration in performance between the first and fourth cycles.

It is clear that efficient sulfidation and regeneration can be achieved using a wide variety of CeO_2 sources. Further research, therefore, should concentration on identifying a low cost, plentiful source of CeO_2 in order to minimize the unit sorbent cost to improve the economics of the process.

CHAPTER 9. PROCESS ANALYSIS

A complete process flowsheet for a two-stage desulfurization process using cerium-based sorbent for bulk H_2S removal followed by a zinc-sorbent polishing step has been synthesized. The process is based on the regeneration of Ce_2O_2S using SO_2 for the direct production of elemental sulfur and regeneration of ZnS using dilute oxygen to produce SO_2. Off-gases from the ZnS regenerator are recycled to the gasifier where SO_2 is reduced to H_2S and recycled through the desulfurization system. Complete material and energy balances for this process were established using the software package PRO/II based upon a specified feed rate of Shell gas containing 1% H_2S. Major process equipment was sized and capital and annual levelized operating costs were estimated. The sensitivity of the annual levelized cost estimate to variations in major cost items was then investigated.

A single-stage desulfurization process using zinc sorbent with elemental sulfur recovery using the direct sulfur recovery process (DSRP) (Gangwal and Portzer, 1995) was analyzed using a similar procedure so that the two approaches to coal gas desulfurization with elemental sulfur recovery could be directly compared.

9.1. Two-Stage Desulfurization Using Cerium Sorbent With SO_2 Regeneration

A detailed block flow diagram of the two-stage process is shown in Figure 68. All major processing units including reactors, heat exchangers, pumps, compressors, and the steam drum are included. All reactors in this process are considered to be fluidized beds. Primary process flows are indicated by solid lines while secondary flows of cooling water and steam are shown as dashed lines. The stream numbers in Figure 68 were defined for the PRO/II material and energy balance calculations which are described subsequently.

Feed (stream 101) from a Shell gasifier is cooled before entering the primary desulfurization reactor (stream 1) containing cerium sorbent where the majority of the sulfur is removed. Product gas from the primary sorber (stream 2) passes through two heat exchangers before entering the secondary sorber (stream 71) containing zinc sorbent. Final sulfur removal occurs in this vessel and desulfurized coal gas (stream 11) meets IGCC sulfur specifications.

Spent sorbent (stream 3) from the primary sorber is transferred to the primary regenerator where Ce_2O_2S reacts with SO_2 to produce CeO_2 and liberate elemental sulfur. Regenerated sorbent (stream 4) is recycled to the primary sorber (stream 14) after a bleed of spent sorbent (stream 15) is removed and replaced with fresh sorbent (stream 12). The sorbent replacement rate, which is required to maintain constant sorbent activity with time, is a major factor in the total process cost. Elemental sulfur in the product gas from the primary regenerator (stream 5) is separated in the sulfur condenser. Excess SO_2 (stream 7) is compressed and recycled to the regenerator (stream 22). A portion of the elemental sulfur product is burned using oxygen (stream 8) to replace the quantity reacted. The final elemental sulfur product (stream 32) may be sold to offset a portion of the desulfurization cost.

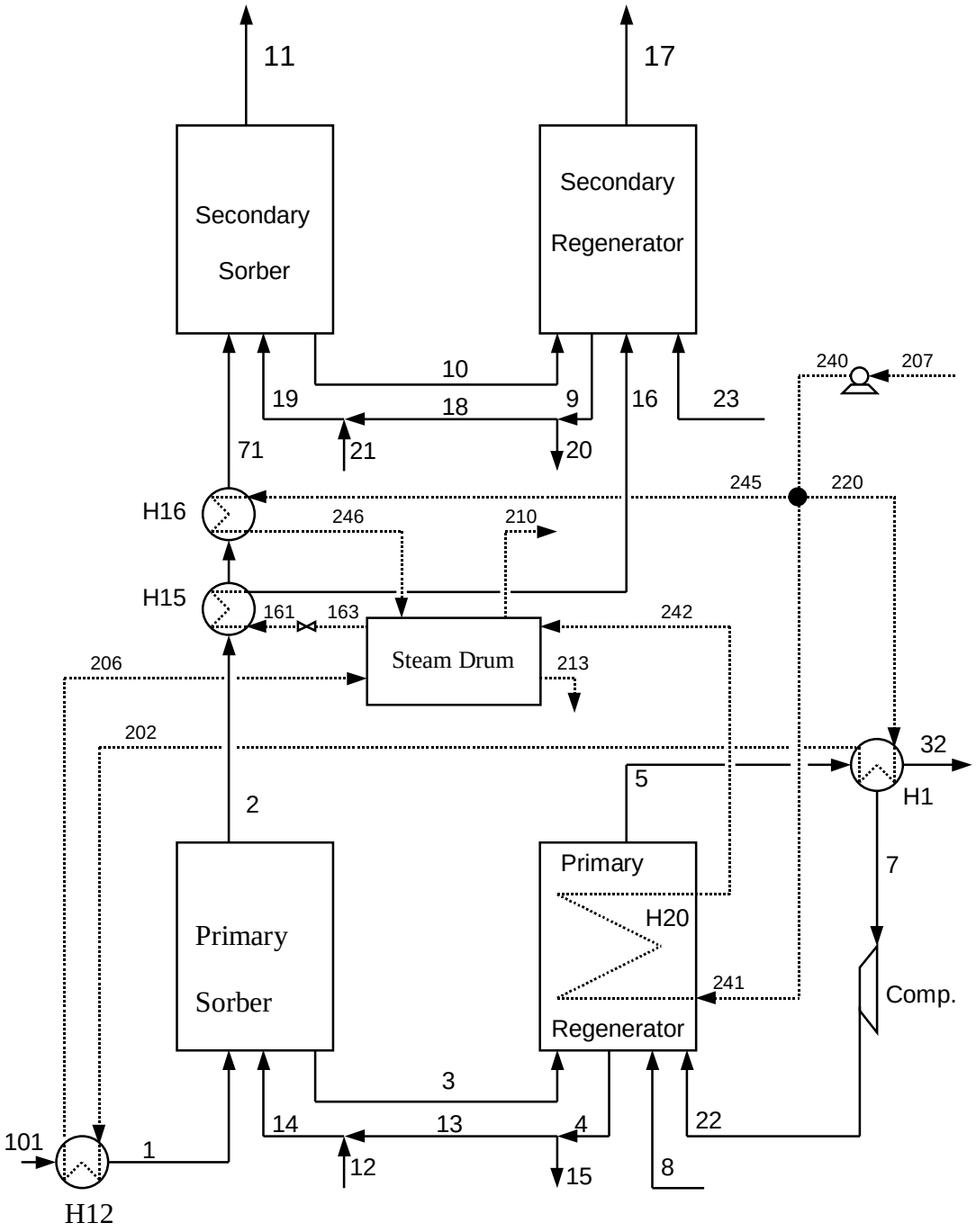

Figure 68. Two-Stage Desulfurization with SO_2 Regeneration

Spent zinc sorbent from the secondary sorber (stream 10) is transported to the secondary regenerator where ZnS reacts with O_2 (stream 23) to produce ZnO and SO_2. The regenerated sorbent (stream 9) is recycled (stream 19) after appropriate discharge of spent sorbent (stream 20) and fresh sorbent make-up (stream 21). Temperature control in the secondary regenerator is accomplished by diluting the O_2 with steam (stream 16). Secondary regenerator off-gas (stream 17) containing SO_2 and excess steam is recycled to the gasifier where the SO_2 is reduced H_2S, which is subsequently captured by being recycled to the primary sorber with the gasifier product.

Water and steam flows in the process are designated by dashed lines in the figure and all stream numbers are designated by 2xx. Heat is removed in the primary regenerator for temperature control, from the primary regenerator product gas to condense elemental sulfur, and in the single heat exchanger prior to the primary sorber and the two heat exchangers between the primary and secondary sorbers. Steam is consumed (stream 16) in the secondary regenerator and export steam (stream 210) is produced as a by-product.

9.2. Single-Stage Desulfurization Using Zinc Sorbent With DSRP

A detailed block diagram of this process is shown in Figure 69. Product gas from the Shell gasifier (stream 101) is cooled in a series of three heat exchangers. A slip stream of coal gas (stream 3) is removed and fed to the DSRP reactor to provide reducing gas needed to convert SO_2 to elemental sulfur. The remaining coal gas (stream 2) is fed to the sorber where H_2S reacts with ZnO to produce a desulfurized product gas (stream 11) which meets IGCC specifications. Spent sorbent (stream 9) is transferred to the regenerator where it reacts with O_2 from air (stream 10) to produce ZnO and SO_2. The regenerated sorbent (stream 8) is recycled to the sorber (stream 4) after appropriate discharge of spent sorbent (stream 6) and fresh sorbent make-up (stream 5).

Product gas from the regenerator (stream 12) flows to the DSRP reactor where SO_2 is reduced to elemental sulfur by reaction with H_2 and CO from the coal gas slip stream (stream 3). Elemental sulfur (stream 32) is separated in the sulfur condenser. Most of N_2-rich product gas from the condenser (stream 17) is compressed and recycled to the regenerator (stream 14). A portion of the condenser product gas is discharged to the atmosphere (stream 24) to maintain carbon and nitrogen balances. A small amount of sulfur is also present in this discharge stream. The overall energy balance is satisfied by generating steam. Boiler feed water and steam flows are shown by dashed lines numbered 2xx and export steam (stream 210) is produced.

9.3. Design Basis

Both processes were designed to treat 17,000 lb mol/hr of Shell gas whose temperature, pressure, and composition are presented in Table 17. The flow rate was chosen to match that used by Buchanan et al. (1994) so that cost comparisons could be made. The electrical output in this study ranged from 253 to 292 MW (net), depending on the type of gasifier and cleanup process employed. Only the Shell gas was considered since application of the CeO_2 sorbent is limited to highly reducing gases. Other assumptions and decisions used in the base design case are listed below.

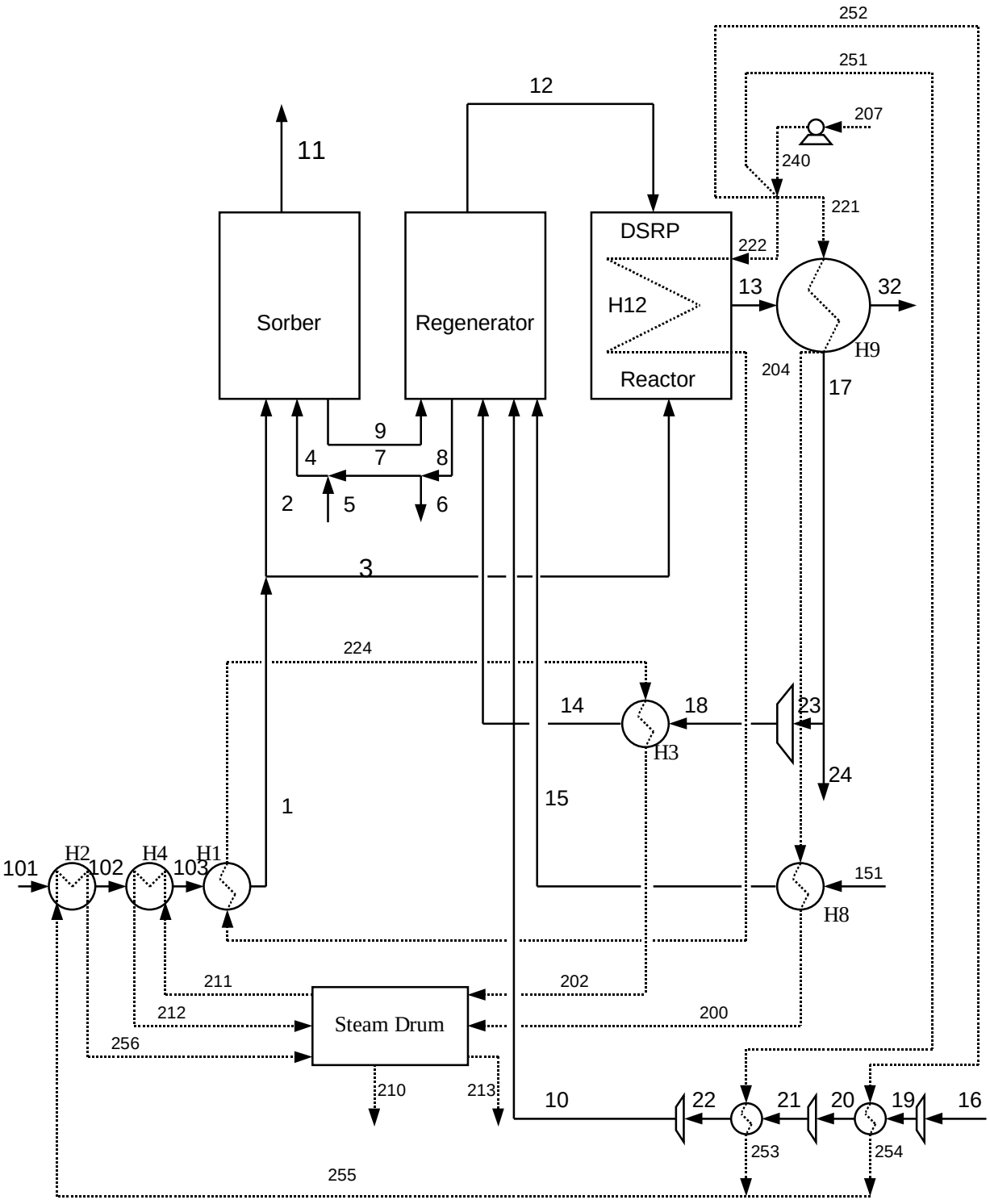

Figure 69. Single-Stage Desulfurization with DSRP

Table 17. Design Flow Rate, Temperature, Pressure, and Composition of Shell Gas

Flow Rate	17000 lb mol/hr
Temperature	1850°F
Pressure	25 atm
Composition	Mol Fraction
CO	0.60
H_2	0.29
CO_2	0.02
H_2O	0.05
H_2S	0.01
N_2	0.03

1. Pressure drop through the process was neglected, i.e., all process units operated at 25 atm.

2. H_2S removal in all desulfurization reactors was based on the achievement of thermodynamic equilibrium at the specified temperature and pressure.

3. The sorbent feed rate to all desulfurization reactors provided 100% excess over the stoichiometric quantity required for complete H_2S removal.

4. The sorbent discharge and make-up rates were fixed at 1% of the sorbent circulation rate, corresponding to an average sorbent lifetime of 100 sulfidation-regeneration cycles. This value was totally arbitrary and was found to be too large to permit either process to operate economically. The material and energy balances of the remainder of the processes are independent of the discharge/replacement rate, and this parameter was considered in the cost sensitivity analysis.

5. The oxygen feed rate to the secondary regenerator of the two-stage cerium desulfurization process was set at 10% excess over the stoichiometric quantity needed for complete ZnS regeneration. The reaction is irreversible. The mole fraction of oxygen in the gas feed to the secondary regeneration was fixed at 0.03, with steam as the diluent.

6. The flow rate of SO_2 to the primary regenerator in the two-stage process was determined by heat transfer requirements for this highly exothermic reaction. The heat transfer analysis is discussed at a later point in this chapter.

7. The primary and secondary sorbers as well as the secondary regenerator in the two-stage process were modeled as adiabatic fluidized-bed reactors with flow rates of inlet

streams adjusted to produce the desired operating temperature. The primary regenerator was modeled as a nonadiabatic fluidized-bed reactor. The highly exothermic regeneration reaction required that special attention be given to the heat transfer characteristics of the reactor.

8. Both the sorber and regenerator in the single-stage process were modeled as adiabatic fluidized-bed reactors with temperatures and flow rates of inlet streams adjusted to produce the desired operating temperature. The DSRP reactor was modeled as a fixed-bed nonadiabatic reactor with sufficient heat transfer capability to produce the desired operating temperature.

9. Nominal operating temperatures for the reactors and sulfur condenser in both the two-stage and single-stage processes were fixed at levels shown in Table 18. The operating temperatures of the cerium sorbent reactors were fixed on the basis of experimental results from this study while temperatures of the zinc sorbent and DSRP reactors were based on current operating practice.

10. The cerium sorbent was assumed to be pure CeO_2 while the zinc sorbent was assumed to be Zn_2TiO_4.

Table 18. Nominal Reactor and Sulfur Condenser Temperatures

Two-Stage Desulfurization Using Cerium Sorbent With SO_2 Regeneration	Temperature, K
Primary Sorber	1073
Primary Regenerator	873
Secondary Sorber	873
Secondary Regenerator	1000
Sulfur Condenser	373
Single-Stage Desulfurization Using Zinc Sorbent With DSRP	
Sorber	873
Regenerator	1000
DSRP Reactor	873
Sulfur Condenser	373

9.4 Material and Energy Balance Results

PRO/II was used to complete the material and energy balance calculations for the processes shown in Figures 68 and 69 using the design criteria summarized in the previous section. A summary of the results for two-stage desulfurization using cerium sorbent and SO_2 regeneration is presented in Table 19 while results for single-stage desulfurization using zinc sorbent and DSRP for elemental sulfur production is shown in Table 20. The first column presents the total stream flow rate in units of lb mol/hr while the second presents sulfur flow rate in units of lb/hr. Only terminal, i.e., overall process input and output streams are shown in these tables. Flow rates, compositions, and temperatures of all streams shown in Figures 68 and 69 may be found in Zhang's thesis (1997).

The coal gas feed rate and the amount of sulfur in the coal gas are the same in both processes. The flow rate of desulfurized coal gas in the two-stage process is equal to the coal gas feed rate while the desulfurized coal gas rate in the single-stage process is reduced by 3% because of the slip stream diverted to the DSRP reactor. The composition and temperature of the desulfurized coal gas product are identical in each case, and the apparent difference in sulfur rate between 5 lb/hr and 6 lb/hr is due to round-off. The lower production rate of elemental sulfur in the two-stage process is somewhat misleading since SO_2 in the secondary regenerator product gas is recycled to the gasifier and eventually captured as elemental sulfur. Thus the elemental sulfur production rates are equal when this recycle is included. There are, however, two disadvantages associated with the elemental sulfur product in the single-stage process. About 5 lb/hr of sulfur are discharged to the atmosphere in the recycle purge gas. In addition, much of the H_2O present in the coal gas slip stream and produced in the DSRP reactor is removed in the sulfur condenser so that the liquid product in only about 62 mol% sulfur. Further purification of the sulfur product was not considered. In contrast, only pure sulfur is condensed in the two-stage process and further purification is not required.

Sorbent make-up and discharge rates must obviously be equal, but a much larger amount of cerium sorbent must be replaced in the two-stage process compared to zinc sorbent in the single stage process. This is due to the different stoichiometric sulfur capacities of the two sorbents, 0.093 g S per g of CeO_2 compared to 0.264 g S per g of Zn_2TiO_4. This difference in sorbent replacement rates results in a major economic advantage for the single-stage process.

Oxygen is required as feed to both the primary and secondary regenerators in the two-stage process. The oxygen is assumed to be purchased from the air separation plant associated with the gasifier. The steam fed to the secondary regenerator is obtained from steam generated within the process, which accounts for the difference between the feed water make-up and export steam production rates. Nitrogen fed to the regenerator in the single-stage process is assumed to be available from the air separation unit associated with the gasifier. No process steam is required in the single-stage process so that water make-up and export steam rates are equal. The amount of export steam, however, is only about 63% of the amount available from the two-stage process.

Table 19. Material Balance Summary for Two-Stage Desulfurization With SO_2 Regeneration

Input Stream Description (Number)	Stream Flow Rate, lb mol/hr	Sulfur Flow Rate, lb/hr
Coal Gas from Gasifier (101)	17,000	5500
Cerium Sorbert Make-up (12)	6.9	---
Zinc Sorbent Make-up (21)	0.2	---
O_2 to Primary Regenerator (8)	150	---
Steam to Secondary Regenerator (16)	970	---
O_2 to Secondary Regenerator (23)	30	---
Feed Water (207)	13,000	---
Output Stream Description (Number)		
Desulfurized Coal Gas (11)	17,000	6
Cerium Sorbent Discharge (15)	6.9	---
Zinc Sorbent Discharge (20)	0.2	---
Secondary Regenerator Off-Gas (17)	990	581
Elemental Sulfur Product (32)	150	4913
Export Steam (210)	12,000	---

Note: Refer to Figure 68 for stream numbers

Table 20. Material Balance Summary for Single-Stage Desulfurization With DSRP

Input Stream Description (Number)	Stream Flow Rate, lb mol/hr	Sulfur Flow Rate, lb/hr
Coal Gas from Gasifier (101)	17,000	5500
N_2 to Regenerator (15)	1100	---
Air to Regenerator (16)	1320	---
Zinc Sorbent Make-up (5)	1.7	---
Feed Water (207)	7590	---
Output Stream Description (Number)		
Desulfurized Coal Gas (11)	16,500	5
Zinc Sorbent Discharge (6)	1.7	---
Elemental Sulfur Product (32)	276	5490
Recycle Gas Purge (24)	2470	5
Export Steam	7590	---

Note: Refer to Figure 69 for stream numbers

9.5 Process Design

Sizing the reactor vessels and other major process equipment was based largely on previous designs of similar systems. Two reports by Chen et al. (1991 and 1992) were particularly useful. Design decisions and assumptions are listed below.

1. Both processes, including all sorbers, regenerators, and the DSRP reactor were sized on the basis of four equal parallel trains (Chen et al., 1991).

2. The fluidized-bed sorbers and regenerators were sized on the basis of a superficial gas velocity of 1 ft/s and fluidized-bed depth of 6 ft (SV = 600 hr^{-1}) (Chen et al. 1992). The total height of the fluidized-bed reactors included freeboard which was set at 50% of the fluidized bed depth.

3. The fixed-bed DSRP reactor was sized on the basis of a space velocity of 4560 std cm^3/cm^3 hr reported by Gangwal (1995).

4. Special considerations for including heat transfer tubes in the primary regenerator of the two-stage process and in the DSRP fixed-bed reactor were made. The remaining reactors operated adiabatically.

5. All reactor vessels contained six inches of refractory lining as specified by Chen et al. (1991).

6. Vessel wall thickness was determined using the following empirical equation from Peters and Timmerhaus (1991)

$$t = (PR_i/SE_j - 0.6P) + C_c \qquad (15)$$

where t = wall thickness, in.
P = operating pressure, psia
R_i = vessel inside radius, in.
E_j = joint efficiency = 0.85 (Peters and Timmerhaus, 1991)
C_c = corrosion allowance = 0.125 (Peters and Timmerhaus, 1991)
S = maximum allowable working stress = 13,700 psi for carbon steel over a temperature range of –20 to 650°F (Peter and Timmerhaus 1991)

An approximate heat transfer analysis was used to estimate that the maximum vessel wall temperature was about 252°F, thereby justifying the use of the value of S specified above.

Including heat transfer surface in the primary regenerator of the two-stage process and the DSRP reactor of the fixed-bed process required that these vessels receive special consideration. 1.25 inch outside diameter by 1 inch inside diameter heat transfer tubes having an outside surface area of 0.327 ft^2/ft were placed in a square array with a tube pitch of about 2.5 inches. The heat transfer area and number of tubes needed were calculated from

$$A = \frac{Q}{U\Delta T_m} \tag{16}$$

$$n = \frac{A}{LA_L} \tag{17}$$

where A = heat transfer area, ft^2
Q = heat removal needed to satisfy vessel temperature specifications, Btu/hr
U = overall heat transfer coefficient, Btu/hr ft^2 °F
n = number of heat transfer tubes
L = tube length, ft
A_L = outside heat transfer area per length of tubing = 0.327 ft^2/ft

A value of U = 30 Btu/hr ft^2 °F, which is in the middle of a range of heat transfer coefficients for tubes in fluidized beds from a number of sources (Seko et al., 1983; Piepers et al., 1983; Donsi et al., 1983), was used.

Heat transfer and gas flow rate requirements in the DSRP reactor were both satisfied using this approach. However, for the primary regenerator in the two-stage process the gas flow and heat transfer requirements were not compatible. This is, it was impossible to include the required heat transfer area while maintaining a superficial gas velocity of about 1 ft/s. This problem was solved by increasing the SO_2 recycle rate to the primary regenerator. The larger recycle rate reduced the amount of heat which had to be removed and increased the volumetric gas feed rate to the reactor. A trial-and-error approach was used to determine a recycle rate consistent with both fluidization and heat transfer requirements.

Final reactor vessel dimensions are summarized in Table 21. All fluidized-bed reactors are of equal height due to the equal contact time. In two-stage desulfurization with SO_2 regeneration the primary and secondary sorbers are of almost equal diameter even though the sulfur removal duty is quite different in each. Diameter is determined by gas throughput, not sulfur removal. The diameters of the regenerators are significantly smaller because of smaller regeneration gas flow rates. The larger diameter of the primary regenerator is needed to accommodate the 100 heat transfer tubes inside the fluidized bed. The 1 ft difference between the open vessel diameter and metal wall inside diameter is due to the 6 inches of refractory lining. Finally, the differences in vessel wall thickness are due to the different diameters and operating temperatures.

9.6 Capital Cost Estimates

Purchased equipment cost estimates for all major process equipment were based on equipment sizes or other equipment characteristics and cost factors from literature sources and informal vendor quotes. A summary of the major pieces of process equipment, the basis used to estimate cost, and the purchased equipment cost for the two-stage process with SO_2 regeneration is presented in Table 22. A similar summary for single-stage desulfurization with DSRP is found in Table 23.

Table 21. Reactor Dimensions

	Height, ft	Open Vessel Diameter, ft	Metal Wall Inside Diameter, ft	Metal Wall Thickness, in	Number of Heat Transfer Tubes
Two-Stage Desulfurization With SO_2 Regeneration					
Primary Sorber	9	8.8	9.8	2.0	0
Secondary Sorber	9	8	9	1.9	0
Primary Regenerator	9	2.3	3.3	0.8	0
Secondary Regenerator	9	1.4	2.4	0.6	100
Single-Stage Desulfurization With DSRP					
Sorber	9	7.9	8.9	1.8	0
Regenerator	9	6.5	7.5	1.6	0
DSRP Reactor	11.5	5.0	6.0	1.3	64

The cost basis for reactor vessels was the mass of steel. This was calculated from the vessel dimensions of Table 21 and includes a 15% increase for nozzles, manholes, and fittings (Peters and Timmerhaus, 1991). The purchased cost was calculated from an empirical equation of Peters and Timmerhaus (1991)

$$PEC = 80\, w^{0.66} \qquad (18)$$

where PEC = purchased equipment cost, 1990 $ (cost index = 356)
w = vessel weight, lb

This 1990 cost estimate was updated to the reference year of 1996 using the Chemical Engineering plant cost index of 382. Each value in Tables 22 and 23 represents the total cost of the four parallel trains. The refractory cost estimate was based on an informal vendor quote (Milton, 1996).

The purchased cost of waste heat boilers was based on an informal vendor quote (Willis, 1996) of $75,000 (1996 basis) for a capacity of 15,000 lb/hr of steam. The "0.6 factor rule" (Peters and Timmerhaus, 1991) was used to adjust the base cost for different steam capacities. The purchased cost of shell-and-tube heat exchangers was taken from Peters and Timmerhaus (1991) based on the heat transfer area. Costs were updated to the 1996 base year using the appropriate indices.

Compressor costs were based on horsepower and were taken from Peters and Timmerhaus (1991) and updated using the appropriate cost indices. Other sources of compressor cost data were consulted because of the importance of the three-stage air compressor cost in the single-stage process with DSRP. The Peters and Timmerhaus cost was in the middle of the range of values from other sources. Pump cost estimates were taken from Kirk-Othmer (1981) based on the product of the flow rate and head (gpm x ft) and were updated using the appropriate cost indices. The steam drum is simply a stainless steel high pressure storage tank, and the cost was estimated from Peters and Timmerhaus (1991) and updated to 1996.

Table 22. Major Equipment, Cost Basis, and Purchased Cost
For Two–Stage Desulfurization With SO_2 Regeneration

Equipment Item	Cost Basis	Purchased Eqpt. Cost, $10^6$$, 1996
Reactor Vessels (vessel weight, lb)		
Primary Sorber	4.1×10^4	0.380
Secondary Sorber	3.3×10^4	0.330
Primary Regenerator	4.0×10^3	0.082
Secondary Regenerator	2.1×10^3	0.054
Refractory	---	0.040
Sub Total	---	0.890
Heat Exchangers[1]		
Waste Heat Boilers (lb steam/hr)		
H12	52,300	0.159
H15	7,600	0.050
H16	36,200	0.127
Shell and Tube (area, ft^2)		
H1	1,530	0.021
Sub Total	---	0.357
Recycle Compressor (HP)	118	0.043
Pump, Flow Rate (gmp)	240	0.049
Head (ft)	2930	
Steam Drum (volume, gal)	2800	0.020
Total Purchased Equipment Cost		1.350

[1]Refer to Figure 68 for exchanger identification

Table 23. Major Equipment, Cost Basis, and Purchased Cost
For Single–Stage Desulfurization With DSRP

Equipment Item	Cost Basis	Purchased Eqpt. Cost, $10^6$$, 1996
Reactor Vessels (vessel weight, lb)		
Sorber	$3.2x10^4$	0.325
Regenerator	$2.2x10^4$	0.252
DSRP Reactor	$1.7x10^4$	0.210
Refractory	---	0.048
Sub Total	---	0.840
Heat Exchangers[1]		
Waste Heat Boilers (lb steam/hr)		
H2	15,000	0.075
H4	31,500	0.117
H1	62,600	0.177
Shell and Tube (area, ft^2)		
H8	1,200	0.018
H3	3,600	0.043
H9	14,700	0.214
Sub Total	---	0.644
Compressors (HP)		
Air Compressor		
Stage 1	830	
Stage 2	1,000	
Stage 3	1,000	0.980
Recycle	390	0.150
Sub Total	---	1.130
Pump, Flow Rate (gpm)	270	0.049
Head (ft)	2930	
Steam Drum, (volume, gal)	3400	0.020
Total Purchased Equipment Cost		2.683

[1]Refer to Figure 69 for exchanger identification

The total puchased equipment cost for single-stage desulfurization with DSRP shown in Table 23 is approximately twice that required for two-stage desulfurization with SO_2 regeneration. Most of that difference is associated with the large three-stage compressor needed to supply air to the regenerator. The primary regenerator in the two-stage process with SO_2 regeneration does not require such a compressor. Instead, oxygen for regeneration is purchased from the air separation unit associated with the gasifier and is treated as an operating cost.

The estimated purchased equipment cost of the reactor vessels is approximately equal in the two processes, with the four vessels needed for two-stage desulfurization with SO_2 regeneration estimated to cost about 6% more than the three vessels needed for single-stage desulfurization with DSRP. The cost of the waste heat boilers and shell-and-tube heat exchangers in the single-stage process with DSRP is estimated to be about 80% larger than in the two-stage process with SO_2 regeneration. Much of this cost difference is associated with the sulfur condenser (H9 in the single-stage process and H1 in the two-stage process). The condenser in the single-stage process is much larger because the elemental sulfur concentration in the feed stream is only about 1.7% compared to about 15% for the two-stage process. The estimated purchased equipment costs for pumps and steam drums are equal in the two processes and together contribute only a small fraction of the total purchased equipment cost.

Process capital equipment cost includes such items as equipment installation, instrumentation, and piping, while the total capital requirement includes additional costs such as engineering fees, spare parts and working capital. The process capital cost was taken to be 327% of the purchased equipment cost using cost factors from Peters and Timmerhaus (1991). The total capital requirement was estimated to be 493% of the purchased equipment cost using factors from Buchanan et al. (1994). With these multipliers the process capital requirement escalated to $4.42 million and $8.77 million for the two-stage and single-stage processes, respectively. Similarly the total capital estimates become $6.64 million and $13.22 million for the two-stage and single-stage processes.

It is important, whenever possible, to compare capital cost estimates for similar processes from different sources. Buchanan et al. (1994) and McMichael and Gangwal (19091) have reported economic estimates for single-stage desulfurization with DSRP under somewhat similar, but not identical conditions. McMichael and Gangwal only considered the sulfur recovery costs associated with the DSRP process and did not include the sulfidation and regeneration steps. Buchanan et al. evaluated an entire IGCC system including gasification, particulate removal, halogen removal, desulfurization/regeneration, and sulfur recovery. However, their estimate of the process capital requirement for desulfurization/regeneration and sulfur recovery was reported separately. The operating conditions of the three studies were also somewhat different.

For the sake of comparison, approximate methods were used to convert the estimated process equipment costs from the three studies to a common basis. The final estimates of the total process equipment costs are $7.5 million according to McMichael and Gangwal (1991), $7.6 million according to Buchanan et al (1994), and $8.5million from this study. Although the current estimate is 15% greater than the estimate of McMichael and Gangwal, we feel that this level of agreement is reasonable at this stage of the evaluation.

9.7 Operating Cost Estimates

The total operating cost is divided into fixed and variable operating costs. The fixed operating costs are independent of the operating rate and include such items as operating and maintenance labor and administration. The variable operating cost is determined by the consumption and production rates of raw materials, by-products, and utilities coupled with their unit costs.

The total fixed operating cost was taken to be 5.45% of the process capital cost in agreement with McMichael and Gangwal (1991). Table 24 summarizes the consumption or production rates of raw materials, by-products and utilities for two processes. All values except DSRP catalyst consumption rate were obtained directly from PRO/II material and energy balance calculations. The DSRP catalyst consumption rate is from Buchanan et al. (1994). Both processes require boiler feed water, power, and zinc sorbent, and both produce steam and elemental sulfur. Single-stage desulfurization with DSRP also requires nitrogen diluent to the regenerator, DSRP catalyst replacement, and purchase of the coal gas slip stream to the DSRP reactor. Two-stage desulfurization with SO_2 regeneration requires the purchase of oxygen and cerium sorbent.

Table 24. Utilities and Chemicals Consumption and Production Rates

	Two-Stage Desulfurization with SO_2 Regeneration	Single-Stage Desulfurization with DSRP
Utilities		
Boiler Feed water	6482 lb mol/hr	7564 lb mol/hr
Power	384 HP	3540 HP
Chemicals		
Coal Gas	0	435 lb mol/hr
Oxygen	177 lb mol/hr	0
Nitrogen	0	1100 lb mol/hr
Zinc Sorbent	0.08 lb mol/hr	1.68 lb mol/hr
Cerium Sorbent	6.88 lb mol/hr	0
DSRP Catalyst	0	0.57 ton/year
Credits		
Steam	6050 lb mol/hr	7556 lb mol/hr
Sulfur	164 lb mol/hr	171.5 lb mol/hr

Unit cost estimates used in the base case evaluation are summarized in Table 25 along with the source of each estimate. Data are updated to the 1996 reference year in the last column. Because of the uncertainty in many of these unit costs, the sensitivity of the total process cost to variations in selected unit costs was analyzed and is discussed subsequently.

Table 25. Unit Costs and Credits for Utilities and Chemicals

Item	Unit Cost	Date	Reference	1996 Cost
Utilities				
Boiler feed water	$11.2/1000gal	1987	McMichael and Gangwal (1991)	$13.2/1000gal
Electricity	$0.059/kwh	1987	McMichael and Gangway (1991)	$0.070/kwh
Chemicals				
Coal gas	$1.066/lb mol	1987	McMichael and Gangway (1991)	$1.26/lb mol
Nitrogen	$25/ton	1996	Cammarata (1997)	$25/ton
Oxygen	$40/ton	1996	Cammarata (1997)	$40/ton
Zinc Sorbent	$7000/ton	1993	Buchanan et al. (1994)	$7500/ton
Cerium Sorbent	$6400/ton	1996	Stanford Materials Company (1997)	$6400/ton
DSRP Catalyst	$4000/year	1993	Buchanan et al. (1994)	$4250/ton
Credit				
Steam	$4.9/1000lb	1981	EPRI (1982)	$6.3/1000lb
Sulfur	$76.4/ton	1987	McMichael and Gangwal (1991)	$90/ton

Annual operating cost estimates for the two processes are compared in Table 26. The dominant cost item in two-stage desulfurization with SO_2 regeneration is cerium sorbent replacement at $21.42 million annually. All other costs are, in comparison, quite small. Zinc sorbent replacement is the largest operating cost item in the single-stage process with DSRP at $8.62 million, but this is only 40% of the estimated cerium sorbent replacement cost. The zinc sorbent cost is followed, in decreasing order, by the cost of coal gas, nitrogen, boiler feed water, and power.

By-product credits are slightly in favor of the single-stage process because of the increased export steam production rate. The sulfur by-product of both processes is evaluated at the same unit cost, although, as previously discussed, the sulfur product in the single-stage process is contaminated with water and additional processing would be required before the sulfur could be sold.

Table 26. Comparison of Operating Cost Estimates for the Two Processes, 10^6\$, 1996 Basis

	Two-Stage Desulfurization With SO_2 Regeneration	Single-Stage Desulfurization With DSRP
Fixed Operating Cost	.024	0.48
Variable Operating Costs		
Boiler Feed Water	1.05	1.23
Power	0.11	1.05
Zinc Sorbent	0.41	8.62
Cerium Sorbent	21.42	---
Oxygen	0.65	----
Nitrogen	---	2.20
Coal Gas	---	3.11
DSRP Catalyst	---	0.004
By-Product Credits		
Steam	(3.91)	(4.88)
Sulfur	(1.34)	(1.41)
Total	18.63	10.40

9.8 Levelized Cost

The method of levelized cost (Electric Power Research Institute, 1982) was used to develop the final base case cost comparison. Levelization of the operating cost is achieved by multiplying the first year operating cost from Table 26 by the factor L_n which distributes the summation of the present worth of future operating costs equally over the project lifetime. Levelization distributes the capital costs over the project lifetime by multiplying the estimated capital cost by the factor P_n. For an annual escalation factor of 6% and a ten-year analysis period, the values of L_{10} and P_{10} are 1.321 and 0.195, respectively (O'Hara et al. 1987).

Tables 27 and 28 summarize the annual levelized capital and operating costs for the two processes along with percent contribution of each item to the total levelized cost. On this total levelized cost basis the two-stage process with SO_2 regeneration is almost 60% more expensive than single-stage desulfurization with DSRP. The total cost for two-stage desulfurization with SO_2 regeneration is totally dominated by the cost of the cerium sorbent, which alone is larger than the estimated total cost. In other words, by-product credits from sales of sulfur and steam exceed the sum of the cost of all items except the sorbent replacement cost. The next largest cost items are boiler feed water and capital costs, but these contribute only 5.4% and 5.0% respectively, compared to 109.2% for sorbent replacement.

Table 27. Levelized Cost and Percentage of Major Items for Two-Stage Desulfurization with SO_2 Regeneration, $10^6$$, 1996 Basis

Capital cost	Levelized Cost	% of Capital Levelized Cost	% of Total Levelized Cost
Pressure Vessels	0.86	65.4	3.3
Heat Exchangers	0.35	26.5	1.3
Compressors	0.04	2.9	0.1
Pump	0.05	3.7	0.2
Steam Drum	0.02	1.5	0.1
Levelized Capital Cost	1.31	100	5.0
Levelized Fixed Operating Cost	0.32		1.2
Variable Operating Cost		% of Operating Levelized Cost	
Boiler Feed Water	1.39	5.7	5.4
Power	0.15	0.6	0.6
Oxygen	0.86	3.5	3.3
Zinc Sorbent	0.54	2.2	2.1
Cerium Sorbent	28.30	115.9	109.2
Credit			
Steam	(5.17)	-21.2	-20.0
Sulfur	(1.77)	-7.3	-6.8
Levelized Variable Operating Cost	24.29	100	93.7
Total Levelized Cost	25.92		100

Table 28. Levelized Cost and Percentage of Major Cost Items for Single-Stage Desulfurization with DSRP, $10^6$$, 1996 Basis

Captial Cost	Levelized Cost	% of Capital Levelized Cost	% of Total Levelized Cost
Pressure Vessels	0.81	31.3	4.9
Heat Exchangers	0.62	23.9	3.8
Compressors	1.09	42.2	6.7
Pump	0.05	1.9	0.3
Steam Drum	0.02	0.7	0.1
Levelized Capital Cost	2.58	100	15.8
Levelized Fixed Operating Cost	0.63		3.8
Variable Operating Cost		% of Operating Levelized Cost	
Coal Gas	4.11	30.8	25.2
Boiler Feed Water	1.62	12.2	10.0
Power	1.39	10.4	8.5
Nitrogen	2.91	21.8	17.8
Zinc Sorbent	11.39	85.4	69.8
DSRP Catalyst	0.005	0.04	0.03
Credit			
Steam	(6.45)	-48.3	-39.5
Sulfur	(1.86)	-14.0	-11.4
Levelized Variable Operating Cost	13.11	100	80.3
Total Levelized Cost	16.32		100

The replacement of zinc sorbent is also the most expensive item in the total levelized cost of the single-stage process with DSRP, but the $11.39 million for zinc sorbent is only 69.8% of the total cost of $16.32 million. The costs of coal gas to the DSRP reactor and purchased nitrogen are the second and third most important cost items, contributing 25.2% and 17.8%, respectively, of the total cost.

9.9 Cost Sensitivity Analysis

The sensitivity of the total levelized cost was investigated as a function of sorbent replacement rate, sorbent unit cost, oxygen and nitrogen unit costs, and total capital requirement. In the base design case the cerium and zinc sorbent replacement rates were arbitrarily set at 1% of the sorbent circulation rate, which corresponds to an average sorbent lifetime of 100 sulfidation/regeneration cycles. The resulting total levelized costs for both processes (Tables 27 and 28) are such that neither process is likely to be economically competitive. The Kellogg design of the hot gas desulfurization portion of the Piñon Pine IGCC demonstration plant is based on one complete replacement of zinc sorbent inventory per year (Dorchak, 1997). Three complete replacements of the zinc sorbent per year were assumed in the study of Buchanan et al. (1994). These replacement rates, as percentages of sorbent circulation rate, are estimated to be in the range of 0.04% to 0.1% (corresponding to average sorbent lifetimes of 1000 to 2500 cycles), far smaller than used in the base design case of this study. The sorbent replacement cost also depends on the sorbent unit cost, which is also highly uncertain at this stage of development. Keys (1997) estimated a cost range of from $5/lb to $8/lb for zinc sorbent, and Kilbourn (1997) suggested a range of from $3/lb to $8/lb for cerium sorbent. Consequently, in the cost sensitivity analysis the sorbent replacement rate (both sorbents) was varied between 0% (infinite sorbent life) and 1% while unit costs of $3/lb, $5/lb, and $8/lb for both sorbents were considered.

Results of the cost sensitivity analysis are shown in Figure 70. Base levels were assumed for all other cost items, including the zinc sorbent replacement rate in the secondary sorber of the two-stage process. The solid lines in Figure 70 represent cerium sorbent costs while the dashed lines represent zinc sorbent costs. At the base sorbent replacement rate of 1%, single-stage desulfurization using zinc sorbent is less expensive except when the cost of zinc sorbent is high ($8/lb) and the cost of cerium sorbent is low ($3/lb). However, the total levelized cost in each case is too large for either process to be economically competitive.

As the replacement rate is decreased (sorbent lifetime increased) the total cost of both processes decreases as does the cost advantage of the zinc sorbent process. Because of the different slopes, the six lines of Figure 70 form nine points of intersection corresponding to equal total levelized cost for the two processes. These intersection points and associated costs are identified in Table 29. For example, when the unit costs of both sorbents are equal at either $3/lb, $5/lb, or $8/lb, the intersections occur at a total levelized cost of $8.68 million, well below the base case total levelized cost of either process. The sorbent replacement rate at these intersections shifts to the left (smaller sorbent replacement rate) as the sorbent unit cost increases. When the unit cost of both sorbents is $3/lb, equal cost occurs at a sorbent replacement rate of 0.415% (240 cycle lifetime). At an equal sorbent unit cost of $5/lb, the equal cost replacement rate is 0.25% (400 cycles), and is 0.155% (650 cycles) when the unit cost of both sorbents is $8/lb. To the left of the intersection points (smaller sorbent replacement rate)

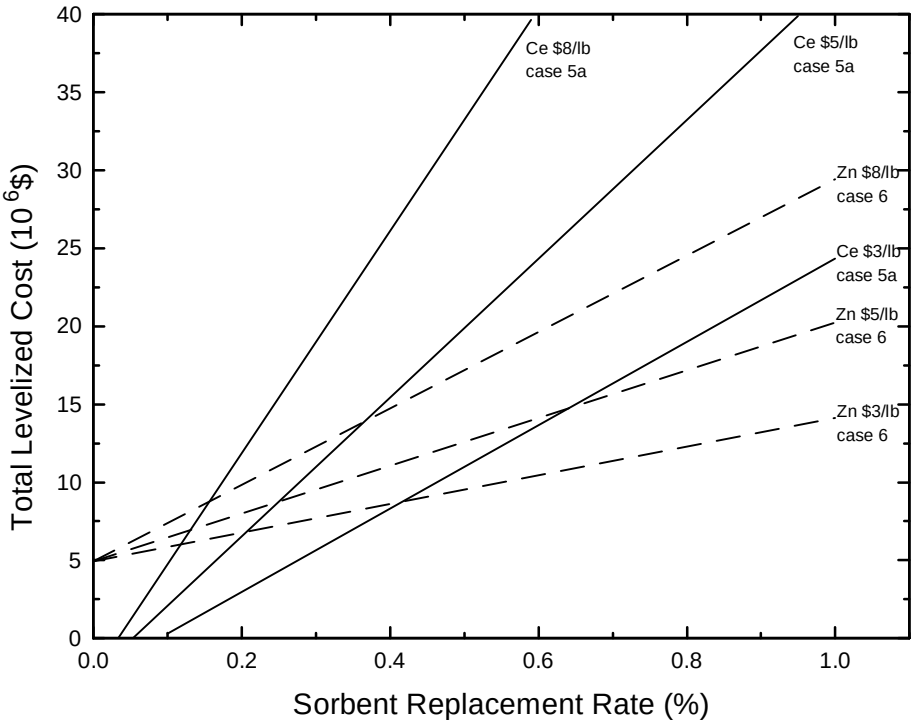

Figure 70. Cost Sensitivity Analysis as a Function of Sorbent Replacement Rate and Sorbent Unit Cost

Table 29. Sorbent Replacement Rates and Total Levelized Costs at the Equal Cost Intersection Points of Figure 70

Cerium Sorbent Unit Cost, $/lb	Zinc Sorbent Unit Cost, $/lb	Sorbent Replacement Rate, % of Circulation Rate	Total Levelized Cost, $10^6$$
8	8	0.155	8.68
8	5	0.13	6.96
8	3	0.12	5.96
5	8	0.37	13.8
5	5	0.25	8.68
5	3	0.21	6.96
3	8	3.0*	76.43*
3	5	0.65	14.84
3	3	0.415	8.68

*calculated values not shown in Figure 70

the total levelized cost for two-stage desulfurization with SO_2 regeneration is lower than that of single-stage desulfurization with DSRP.

Figure 70 also shows that the three cost lines for each sorbent converge to a common point at zero sorbent replacement rate (infinite sorbent lifetime). For single-stage desulfurization with DSRP convergence occurs at $5 million while for two-stage desulfurization with SO_2 regeneration the lines converge at -$2.2 million. In other words, two-stage desulfurization with SO_2 regeneration has the potential to "make money" through the sale of by-product steam and sulfur if the sorbent lifetime is sufficiently large. In contrast, single-stage desulfurization with DSRP will incur a total levelized cost of $5 million even with infinite sorbent lifetime.

As shown in the base case estimates (Tables 27 and 28), the total levelized cost of both processes is dominated by the sorbent replacement cost and is insensitive to other cost items. However, as the sorbent replacement rate decreases, other items such as oxygen, nitrogen and the total capital requirement become more important contributors to the total levelized cost.

The unit costs for both nitrogen and oxygen depend on the air separation method, the size of the separation plant, and also on accounting factors. The base case cost estimate used $25/ton for nitrogen and $40/ton for oxygen. Unit cost ranges of $30/ton to $50/ton for oxygen and $10/ton to $40/ton for nitrogen were selected for the sensitivity analysis. Figure 71 shows the results for sorbent replacement rates between 0.1% and 0.5% of circulation rate (200 to 1000 cycles lifetime). The unit costs of both zinc and cerium sorbents were set at the intermediate value of $5/lb for this analysis.

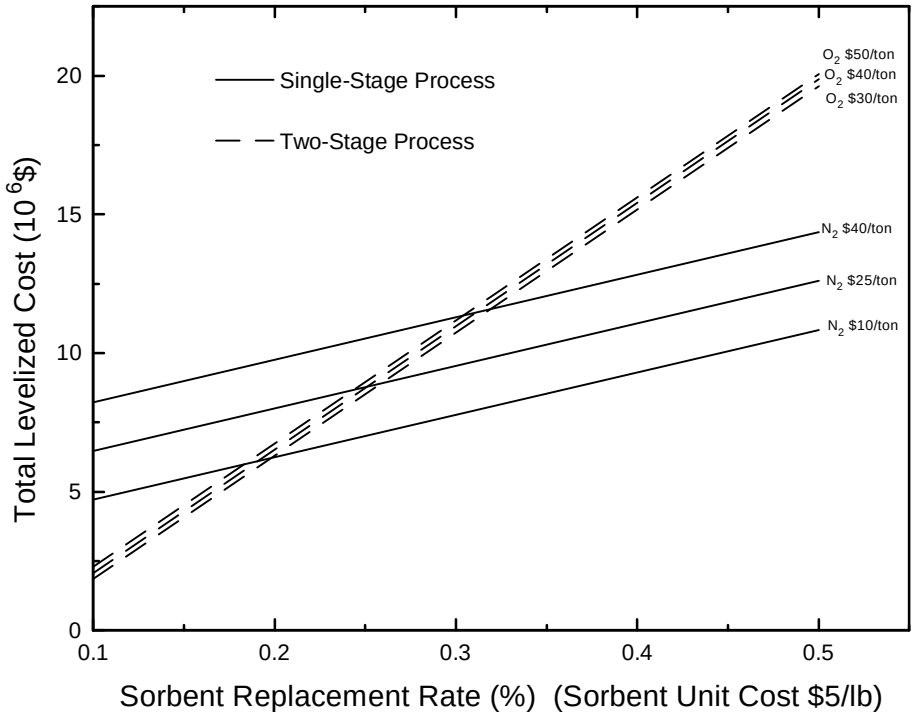

Figure 71. Cost Sensitivity Analysis as a Function of Oxygen and Nitrogen Unit Costs and Sorbent Replacement Rate

For single-stage desulfurization with DSRP, the difference in total levelized cost between nitrogen at $40/ton and $10/ton is $3.53 million. This amounts to about 33% of the total levelized cost at a sorbent replacement rate of 0.5%, and 75% of the total levelized cost at a 0.1% replacement rate. Both percentages are based on a nitrogen unit cost of $10/ton. At base case conditions the nitrogen contributed 17.8% of the total levelized cost.

Oxygen costs for two-stage desulfurization with SO_2 regeneration are much less important because of the higher sorbent replacement cost. The total levelized cost difference between O_2 at $50/ton and $30/ton is $0.46 million. This is a near negligible 2% of the total levelized cost at a sorbent replacement rate of 0.5% but rises to 25% of the total levelized cost when the sorbent replacement rate is 0.1%. Both percentages are based on O_2 at $30/ton. The intersection points in Figure 71 occur over a range of sorbent replacement rates from 0.18% (555 cycles) to 0.32% (312 cycles) and the total levelized costs at these intersections are $11.62 million and $6 million, respectively.

The capital cost estimate also becomes more important as the required sorbent replacement rate decreases. The estimated accuracy of the capital cost estimate is ± 30%, and the sensitivity of the total levelized cost was examined at 70%, 100%, and 130% of the base level capital cost. Results, as a function of sorbent rate replacement between 0.1% and 0.5% of the sorbent circulaton rate and sorbent unit cost of $5/lb, are shown in Figure 72. As the total capital requirement is increased from 70% to 130% of the base value, the total levelized cost of two-stage desulfurization with SO_2 regeneration increases by $0.78 million while an increase of $1.55 million occurs for the single-stage process. The $1.55 million increase represents an increase in the annual levelized cost of about 13% and 27% at sorbent replacement rates of 0.5% and 0.1% respectively. With two-stage desulfurization, the $0.78 million increment represents increases of 4% and 46% at sorbent replacement rates of 0.5% and 0.1%, respectively. The intersection points of the of Figure 72 occur at sorbent replacement rates between 0.21% and 0.29% (345 and 476 cycles) with total levelized costs between $7.3 million and $10.2 million, both well below the total levelized costs for the base design case.

9.10 Conclusions

The process and economic analysis has shown that sorbent replacement cost is the key variable for the economic success of both the single-stage zinc sorbent process with DSRP and the two-stage cerium sorbent process with SO_2 regeneration. The total levelized cost estimated in the base design cases, which assumed a sorbent replacement rate of 1% of the sorbent circulation rate (100 cycle average sorbent lifetime) was $16.3 million for the single-stage process and $25.9 million for the two-stage process. On the basis of a 65% on-stream factor, these annual levelized costs correspond to incremental busbar costs of electricity of about 10.6 and 16.8 mill/kWh, both above levels needed to be economically competitive.

As the required sorbent replacement rate decreases (sorbent lifetime increases), the cost of both processes decreases and, relatively speaking, the two-stage cerium sorbent process becomes more attractive. The sorbent replacement rate at which the levelized costs of the two processes are equal is in the range of 0.1% to 0.4% of the circulation rate (250 to 1000 cycles). The wide range is due to the large uncertainty in other process costs such as the unit costs of

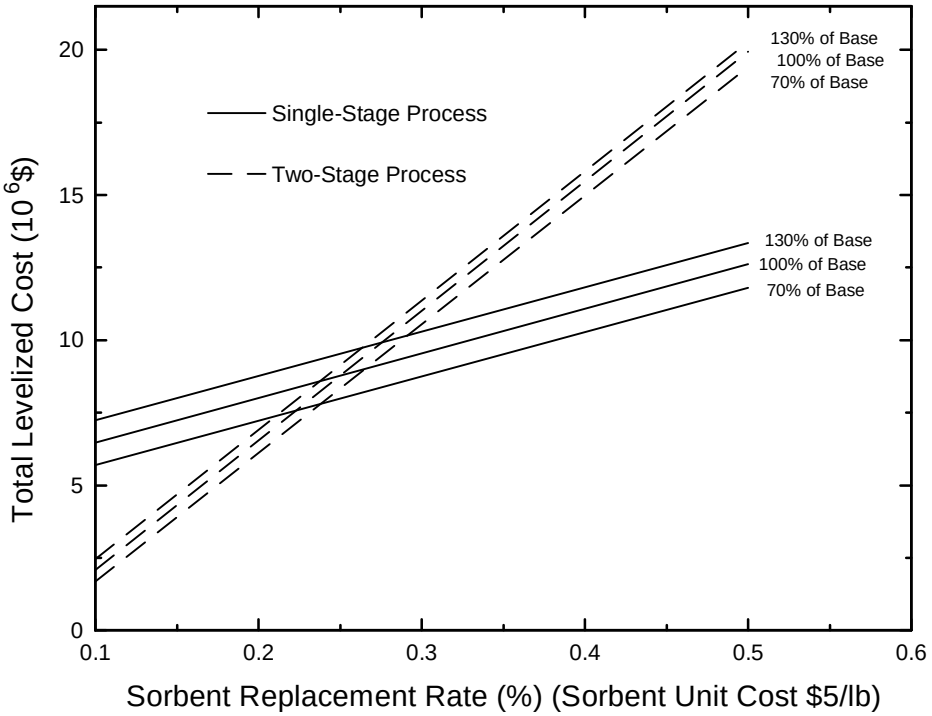

Figure 72. Cost Sensitivity Analysis as a Function of Total Capital Requirement and Sorbent Replacement Rate

sorbent, oxygen, and nitrogen as well as capital costs. However, within this range the total annual levelized cost is reduced to the range of $7.1 to $8.6 million or 4.6 to 5.6 mills/kWh incremental busbar cost. For replacement rates smaller than 0.1% of the sorbent circulation rate, we project that the two-stage process using cerium sorbent should be less costly. In the limit of infinite sorbent lifetime, by-product sale from should be less costly. In the limit of infinite sorbent lifetime, by-product sales from the two-stage process could produce a profit of about $2.2 million per year in annual levelized cost (1.4 mills/kWh). In contrast, the minimum annual levelized cost of the single-stage process using zinc sorbent is estimated to be about $5 million (3.2 mills/kWh).

REFERENCES

Anderson, G.L., and Berry, F.O., 1987, "Development of a Hot Gas Cleanup System," Proceedings of the 7th Annual Gasification and Gas Stream Cleanup Systems Meeting, DOE/METC-87/6079, Vol 2. (DE87006496).

Barin, I., et al., 1977, "Thermochemical Data of Pure Substances," VCH Verlagsgesellschaft, Weinheim, Germany.

Barin, I., et al., 1993, "Thermochemical Data of Pure Substances," VCH Verlagsgesellschaft, Weinheim, Germany.

Bevan, D.J.M., and Kordis, J., 1964, "Mixed Oxides of the Type Mo_2O_3 - - I. Oxygen Dissociation Pressure and Phase Relationship in the System CeO_2 – Ce_2O_3 at High Temperatures," J. Inorg. Nucl. Chem., 26, 1509.

Buchanan, T.L., et al., 1994, Optimization of Gas Stream Cleanup in Three IGCC Systems, Final Report, Task Assignment, 11, DE-AC01-88FE61660.

Cammarata, D., 1997, Personal Communication, Air Products, Baton Rouge, LA.

Chen, H.T., et al., 1992, Sensitivity Effects of Fluidized Bed Hot Gas Desulfurization in IGCC Cost of Electricity, Final Report, Task Assignment 9, DE-AC01-88FE61660.

Chen, H.T. et al., 1991, Sensitivity Effects of Fluidized Bed Hot Gas Desulfurization on IGCC Cost of Electricity, Final Report, Task Assignment 2, DE-AC01-88FE61660.

Copeland, R.A., 1993a, "High Temperature Regenerable H_2S Removal Agents," U.S. Patent 5,271,907.

Copeland, R.A., 1993b, "High Temperature H_2S Removal," Proceedings of the Symposium on Coal-Fired Power Systems '93 – Advances in IGCC and PFBC, DOE/METC-93/6131.

Donsi, G. et al., 1983, Heat Transfer from Vertical Heated Surfaces to Slugging, Pressurized Fluidized Beds, Fluidization, Proceedings of the Fourth International Conference on Fluidization, Kashekojima, Japan.

Dorchak, T., 1997, Personal Communication, U.S. Department of Energy, Morgantown, WV.

Electric Power Research Institute (EPRI), 1982, TAG-Technical Assessment Guide, Report No. EPRI-P-2410-SR.

Gangwal, S.K., et al., 1988, "Multicycle Testing of Zinc Ferrite," DOE/MC/23126-2644.

Gangwal, S.K., and Portzer, J.W., 1995, "Slipstream Testing of Hot-Gas Desulfurization With Sulfur Recovery," Proceeding of the Advanced Coal-Fired Power Systems '95 Review Meeting, DOE/METC-95/1018, Vol. 1, p. 220.

Grindley, T., and Steinfeld, G., 1981, "Development and Testing of Regenerable Gas Desulfurization Sorbents," DOE/MC/16545-1125.

Joshi, D.K., et al., 1979, "Hot Low-Btu Producer Gas Desulfurization in Fixed-Bed of Iron Oxide-Fly Ash," DOE/FE-2257-3.

Kay, D.A.R., and Wilson, W.G., 1989, "Method for the Regeneration of Sulfided Cerium Oxide Back to a Form That is Again Capable of Removing Sulfur From Fluid Materials," U.S. Patent 4,857,280.

Kay, D.A.R., et al., 1993, "High Temperature Thermodynamics and Applications of Rare Earth Compounds Containing Oxygen and Sulfur in Fuel Gas Desulfurization and SO_2 and NO_x Removal, J. of Alloys and Compounds, 192, 11.

Keys, K., 1997, Personal Communication, United Catalysts, Inc., Louisville, KY.

Kilbourn, B., 1997, Personal Communication, Molycorp, Fairfield, NJ.

Kirk-Othmer, 1981, Encyclopedia of Chemical Technology, Mark, H.F., ed., John Wiley and Sons, New York, NY.

Kirkpatrick, M.O., and Pike, R.W., 1994, "Linking Database Management Systems and Chemical Engineering Application Programs - - Prediction of Chemical Equilibrium," AIChE Symposium Series, C.C. Chen and S. Watansiri, eds., Vol. 90, No. 298, pp. 174-187.

Lopez, A., et al., 1994, "Advanced Sulfur Control Concepts in Hot-Gas Desulfurization Technology: Phase I. Feasibility of the Direct Production of Elemental Sulfur During Regeneration of High Temperature Desulfurization Sorbents," Topical Report, DOE Contract No. DE-AC21-94MC30012.

Lopez, A., et al., 1997, "Advanced Sulfur Control Concepts in Hot Gas Desulfurization Technlogy: Phase II. Exploratory Studies on the Direct Production of Elemental Sulfur During the Regeneration of High Temperature Desulfurization Sorbents," Topical Report, DOE Contract No. DE-AC21-94MC30012.

McMichael, W.J., and Gangwal, S.K., 1991, Sulfur Recovery From Hot Gas Desulfurization Processes, Final Report, DE-AC21-86MC23260.

Meng, V.V., and Kay, D.A.R., 1987, "Gaseous Desulfurization Using Rare Earth Oxide," in High Tech. Ceramics, P. Vincinzini, ed., Elsevier Science Publishers, Amsterdam.

Nielsen, P.E.H., et al., 1991, "Steam Regenerable Sulfur Absorption Masses and Their Application in IGCC Plants," paper presented at EPRI Coal Gasification Conference, San Francisco.

O'Hara, J.B., et al., 1997, Sulfur Recovery From Hot Coal Gas Desulfurization Processes, DOE/MC/21097-2338 (DE 870064777).

Patrick, V., and Gavalas, G.R., 1993, "Reduction, Sulfidation, and Regeneration of Mixed Iron-Aluminum Oxide Sorbent," Industrial and Engineering Chemistry Research, 32, 519.

Peters, M., and Timmerhaus, K., 1991, Plant Design and Economics for Chemical Engineers, Fourth Ed., McGraw-Hill, New York, NY.

Piepers, H.W., et al., 1983, Heat Transfer on a Vertical Tube Bundle Immersed in a 0.70M Fluidized Bed, Fluidization, Proceedings of the Fourth International Conference on Fluidization, Kashikoyuna, Japan.

Schrodt, J.T., and Best, J.E., 1978, "Sulfur Recovery From Fuel Gas Desulfurization Sorbent," AIChE Symposium Series, 74, No. 175, 189.

Seko, H., et al., 1983, Heat Transfer Characteristics Along Vertical Tubes in a Fluidized Bed at Elevated Temperature, Fluidization, Proceedings at the Fourth International Conference on Fluidization, Kashikoyuna, Japan.

Sohn, H.Y., and Kim, D., 1987, "Intrinsic Kinetics of the Reaction Between Zinc Silfide and Water Vapor," Metall. Trans. B, 18B, 451.

Stanford Materials Co., 1997, Internet Product Catalog, http://www.stanford.materials.com.

Tamhankar, S.S., et al., 1985, "Kinetic Study on the Reactions Involved in Hot Gas Desulfurization Using a Regenerable Iron Oxide Sorbent: III. Reactions of the Sulfided Sorbent With Steam and Steam-Air Mixtures," Chemical Engineering Science, 40, 1019.

Tseng, S.C., et al., 1991, "Kinetic Studies on the Reactions Involved in Hot Gas Desulfurization Using a Regenerable Iron Oxide Sorbent: II. Reactions of Iron Sulfide With Oxygen and Sulfur Dioxide," Chemical Engineering Science, 36, 1287.

U.S. DOE, 1966a, "The Piñon Pine Integrated Gasification Combined Cycle Project," Clean Coal Technology Topical Report 8, U.S. DOE, Office of Fossil Energy.

U.S. DOE, 1996b, "The Tampa Electric Integrated Gasification Combined Cycle Power Plant," Clean Coal Technology Topical Report 6, U.S. DOE, Office of Fossil Energy.

Van der Waal, W.J.J., 1987, "Desulfurization of Process Gas by Means of Iron Oxide on Silica Sorbents," Ph.D. Dissertation, University of Utrecht.

Wakker, J.P., et al., 1993, "High Temperature H_2S and COS Removal With MnO and FeO on ϒ-Al_2O_3 Acceptors," Industrial and Engineering Chemistry Research, 32, 139.

Willis, J., 1996, Personal Communications, ADCO Companies, Inc., Baton Rouge, LA

Woods, M.C., et al., 1990, "Reaction Between H_2S and Zinc Oxide – Titanium Oxide Sorbents. 1. Single-Pellet Sulfidation Studies," Industrial and Engineering Chemistry Research, 29, 1160.